ESL-TR-88-82

SPLIT-HOPKINSON PRESSURE BAR TESTS

C. ALLEN ROSS

HQ AFESC/RDCM
HQ AIR FORCE ENGINEERING AND SERVICES CENTER
TYNDALL AFB FL 32403-6001

MARCH 1989

FINAL REPORT

OCTOBER 1986 — SEPTEMBER 1988

AFESC

ENGINEERING & SERVICES LABORATORY
AIR FORCE ENGINEERING & SERVICES CENTER
TYNDALL AIR FORCE BASE, FLORIDA 32403

NOTICE

PLEASE DO NOT REQUEST COPIES OF THIS REPORT FROM HQ AFESC/RD (ENGINEERING AND SERVICES LABORATORY). ADDITIONAL COPIES MAY BE PURCHASED FROM:

NATIONAL TECHNICAL INFORMATION SERVICE
5285 PORT ROYAL ROAD
SPRINGFIELD, VIRGINIA 22161

FEDERAL GOVERNMENT AGENCIES AND THEIR CONTRACTORS REGISTERED WITH DEFENSE TECHNICAL INFORMATION CENTER SHOULD DIRECT REQUESTS FOR COPIES OF THIS REPORT TO:

DEFENSE TECHNICAL INFORMATION CENTER
CAMERON STATION
ALEXANDRIA, VIRGINIA 22314

UNCLASSIFIED
SECURITY CLASSIFICATION OF THIS PAGE

REPORT DOCUMENTATION PAGE

Form Approved
OMB No 0704-0188

1a REPORT SECURITY CLASSIFICATION Unclassified	1b RESTRICTIVE MARKINGS
2a SECURITY CLASSIFICATION AUTHORITY NA	3 DISTRIBUTION/AVAILABILITY OF REPORT Approved for public release. Distribution unlimited.
2b DECLASSIFICATION/DOWNGRADING SCHEDULE NA	
4 PERFORMING ORGANIZATION REPORT NUMBER(S) ESL-TR-88-82	5 MONITORING ORGANIZATION REPORT NUMBER(S)
6a NAME OF PERFORMING ORGANIZATION HQ AFESC 6b OFFICE SYMBOL (If applicable) RDCS	7a NAME OF MONITORING ORGANIZATION
6c ADDRESS (City, State, and ZIP Code) HQ Air Force Engineering and Services Center Tyndall AFB FL 32403-6001	7b ADDRESS (City, State, and ZIP Code)
8a NAME OF FUNDING/SPONSORING ORGANIZATION 8b OFFICE SYMBOL (If applicable)	9 PROCUREMENT INSTRUMENT IDENTIFICATION NUMBER
8c ADDRESS (City, State, and ZIP Code)	10 SOURCE OF FUNDING NUMBERS PROGRAM ELEMENT NO PROJECT NO: 2673 TASK NO WORK UNIT ACCESSION NO: 93

11 TITLE (Include Security Classification)
(U) Split-Hopkinson Pressure Bar Tests

12 PERSONAL AUTHOR(S)
C. Allen Ross

13a TYPE OF REPORT	13b TIME COVERED	14 DATE OF REPORT (Year, Month, Day)	15 PAGE COUNT
Final	FROM 86/10/1 TO 88/9/30	March 1989	

16 SUPPLEMENTARY NOTATION
Availablility of this report is specified on reverse of front cover.

17 COSATI CODES		
FIELD	GROUP	SUB-GROUP

18 SUBJECT TERMS (Continue on reverse if necessary and identify by block number)
Hopkinson Bar, Kolsky Device, Wave Propagation, Transmission Ratio, Strain-Rate, Load-Rate, Partially Saturated Soil, Wave Speed

19 ABSTRACT (Continue on reverse if necessary and identify by block number)

This report summarizes work conducted on the Engineering and Services Laboratory (ESL) split-Hopkinson pressure bar (SHPB). The SHPB was modified to permit both tensile and compressive testing on cementitious materials. Direct tension tests were performed on concrete by cementing the specimen to the SHPB. Splitting cylinder tests were also conducted in the SHPB. Tensile strength data versus strain rate is presented for concrete. The strain rate sensitivity of tensile data appears to be two to four times greater than the compressive data for the same strain rate. Tests on dry and moist soils were also conducted in the SHPB. For these tests the loading pulse time is much smaller than the transit time of the specimen. Both wave speed and stress transmissibility through the specimen were monitored. Although not completely conclusive effects of compaction with moisture may cause large increases in wave speed transmissibility, and stiffness in sandy soils, at low values of moisture content. These results show the importance of needed research in the area of stress transmission in partially saturated soils.

20 DISTRIBUTION/AVAILABILITY OF ABSTRACT	21 ABSTRACT SECURITY CLASSIFICATION
☒ UNCLASSIFIED/UNLIMITED ☐ SAME AS RPT ☐ DTIC USERS	Unclassified
22a NAME OF RESPONSIBLE INDIVIDUAL Dr C. A. Ross	22b TELEPHONE (Include Area Code) / 22c OFFICE SYMBOL

DD Form 1473, JUN 86 Previous editions are obsolete SECURITY CLASSIFICATION OF THIS PAGE

(The reverse of this page is blank.)

PREFACE

This report was prepared by Dr C. A. Ross, University of Florida, as a final report of work accomplished under a University Resident Research Program of the Air Force Systems Command (AFSC). This work was conducted for the Air Force Engineering and Services Center, Engineering and Services Laboratory, Facility Systems and Analysis Branch (AFESC/RDCS) Tyndall AFB FL 32403-6001. Mr W. S. Strickland (AFESC/RDCS) served as the program technical manager. This report summarizes work conducted between 1 Oct 1986 to 30 Sep 1988.

This report has been reviewed by the Public Affairs Office and is releasable to the National Information Service (NTIS). At NTIS, it will be available to the general public, including foreign nationals.

This technical report has been reviewed and approved for publication.

W. S. STRICKLAND
Chief, Facility Systems and Analysis Branch

LAWRENCE D, HOKANSON, Colonel, USAF
Director, Engineering and Services Laboratory

R. J. MAJKA, Lt Col, USAF
Chief, Engineering Research Division

(The reverse of this page is blank.)

TABLE OF CONTENTS

TABLE OF CONTENTS
(Concluded)

LIST OF FIGURES

LIST OF FIGURES
(Concluded)

SECTION I

INTRODUCTION

A. OBJECTIVE

The major objective of this work was to develop a method for testing mortar and concrete at high strain rates of 10/sec and higher. A second objective was to experimentally study the effects of compaction and moisture on wave speed and stress transmission in soils.

B. BACKGROUND

The effect of increasing strain rate on strength properties of many materials has been recognized for many years and efforts to test at high strain rates using bar impact began approximately 75 years ago. It is generally safe to say that most materials, with the exception of some work hardened aluminum alloys, experience some increase in strength with increases in load or strain rate. These increases in strength begin to show up in strain rate ranges of 10^{-7}/sec to 10^{-2}/sec and larger increases are evident in the strain rate range of 10/sec to 10^{3}/sec. Mortar and concrete compressive tests are easier to conduct than tensile tests and some experimental compressive strength properties in the strain-rate range of 10^{-7}/sec to 10^{3}/sec have been determined. However, in the intermediate-strain-rate range of 10^{-1}/sec to 10/sec testing is very difficult and compressive data is scarce in this region of strain rate.

Tensile strength testing of concrete and mortar is difficult, even in the low or quasi-static strain rate range. To emphasize this statement the American Society of Testing Materials (ASTM) does not recognize a standard method for testing of mortar or concrete in direct tension. The splitting cylinder method, an indirect tensile test, is recognized by ASTM as a concrete tensile strength test in the low-strain-rate range.

High-strain-rate tensile tests of concrete have been attempted using impact of long concrete rods with various steel projectiles. However, this is an indirect method because a compression pulse is used to reflect from the free end of the concrete bar and reload the bar in tension on the return pulse. This method appears to give very high tensile strength (as much as 50 percent of the compressive strength) in the strain rate of 10/sec to 10^{2}/sec. These same high-strength values were not evident in tensile tests of concrete using a gravity-driven split-Hopkinson pressure bar (SHPB) in the range of 1.0/sec to 10/sec.

In the area of conventional weapons, loading pulses having rise times in the area of 1.0 millisec may impose strain rates in the range of 10/sec up to 10^{3}/sec on materials and structures. Therefore, it is important to the USAF civil engineering community to know the effects of these loadings or strain rates on tensile strength of structural materials. Very little data is available on tensile strength of concrete and mortar at strain rates associated with close-in conventional weapons.

Also, associated with conventional weapons is the problems of predicting the free-field pressure at some distance from an underground explosion, given the weapon weight and soil properties of density and wave speed. The problem is that errors of $\pm$ 75 percent (and sometimes greater) exist in these estimates. In an effort to try and sort out some of the variations a study was initiated by AFESC/RDC. Under contract to AFESC/RDC, Southwest Research Institute (SWRI) of San Antonio TX developed a large 2-inch (51mm) diameter SHPB to test soil in confined laboratory tests. The results of this work showed soils of varying particle size and moisture content have considerable scatter in the data even when tested in a controlled laboratory environment. However, in constant dry density soil tests a phenomenon was observed, showing increases in wave speed and stress transmission for saturations up to approximately 60 to 70 percent and decreasing beyond.

With the need for further study in the area of effects of high strain rate on tensile strength of concrete and effects of moisture on soil wave speed and transmissibility it was decided to move the SHPB to AFESC/RDC, Tyndall AFB, FL. This SHPB was used in the investigations described in this report.

C. APPROACH

For the soils work an approach, similar to that done at SWRI, would continue on different soils with varying particle sizes and moisture contents. Soils would be tested in the SHPB with varying confinements. Additionally, tests would be run on soil specimens which would be compacted dry and moisture added later and conversely soils compacted after moisture was added. These tests would be an attempt to determine if the observed phenomenon was a result of combined compaction and capillary pressure or a result of these acting rather independently.

For strain rate effects on tensile strength of concrete, two methods of tensile loading in the SHPB would be attempted. One, a method of indirect tension, developed previously for metals, where a compressive pulse is converted to a tensile pulse by reflection from the bar free end, and second, a direct tension method, by inducing a tensile pulse directly into the SHPB. During the course of the research the splitting cylinder method was also attempted.

SECTION II

DYNAMIC MATERIAL TESTING

A. GENERAL DESCRIPTION OF MATERIAL RESPONSE

1. Introduction

A general mathematical material description, model or constitutive equation should cover the entire range of load or strain rates that may be expected in the loading environment. However, this type of general description is very difficult to formulate and for most material the end result may be a piecewise description in a series of narrow bands of strain rate. In addition, the dynamic material testing may require different types of testing devices for each band of strain rate data. A general consideration of dynamic material testing is reported in References 1 and 2 and is reproduced in Figure 1. The breakdown presented in Figure 1 is more representative of metals and other materials may be classified in slightly different categories. However, trying to establish strain rate regions is not as important as trying to accurately determine the strain rate for a given material response or test procedure.

In the intermediate and high strain rate regions both inertia and wave propagation effects become important. In this region, emphasis must be placed on differentiating between average stresses and strains that occur when multiple waves propagate within a body, as opposed to the nonuniform stresses or strains that occur in the rise time of a single high-intensity stress wave passing across the specimen or body. In the strain rate region of 10 to 10^4/sec the stress- and strain-averaging assumptions become a major part of the stress and strain analysis.

2. Low Strain Rate Machines.

In the very low or "creep" regime testing is usually accomplished under constant load and very precise displacement measurements are made. This region of strain rate extends from a range of 10^{-10}/sec up to approximately 10^{-6}/sec. The quasistatic region of strain rate extends from the upper end of the creep range to the lower end of the intermediate range or from approximately 10^{-6}/sec to approximately 1.0/sec. In this region, material testing is conducted using standard hydraulic or screw machine material testers. The material strength associated with the lower end of this strain rate range is many times denoted as the quasistatic or static material strength and used as a base for strength comparisons at higher strain rates.

3. Intermediate Strain Rate Machines

Pneumatic or hydraulic machines have been used to test materials up to strain rates of 10^{-1} to 10^{+1}/sec. These machines usually use some ram device which is accelerated to some velocity and maintained constant during

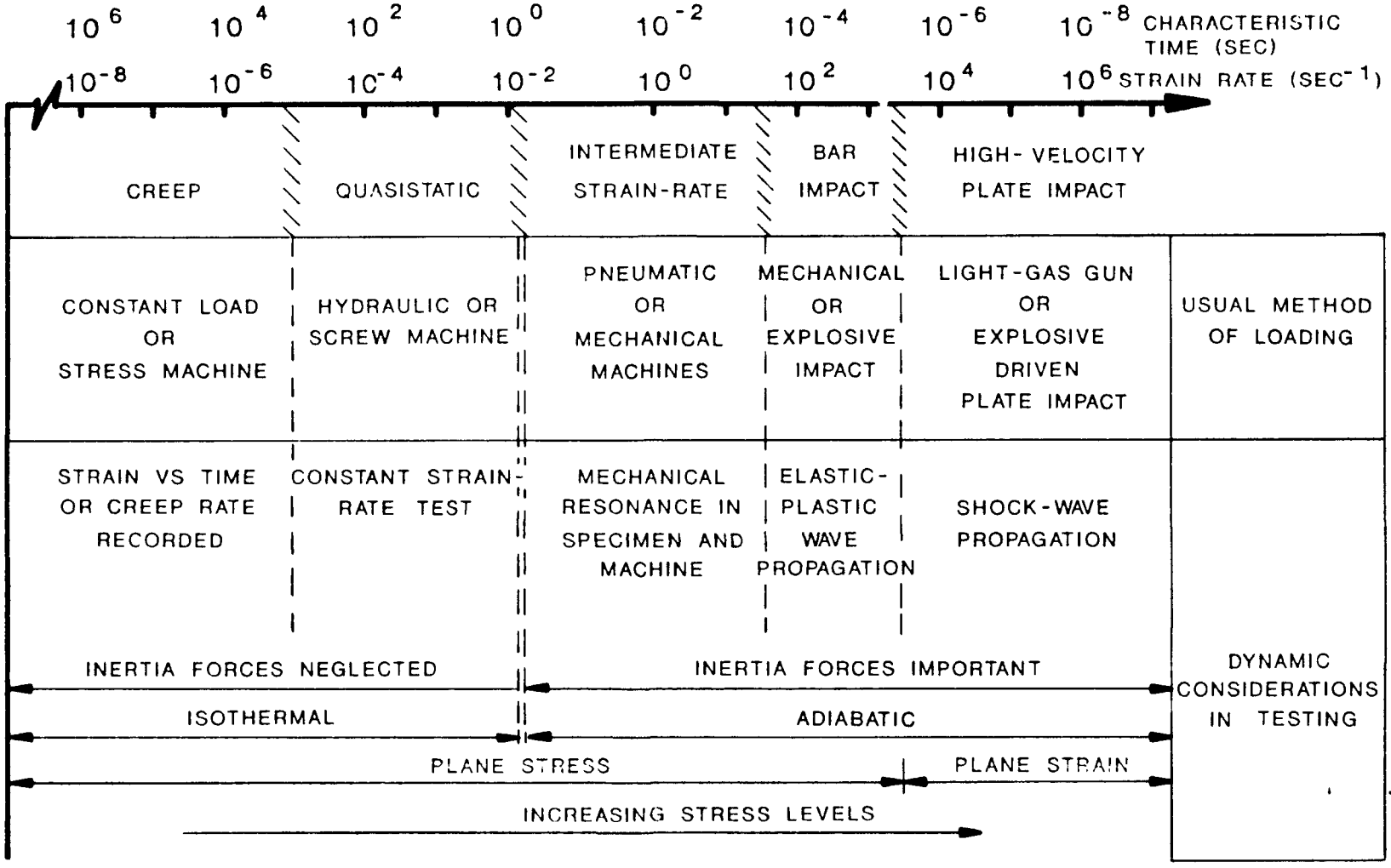

Figure 1. Dynamic Aspects of Mechanical Testing (Reference 1).

the duration of the test. These type machines may be used to bridge the gap in testing from the upper end of screw-type machines at approximately 10^{-1}/sec to the lower end of split-Hopkinson pressure bar range of approximately 10/sec. At the higher velocity end of the hydraulic rams, wave propagation and inertia effects in the load cells and fixtures must be considered in detail. This area of testing is rather difficult, but is important in the general area of concrete and cementitious materials.

4. High Strain Rate Machines.

Depending on type of equipment and size, the high strain rate range usually extends from approximately 10/sec up to around 10^4/sec. Several test devices, such as expanding rings, are used for material testing in this region but probably most used is the Kolsky device or split-Hopkinson pressure bar (SHPB). This device will be described in more detail in later sections. The more common SHPB equipment is usually driven by compressed gas and projectile impact but some are driven by explosives and others by a torsional spring "slingshot" arrangement. Regardless of loading arrangement, the SHPB device uses a stress wave in a bar to load the specimen, which is usually sandwiched between two bars. However, a variety of special specimen holding arrangements are used to acquire all three loading modes, i.e., compression, shear, and tension.

5. Summary.

Mathematical expressions or constitutive equations of material response should cover the entire range of loading but this becomes difficult since the physics of the problem is governed by changing modes of response or mechanisms with increasing load or strain rate. The devices for gathering strain-rate data in a sense determines the regions of strain rate. Screw machines may be used up to strain rates of approximately 10^{-1}/sec, hydraulic machines may be used to generate strain rate properties from 10^{-1}/sec to 10/sec, split-Hopkinson pressure bars may be used from strain rate of 10 to approximately 10^4/sec and high velocity impact plates or cylinders may be used for strain rates above 10^4/sec.

Wave propagation experiments at very intense stress waves are not ruled out but the use of large deformation plastic waves require prior knowledge of wave speeds and dynamic properties. However, wave speeds and dynamic properties are not known prior to testing, therefore this method of testing requires considerable interaction in testing and analysis. Interpretation and application of the data to material properties is difficult.

The prime objective of this report is to discuss and examine the use of the split-Hopkinson pressure bar (SHPB). The following sections will discuss some preliminary subjects and historical background of the SHPB. Following these, major sections will be devoted to the current operational SHPB at the Engineering and Services Laboratory, Air Force Engineering and Services Center at Tyndall AFB, Florida.

B. SPLIT-HOPKINSON PRESSURE BAR (SHPB)

1. Introduction

The SHPB is a device designed specifically for testing of various materials at strain rates in the approximate range of 10 to 10^4/sec. Properties of materials associated with structural response near exploding conventional weapons, are important in this strain rate range. This devise uses an elastic stress pulse, induced by a short bar impact, to load a specimen sandwiched between two long bars, usually of different size and material than that of the specimen.

2. Bar Impact

In the SHPB operation a short bar impacts a longer bar which induces a stress wave in both bars. The following simple description describes the stress pulse resulting in the bars.

Consider the impact of a short cylindrical bar of Material 1, area A_1, and velocity V_1, against a longer cylindrical bar of Material 2, area A_2, and velocity V_2 with $V_1 \geq V_2$. Using Figure 2 and the condition that the two bars remain in contact for some finite time τ, then the loads in each bar at the interface are equal. Using the change in momentum for the impacted end section of each bar the axial loads become

$$\sigma_1 A_1 = P_1 = P_2 = \sigma_2 A_2 \qquad (1)$$
$$-\rho_1 A_1 C_1 (V_1 - v) = -\rho_2 A_2 C_2 (v - V_2)$$

with the assumption of

$$V_1 \geq v \geq V_2 \qquad (2)$$

and where:

P	=	compressive load
σ	=	compressive stress
A	=	cross section area
ρ	=	density
V	=	initial bar velocity
C	=	pressure wave speed
v	=	interface velocity of bars after impact and prior to separation at time τ
τ	=	pulse length
L	=	bar length
1,2	=	subscripts for bar designations

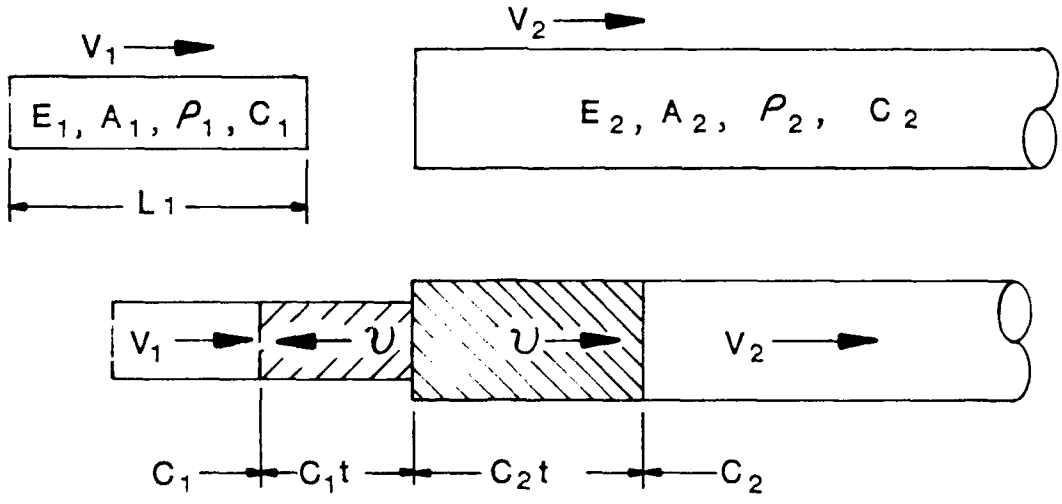

Figure 2. Schematic of Impact of Two Dissimilar Bars.

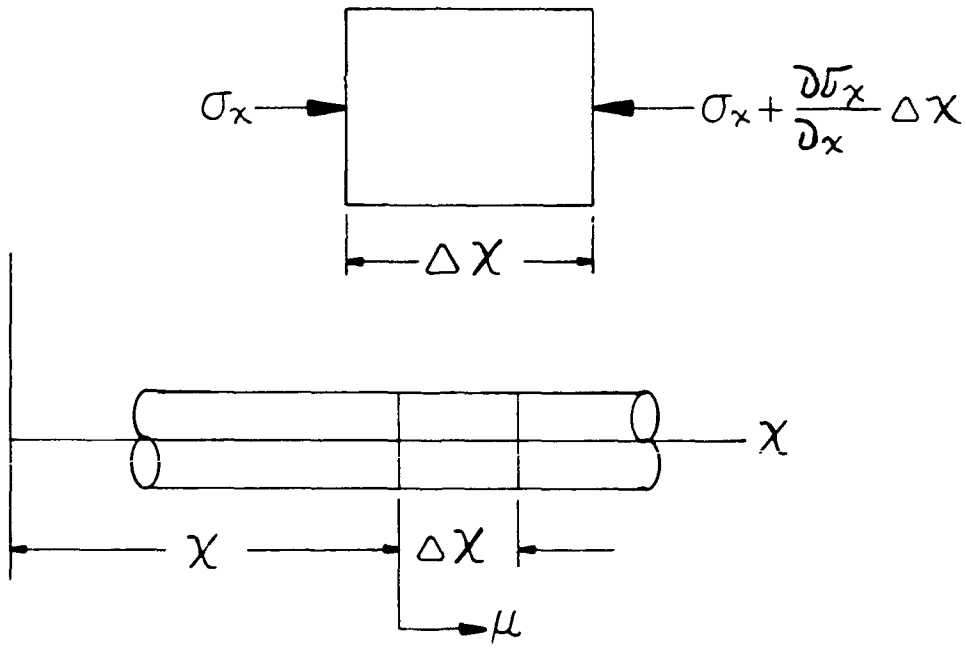

Figure 3. Stresses Associated with Longitudinal Vibration of a Bar.

Solving the second line of Equation (1) for v gives

$$v = \frac{\rho_1 C_1 A_1 V_1 + \rho_2 C_2 A_2 V_2}{\rho_1 C_1 A_1 + \rho_2 C_2 A_2} \tag{3}$$

and the stresses become

$$\sigma_1 = -\rho_1 C_1 \frac{\rho_2 C_2 A_2 (V_1 - V_2)}{\rho_1 C_1 A_1 + \rho_2 C_2 A_2} \tag{4}$$

and

$$\sigma_2 = -\rho_2 C_2 \frac{\rho_1 C_1 A_1 (V_1 - V_2)}{\rho_1 C_1 A_1 + \rho_2 C_2 A_2} \tag{5}$$

If the two bars are of the same material and cross section area then

$$\rho_1 C_1 A_1 = \rho_2 C_2 A_2 = \rho C_0 A \tag{6}$$

and

$$\sigma_1 = \sigma_2 = \sigma \tag{7}$$

The peak stress σ of the stress pulse becomes

$$\sigma = -\rho C_0 \frac{(V_1 - V_2)}{2} \tag{8}$$

and further if $V_2=0$ then the stress becomes

$$\sigma = -\rho \frac{C_0 V}{2} \tag{9}$$

where V is the impact velocity of the short bar.

At impact, a compressive pulse travels in opposite directions from the impacted end of each bar. The leading edge of the compressive pulse reflects from the free end of the short bar of length L_1 as a tensile pulse. Upon its arrival back to the impacted end, the two bars separate leaving a compressive pulse, of length $\tau = 2L_1/C_0$, travelling in the long bar. This means the pulse length τ in the long bar is determined by the time it takes a wave front to travel twice the length of the short bar. The pulse length τ and magnitude σ are two important parameters in tests using a SHPB.

3. Wave Equation for Longitudinal Waves

Consider the free vibration of a bar with area A, Young's modulus E, and density ρ as shown in Figure 3, with the assumption that plane cross sections remain plane and that the stress is uniform across the cross section. Using Newton's second law for a displacement u in the x direction of Figure 3, the equation of motions may be written as

$$-\sigma_x A + (\sigma_x + \frac{\partial \sigma_x}{\partial x} \Delta x) A = \Delta x A \rho \frac{\partial^2 u}{\partial t^2} \tag{10}$$

which reduces to

$$\frac{\partial \sigma_x}{\partial x} = \rho \frac{\partial^2 u}{\partial t^2} \tag{11}$$

Defining the strain in the x direction as

$$\varepsilon_x = \frac{\partial u}{\partial x} \tag{12}$$

and using Young's Modulus E, the LHS of Equation (11) becomes

$$\frac{\partial \sigma_x}{\partial x} = E \frac{\partial^2 u}{\partial x^2} \tag{13}$$

Combining Equations (11) and (13) the wave equation becomes

$$\rho \frac{\partial^2 u}{\partial t^2} = E \frac{\partial^2 u}{\partial x^2} \tag{14}$$

$$\frac{\partial^2 u}{\partial t^2} = C^2 \frac{\partial^2 u}{\partial x^2}$$

where the wave speed is defined as

$$C = (E/\rho)^{1/2} \tag{15}$$

The derivation of the above equation neglects the transverse inertia forces of the bar and is reasonably accurate as long as the pulse or wave length is long compared to the diameter of the bar. The concept of particle velocity may be shown mathematically by examining the solution of Equation (14) for a wave travelling in the direction of decreasing x given as

$$u = f(C_0 t + x) \tag{16}$$

Differentiating both sides of Equation (16) with respect to x yields

$$\frac{\partial u}{\partial x} = f'(C_0 t+x) , \tag{17}$$

where f' is the derivative of f with respect to the argument $(C_0 t+x)$. Also differentiating both sides of Equation (16) with respect to t yields

$$\frac{\partial u}{\partial t} = C_0 f'(C_0 t+x) \tag{18}$$

where f' is same as defined above. Solving Equation (17) or (18) for $f'(C_0 t+x)$ and substituting into the other yields

$$\frac{\partial u}{\partial t} = C_0 \frac{\partial u}{\partial x} \tag{19}$$

Using the definition of strain,

$$\frac{\partial u}{\partial x} = \varepsilon_x = \frac{\sigma_x}{E} \tag{20}$$

in Equation (19) the stress equation becomes

$$\sigma_x = \frac{E}{C_0} \frac{\partial u}{\partial t} , \tag{21}$$

and when using Equation (15) the stress becomes

$$\sigma_x = \rho C_0 \left(\frac{\partial u}{\partial t}\right) \tag{22}$$

where $\partial u/\partial t$ is defined as the particle velocity. An example of this may be seen in Equation (9) where the particle velocity becomes V/2. It is important to point out here that the wave speed C_0 is much larger than the particle velocity. As an example, for a steel bar of ρ =7800 kg/m^3, C_0=5190 m/sec, and σ_x = 40.48 MPa (5870 psi), the particle velocity is 1.0 m/sec.

4. Historical Background

One of the first application of stress pulses in a steel bar was conducted by B. Hopkinson (Reference 3, 1914) on a bar suspended by four strings as shown in Figure 4. For this work a "time-piece" was held magnetically onto the end of the rod. In the test, the momentum of a variable length "time-piece" was measured and these data were used to determine the length and magnitude of the pulse. The exact pressure time curve could not be determined from this Hopkinson bar.

With the advent of electronics, R. M. Davies (Reference 4, 1948) developed an electrical version of the Hopkinson bar using electrical measuring devices. As shown in Figure 5, Davies was able to measure the pulse length and the displacement of the bar end, and subsequently obtained a pressure time curve of the loading function. This device is commonly call. the Davies bar.

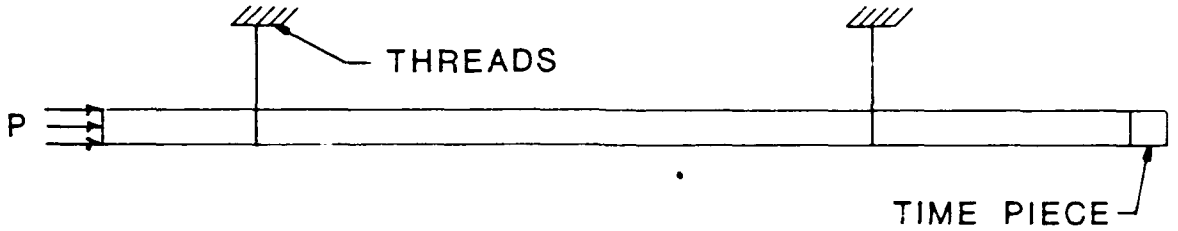

Figure 4. Hopkinson Bar Schematic.

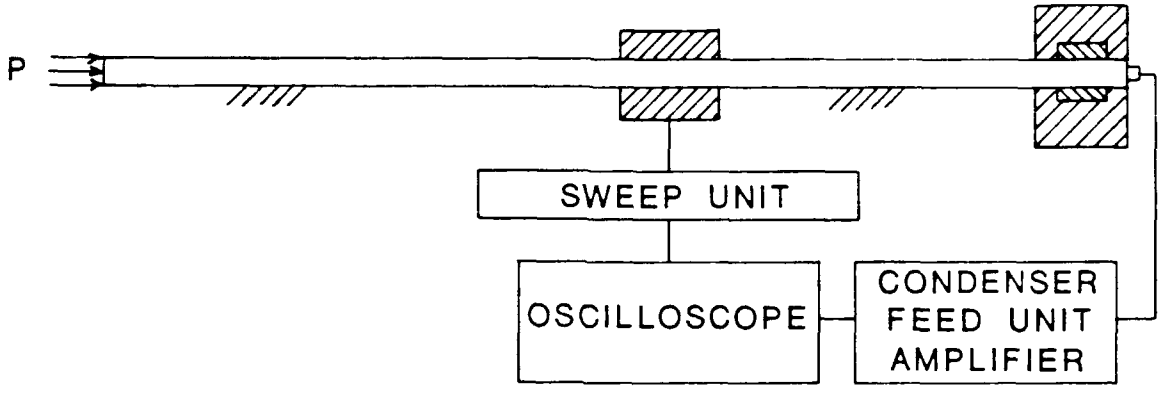

Figure 5. Davies Bar Schematic.

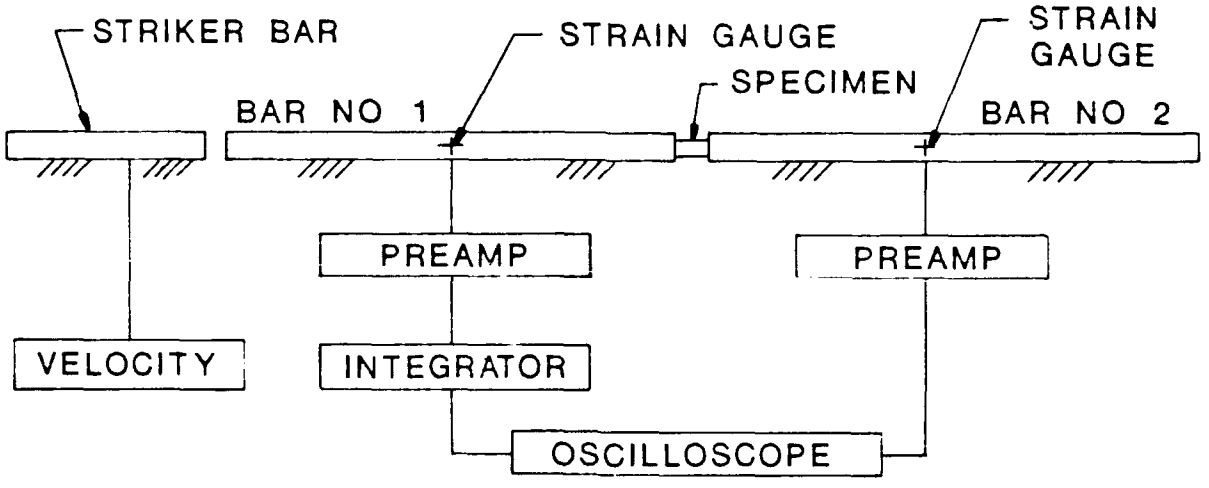

Figure 6. Split-Hopkinson Pressure Bar Schematic (Kolsky Apparatus).

The compressive split Hopkinson pressure bar (SHPB) shown in Figure 6 was developed by Kolsky (Reference 5) and has been used rather extensively. Here, the bar is split and a specimen is sandwiched between two bars and loaded by a pressure pulse. This device, generally referred to as a SHPB is also called a Kolsky apparatus. Several versions of the SHPB are described in Reference 2 and examples of devices for compression, shear, and tension are shown in Figure 7.

For the compressive SHPB of Figure 7a the impact induces a compressive pulse into the input bar which later impinges on the specimen. Part of this pulse is reflected and part of the pulse is transmitted into the output bar. Strain gauge recordings are made for both strain gauge positions. The relations between these strain gauge readings and specimen response will be discussed later. The operation of the shear SHPB of Figure 7b is similar to the compressive SHPB except that a punching shear takes place at the specimen. A tension version of the SHPB is shown in Figure 7c. For this device the impact induces a compressive pulse in the outer tube, and at the free end this pulse is reflected as a tensile pulse in the inner bar. The tensile pulse then loads the specimen in tension. Strain gauge records may be related to specimen response in the same manner as the other versions.

A rather innovative tensile version of a SHPB was developed by Nicholas (Reference 7) and is shown schematically in the lower portion of Figure 8. The initial portion of this type tensile SHPB is similar to the compressive (SHPB) (also shown for comparison in Figure 8). However, for this tensile SHPB, a compressive pulse is passed over a threaded specimen by a split collar and reflects from the free end of Bar 2 as a tensile pulse. The tensile pulse then loads the specimen, and the strain gauges record reflected and transmitted pulses at opposite positions than that of the compressive SHPB.

5. Analysis of the SHPB.

The analysis of the compressive and tensile SHPB may be studied using the same set of equations and principles. For the compressive SHPB Bar 1 is designated as the incident bar and the Bar 2 is the transmitter bar. In case of the tensile SHPB the bar designation is reversed because the tensile pulse, moving in the opposite direction, of Bar 2 becomes the loading or incident pulse. This means that, for the compressive SHPB, the Bar 1 strain gauge senses the incident and reflected strains while the Bar 2 gauge senses the transmitted strains. For the tensile SHPB this is reversed, with the incident and reflected strains measured at the Bar 2 strain gauge and the transmitted strain is measured at the Bar 1 strain gauge.

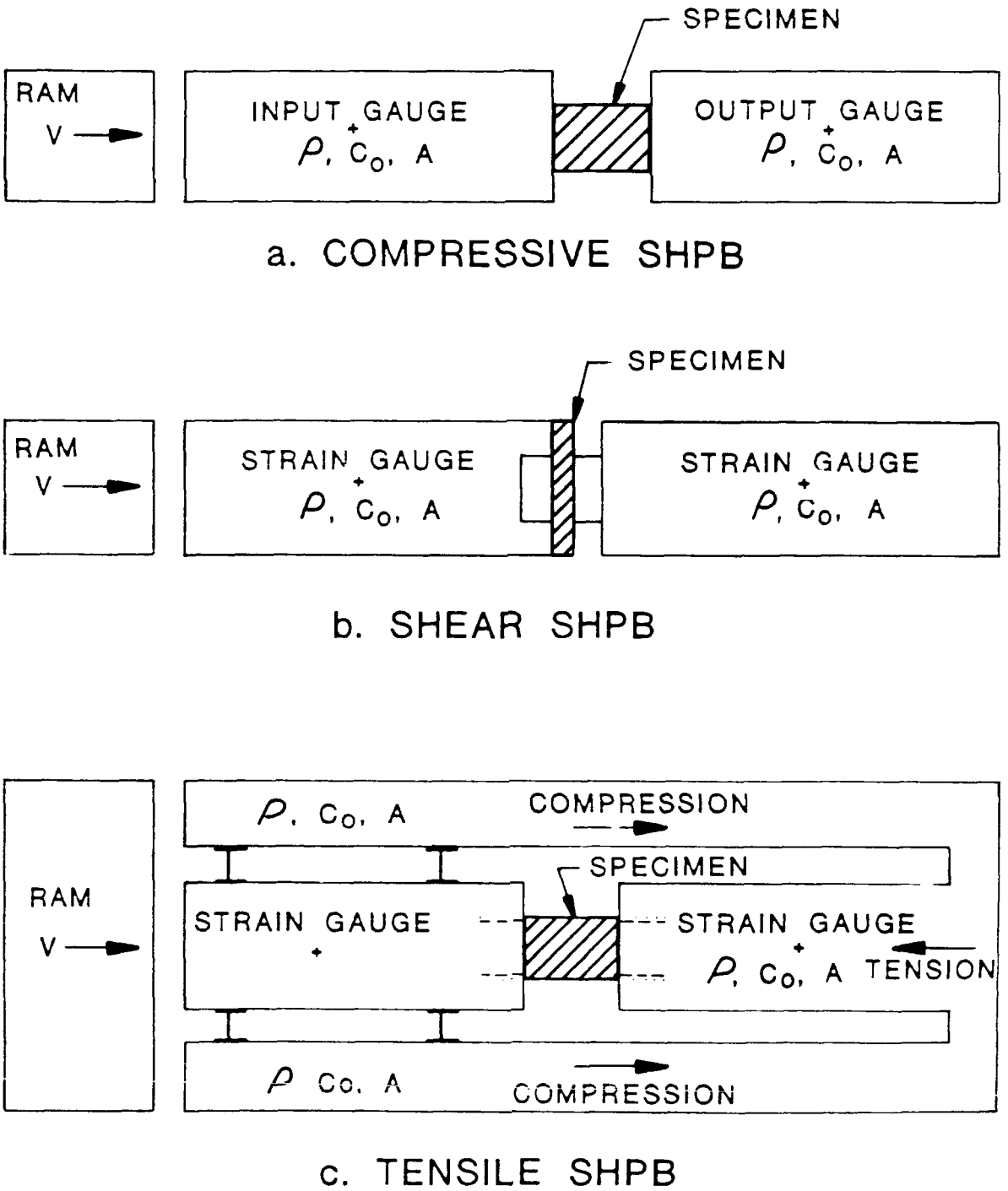

Figure 7. Examples of Compression, Shear, and Tension SHPB. (Reference 2)

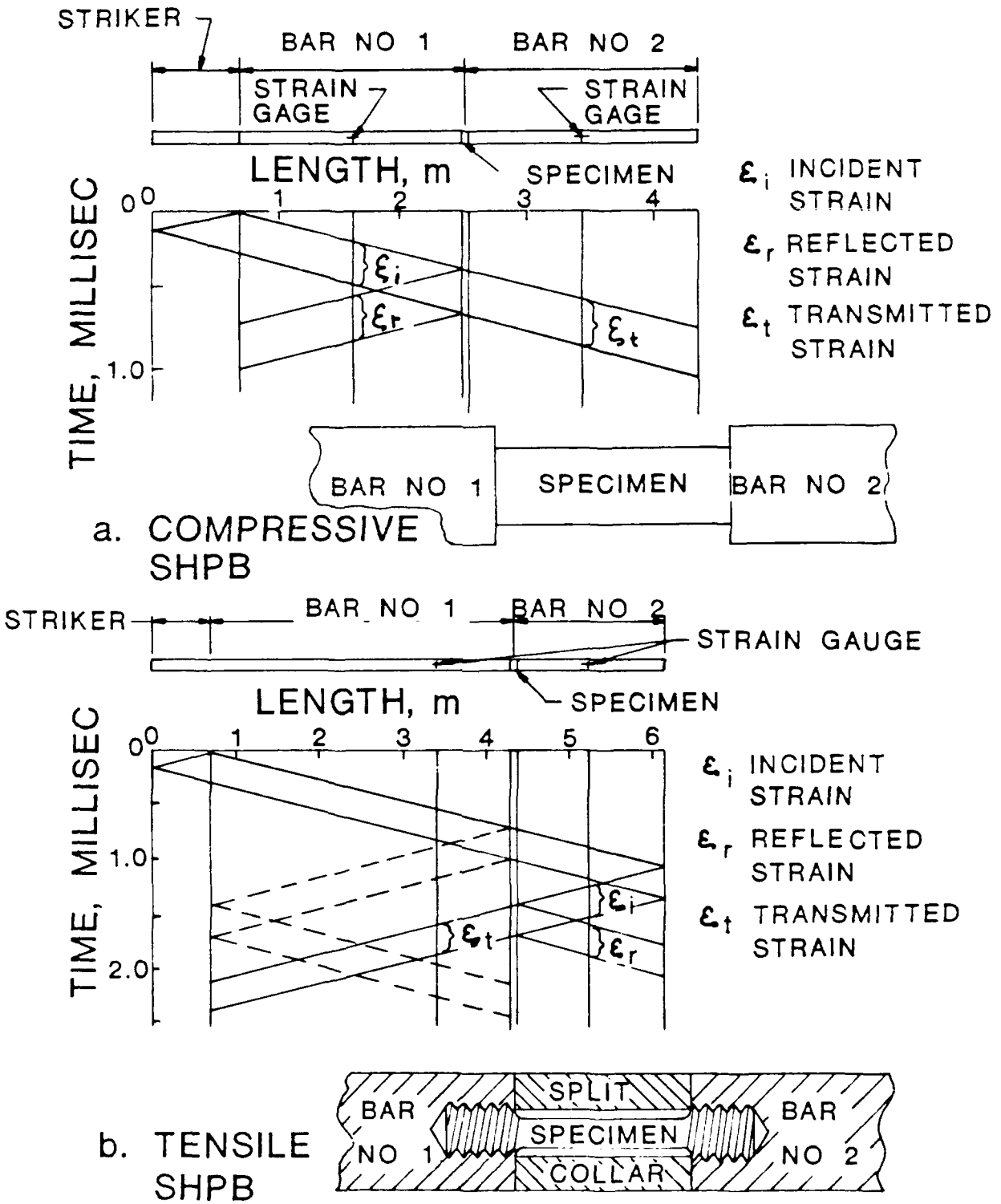

Figure 8. Comparison of Nicholas Type Tensile SHPB and a Compression SHPB.

An analysis of the stresses and strain associated with the specimen of a SHPB may be conducted using a sketch shown in Figure 9 and the following relations (Reference 1). Displacements u_1, and u_2, of opposite ends of the specimen of Figure 9, may be expressed as

$$u_1 = \int_0^t C_0 \varepsilon_1 dt \tag{23}$$

$$u_2 = \int_0^t C_0 \varepsilon_2 dt \tag{24}$$

where t is time.

Assuming stresses, strains, and loads are positive in compression then the displacements may be written in terms of the incident strain ε_i reflected strain ε_r, and transmitted strain ε_t.

$$u_1 = \int_0^t C_0(\varepsilon_i - \varepsilon_r) dt \tag{25}$$

$$u_2 = \int_0^t C_0 \varepsilon_t dt \tag{26}$$

The average strain in the specimen ε_s may be defined as

$$\varepsilon_s = \frac{(u_1 - u_2)}{L_s} \tag{27}$$

where L_s is the specimen length.
Using Equations (25) and (26) in Equation (27) the specimen strain is expressed as

$$\varepsilon_s = \frac{C_0}{L_s} \int_0^t (\varepsilon_i - \varepsilon_r - \varepsilon_t)\, dt \tag{28}$$

Based on strains at the ends of the specimens the forces on each end of the specimen may be written as

$$P_1 = E\varepsilon_1 A = EA\,(\varepsilon_i + \varepsilon_r) \tag{29}$$

$$P_2 = E\varepsilon_2 A = EA\,\varepsilon_t \tag{30}$$

where E and A are the Young's modulus and cross-sectional area of the SHPB, respectively. The average force in the specimen becomes

$$P_{ave} = \frac{EA}{2}(\varepsilon_i + \varepsilon_r + \varepsilon_t) \tag{31}$$

A general assumption is that the forces at the ends of the specimen are equal. The validity of this assumption may be questioned due to large plastic deformation and or crushing which may occur in the specimen. However, momentum principles still hold and differences may occur in the initial stages of the pulse application. Experiments by Malvern (Reference 8) show that this is a valid assumption especially in the latter stages of the pulse application. Using the assumption of $P_1 = P_2$ then

$$\varepsilon_i + \varepsilon_r = \varepsilon_t \tag{32}$$

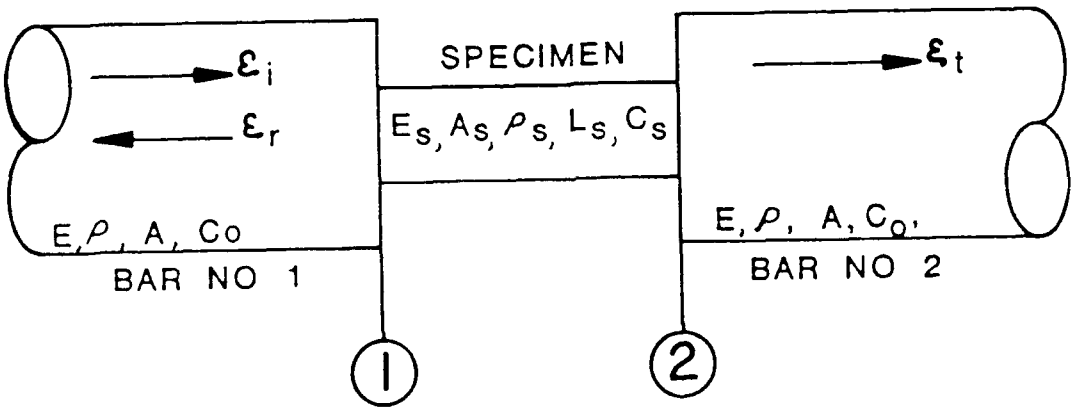

Figure 9. Schematic of Specimen Arrangement for a Compressive SHPB.

and

$$\varepsilon_s = \frac{C_o}{L}\int(\varepsilon_t - \varepsilon_r - \varepsilon_r - \varepsilon_t)dt \tag{33}$$

Using the above equations and the area ratio of bar cross-sectional area A to specimen cross-sectional area A_s, the average strain ε_s, average stress σ_s, and average strain rate $\dot{\varepsilon}_s$ in the specimen may be expressed as

$$\varepsilon_s = \frac{-2C_o}{L_s}\int_o^t \varepsilon_r dt \tag{34}$$

$$\sigma_s = E\,\frac{A}{A_s}\,\varepsilon_t \tag{35}$$

$$\dot{\varepsilon}_s = \frac{-2C_o}{L_s}\,\varepsilon_r \tag{36}$$

The above relations related to the specimen are "average values," based on a previous discussion in Section II.A.2. In normal operation all three strains, ε_i, ε_r and ε_t, are recorded. Calibration of the output using the strain gauge "gauge factor" GF, furnished by the manufacturer, gives a cross check of the alternative strain expression using Equation (9)

$$\varepsilon_i = \frac{\rho C_o}{E}\,\frac{V}{2} = \frac{\rho V}{2C_o} \tag{37}$$

Calibration of the SHPB will be discussed in later sections.

Equations (34), (35), (36), and (37) are related to both compressive and tensile SHPBs and when used in the tensile mode the signs of the strains, stresses, and forces are reversed.

Many SHPBs are in operation throughout the world and the major portion of them have been concerned with the testing of metals, i.e., References 1, 6, and 7. Several studies have been concerned with metal and nonmetal matrix filamentary composites such as References 9, 10, and 11. Rock failure and lateral inertia effects were studied in Reference 12. Concrete strain rate properties and failure mechanisms were examined in References 8 and 13. In addition, soil strain rate properties and constitutive relations were studied in Reference 14 and effects of intermediate strain rate and moisture content on transmissibility of soil were examined in a SHPB in Reference 15. A method for gripping brittle specimens which cannot be threaded for tensile SHPB is presented in Reference 16.

SECTION III

ENGINEERING AND SERVICES LABORATORY SHPB

A. INTRODUCTION

The Engineering and Services Laboratory split-Hopkinson pressure bar (ESL-SHPB) was developed under contract to Southwest Research Institute (Reference 15). The ESL-SHPB was originally configured as a compressive SHPB and the general arrangement is shown in Figure 10. A recent modification was made to make it a dual purpose compression/tension SHPB. An overall description of the bar will be given later.

The ESL-SHPB was originally used to test soil in a compressive mode using only a single pressure wave passed across the soil specimen contained in a steel sleeve as shown in Figure 11. For these tests both strain gauge and pressure recordings were made using the electronic arrangement of Figure 12. The results of these tests are reported in Reference 15. These tests differ from the ordinary SHPB operation, in that the loading pulse was short, compared to the transit time across the specimen. Ordinarily, for the strain-averaging method discussed previously, at least ten reflections and transmissions are required in the specimen to ensure proper averaging. For the soil specimens of Reference 15 only a single wave was desired in order to observe changes in wave shape and magnitude.

The ESL-SHPB was moved from Southwest Research Institute to the Engineering and Services Laboratory (ESL) at Tyndall AFB FL and will be used for tension and compression testing for ductile and brittle materials at strain rates between 5 and 10^3/sec.

B. ESL-SHPB ARRANGEMENT

1. Striker Bar Launcher (Gas Gun)

The striker bar launcher is essentially a compressed gas gun with a quick release device shown schematically in Figure 13. The general operation is to pressurize the inner cylinder which closes off the opening to the barrel. The gun pressure chamber is then pressurized to the desired operating pressure. The inner cylinder pressure required to keep the inner cylinder piston in place is approximately one-third that of the chamber pressure. To launch the striker bar the inner cylinder pressure is simply dumped to the atmosphere and the inner cylinder piston moves opening the port to the barrel. The gas gun configuration and operation is the same for both the compression and indirect tension modes of the ESL-SHPB. The direct tension mode of operation uses a different arrangement and is discussed later.

2. Compressive ESL-SHPB

The dimensions of the compressive ESL-SHPB are shown in Figure 14 with a Lagrange diagram showing the position of the waves relative to time. The striker bar is placed in motion using the above gas gun launch procedures. The general principles and operation are described below.

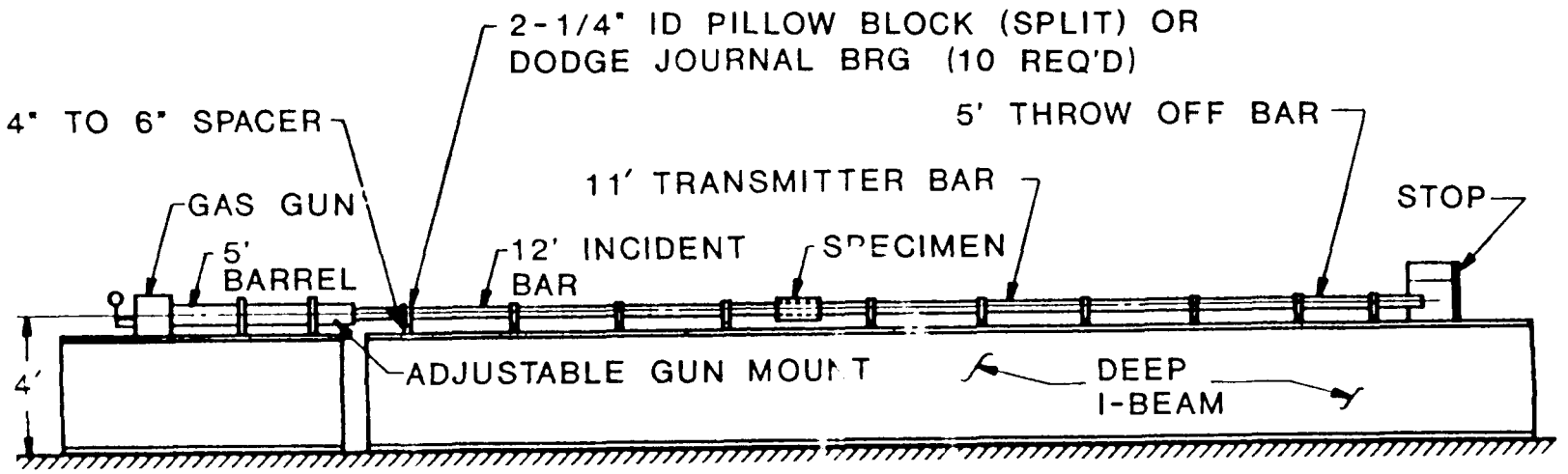

Figure 10. Schematic of 2-inch (5.1 cm) Diameter ESL-SHPB.

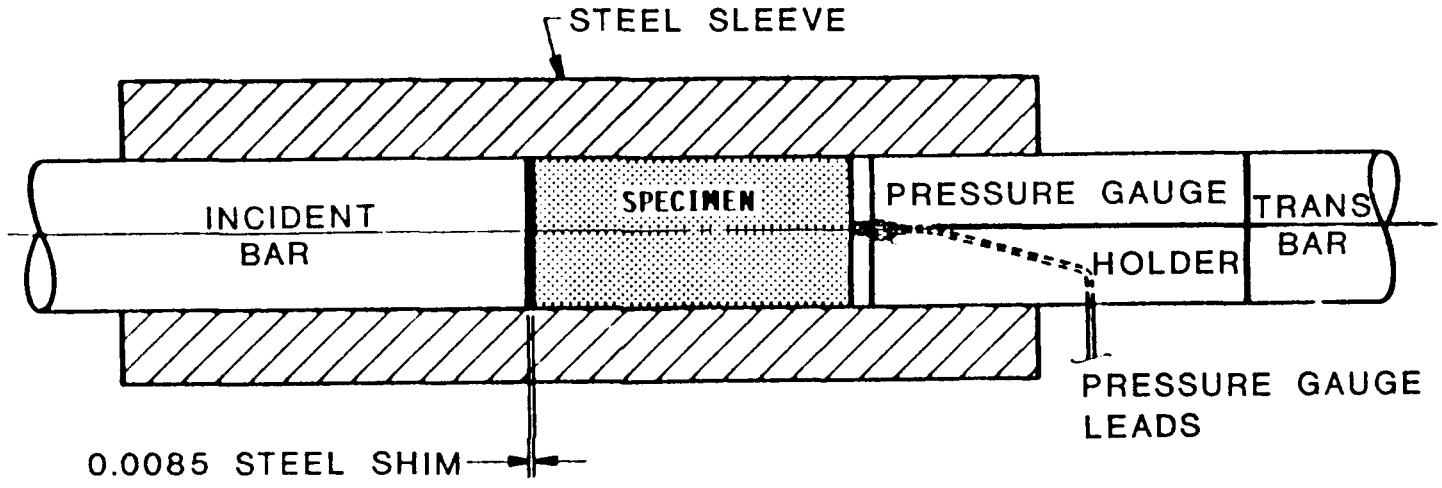

Figure 11. Sketch of Specimen Holder Used in the Original ESL-SHPB (Reference 15).

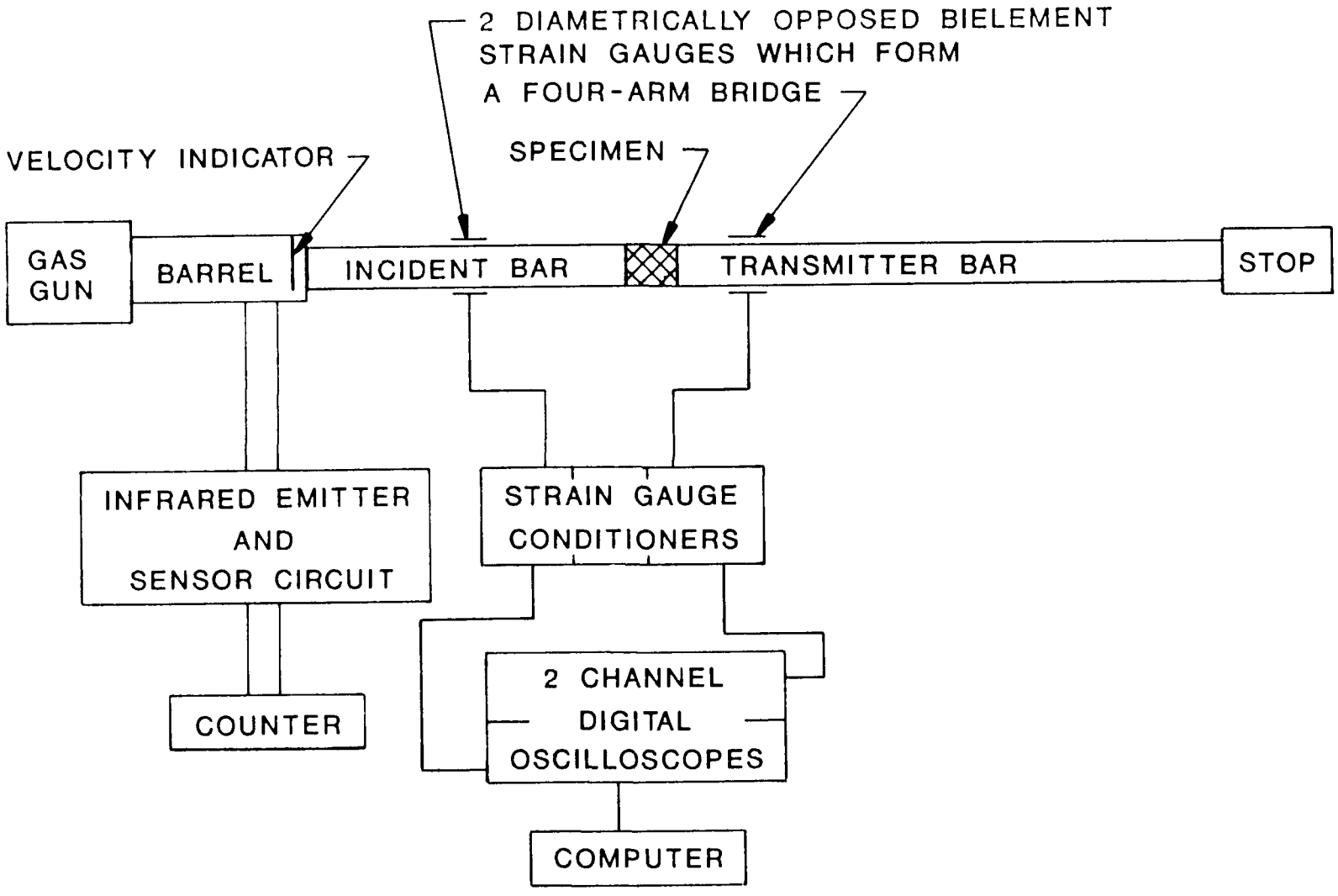

Figure 12. Schematic of Electronic Data Recording System of the ESL-SHPB.

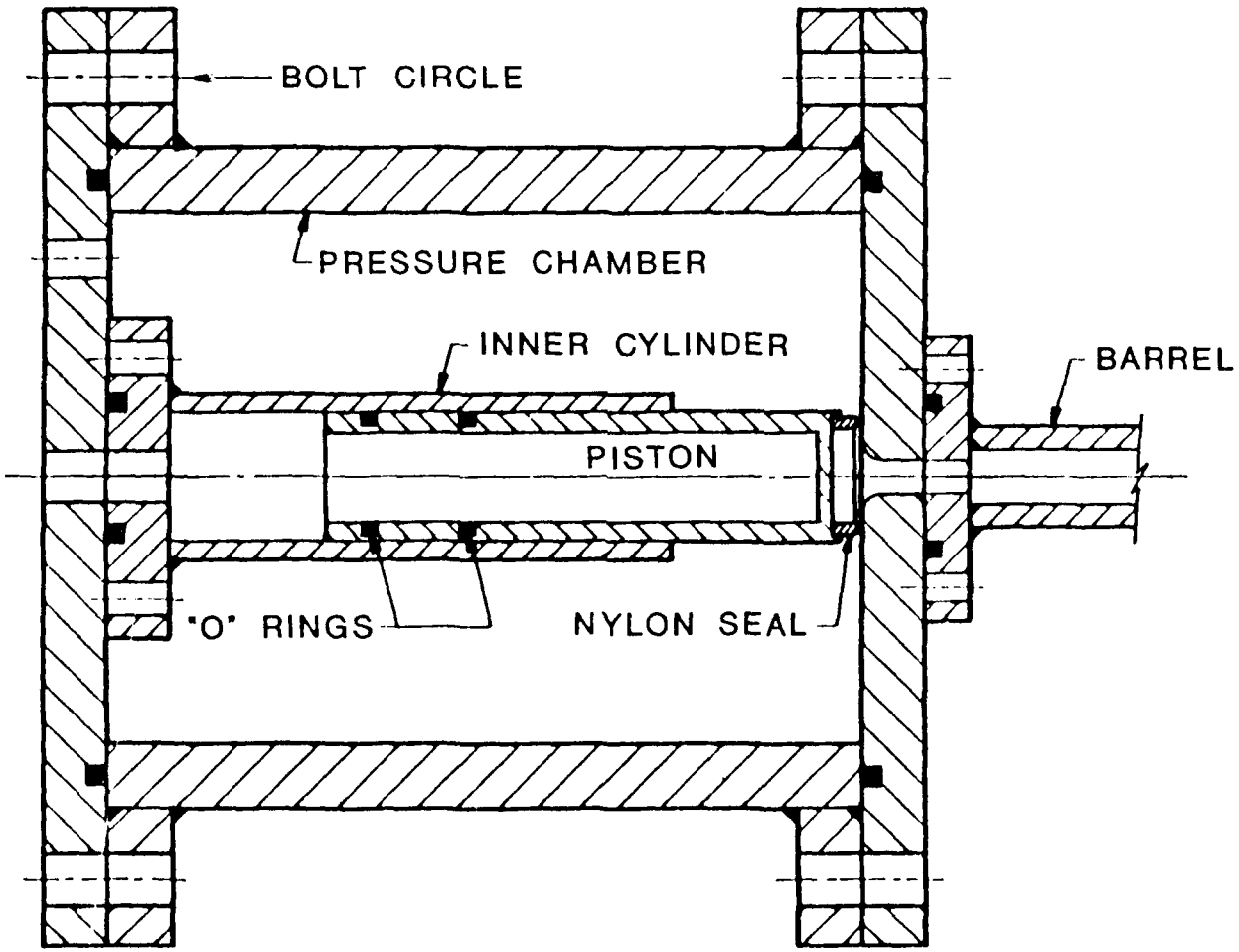

Figure 13. Schematic of the Gas Gun for the ESL-SHPB Striker Bar Launcher.

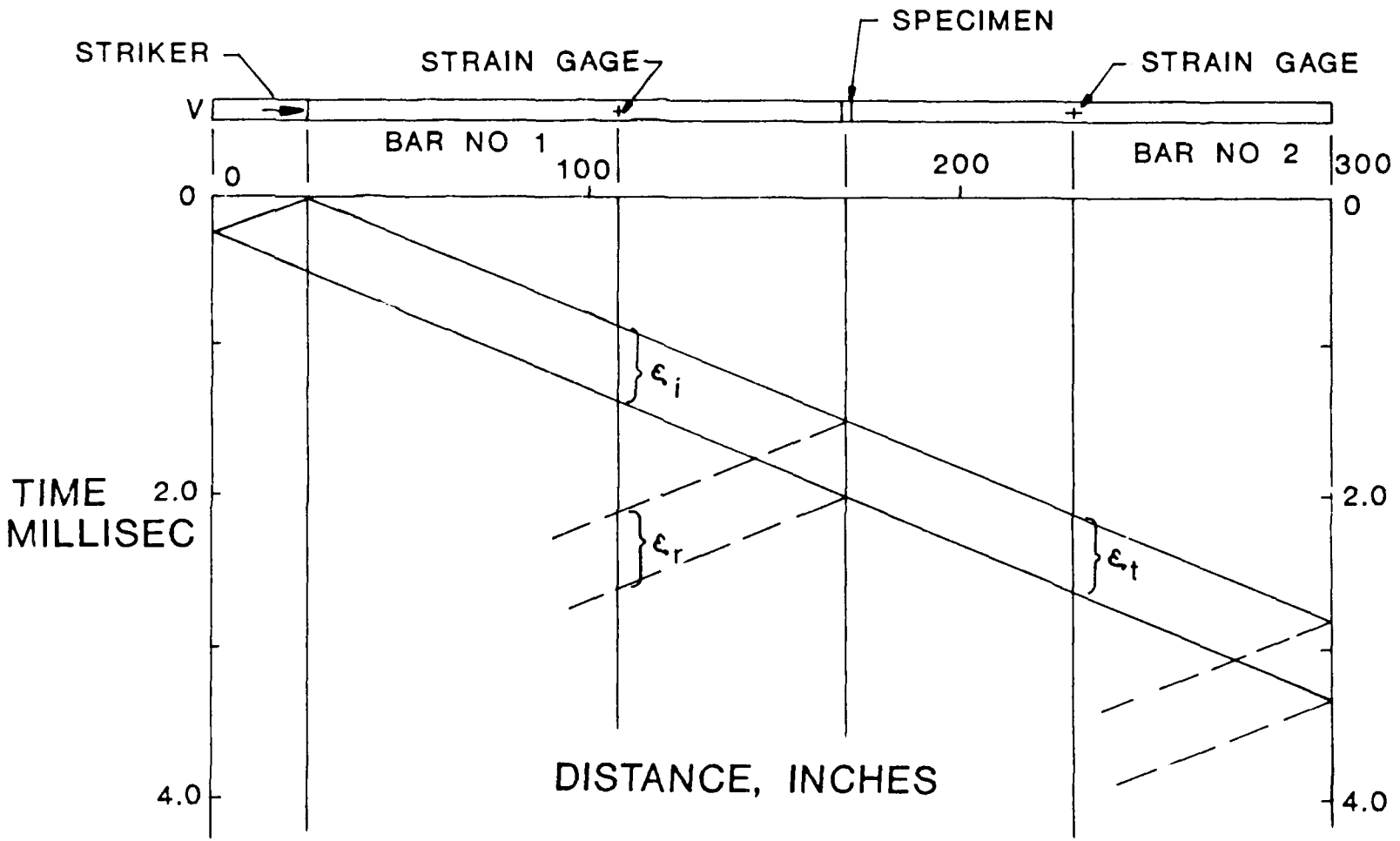

Figure 14. Dimensions and Lagrange Diagram of the FSL-SHPB.

a. A striker bar is put in motion by a launcher and it impacts the incident bar with a velocity V.

b. The impact produces an almost rectangular compressive stress pulse of magnitude $\rho CV/2$ in the striker bar and Bar 1. The pulse length in time is $t_S = 2L_S/C$; ρ is the bar density, C is the bar elastic stress wave speed and L_S is the striker bar length.

c. The compressive stress pulse propagates away from the impacted ends of each bar at a speed of C. When the stress wave reaches the free end of the striker bar it is completely reflected as a tensile wave and it travels back toward the impacted end. This tensile wave unloads the ends of the striker bar and Bar 1, and the bars separate.

d. The compressive pulse travels down Bar 1 and impinges on the specimen sandwiched between Bars 1 and 2. Depending on the physical properties of the sample, portions of the stress pulse are reflected back into Bar 1 and portions are transmitted into Bar 2. The transmitted strain pulse and the integral of the reflected strain pulse are proportional, respectively, to the stress and strain in the specimen.

e. Strain gauges, located equidistant from the specimen to provide time coincident pulses, are used to measure the magnitude and duration of the incident, reflected, and transmitted pulses. These pulses may then be used to generate dynamic stress-strain curves.

Further details on principles of operation and description of the compression SHPB may be found in several publications such as References 1 and 5.

As shown in Figure 14 strain gauges are mounted on both Bars 1 and 2. For the compressive SHPB, Bar 1 strain gauge senses the incident and reflected pulses and the Bar 2 strain gauge senses the transmitted pulse. A typical set of pulses are shown in Figure 15 for a compressive test in the ESL-SHPB. The wave speed in steel is approximately 200,000 in/sec, thus the pulse will travel one inch in 5.0 microseconds. A 257-mircosecond pulse generated from a 25.67-inch long striker bar is used in the display of Figure 15. For the display in Figure 15, it is assumed that the oscilloscope was triggered just before the beginning of the output of strain Gauge 1. Ordinarily, an electronic integrator is placed in the circuit between Strain Gauge 1 and the oscilloscope. This then gives the two signals i.e., an integrated reflected pulse and the transmitted pulse which are used to display a dynamic stress-strain curve. However, for the ESL-SHPB a "math package" is available with the digital oscilloscope and several mathematical operations may be performed on the strain signals. Also, for the ESL-SHPB operation a phase and dispersion correction of Reference 17 will be applied to each signal prior to a stress-strain display, therefore, it is necessary to record the unintegrated reflected signal.

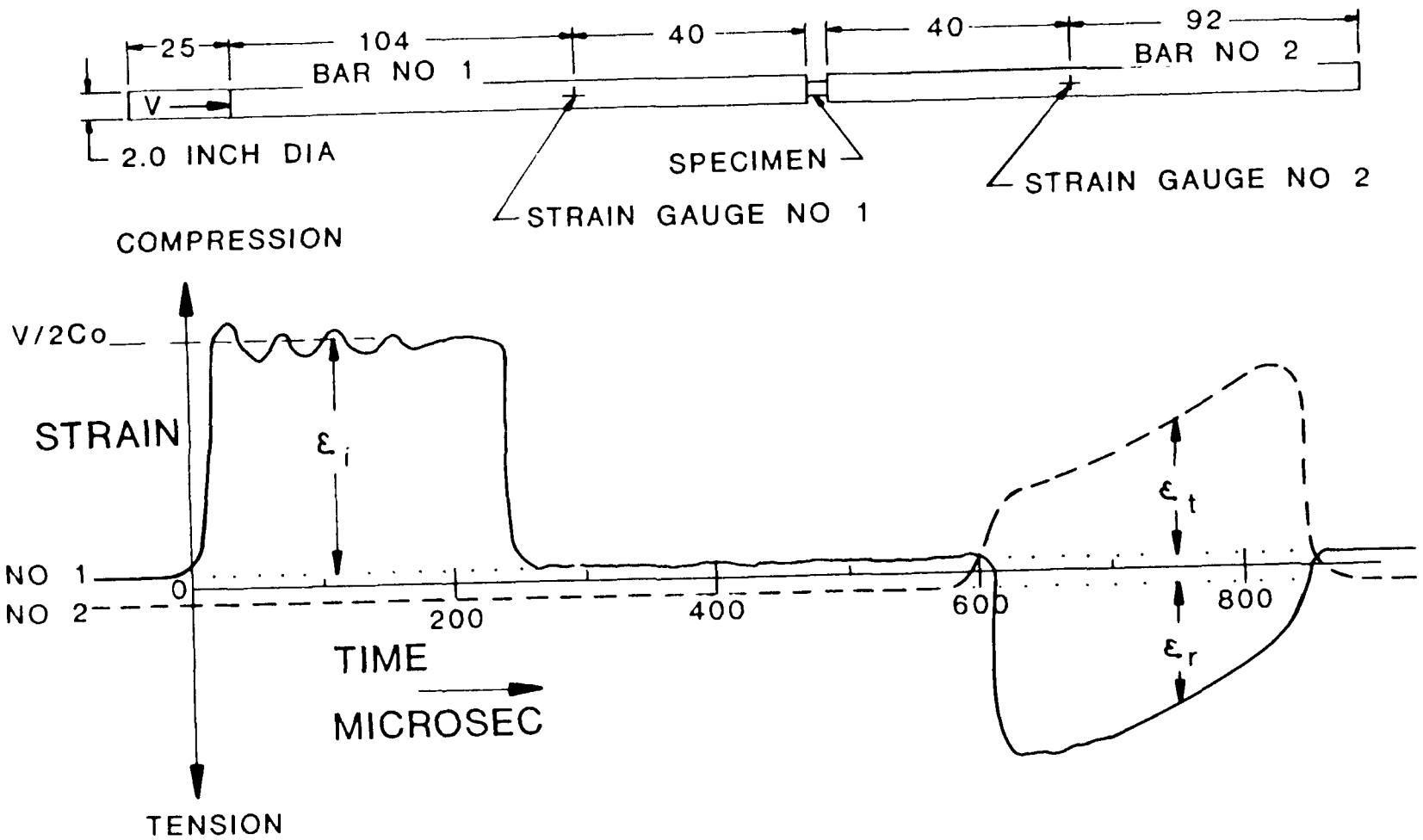

Figure 15. Typical Set of Strain Gauge Signals for the Compressive ESI-SHPB (All Bar Dimensions in Inches).

3. Tensile ESL-SHPB

Initially, it was planned to use an indirect tensile loading method to test tensile specimens at ESL. The indirect method (shown schematically in Figure 16 and 17) was assembled and some mortar testing was attempted using a concrete specimen arrangement shown in Figure 18. The difficulty was that the transmitted pulse through the concrete specimen was of such low magnitude that it was masked by the noise in the instrumentation. The noise in the Strain Gauge 1 circuit is caused by the reflections from the specimen as the incident compression pulse crosses the specimen and collar arrangement. Consequentially, a direct tension system was devised, as shown schematically in Figure 19 and 20. This arrangement eliminated the problem and a very clear transmitted signal was recorded (see results of tensile tests in Section III).

For the indirect tensile ESL-SHPB, shown in Figure 16, the striker bar is launched in the same manner as for the compressive mode as discussed above. The general principles of operation of an indirect tensile SHPB are described below.

a. A striker bar is put in motion by a launcher as it impacts the incident bar with a velocity V.

b. The impact produces an almost rectangular compressive stress pulse of magnitude $\rho CV/2$ in the striker bar and Bar 1. The pulse length in time is $t_S = 2L_S/C$; ρ is the bar density, C is the bar elastic stress wave speed and L_S is the striker bar length.

c. The compressive stress pulse propagates away from the impacted end of each bar at a speed of C. When the stress wave reaches the free end of the striker bar it is completely reflected as a tensile wave and it travels back toward the impacted end. This tensile wave unloads the ends of the striker bar and Bar 1, and the bars separate.

d. The compressive pulse travels down Bar 1 and is passed over the specimen using a split collar as shown in Figure 18. A small portion of the compressive pulse may be reflected at the specimen but is "lost" in the long length of Bar 1 relative to Bar 2. The compressive pulse is transmitted into Bar 2 and is reflected from the free end of Bar 2 as a tensile pulse.

e. The tensile pulse passes over the Bar 2 strain gauge and is recorded as the incident pulse and then impinges on the tensile specimen. Part of this pulse is reflected back into Bar 2 and a portion is transmitted in to Bar 1. These pulses, incident and reflected in Bar 2 and transmitted in Bar 1 are negative of those of the compressive mode. These pulses are then used to form the tensile dynamic stress-strain curve similar to that discussed in 2e above.

The dimensions of the indirect tensile ESL-SHPB are shown in Figure 16 along with the Lagrange diagram. In addition, a typical strain pulse display for the tensile SHPB of Figure 16 is shown for a 25-inch striker bar (250 microseconds) in Figure 17. These pulses are estimates and are not true recordings.

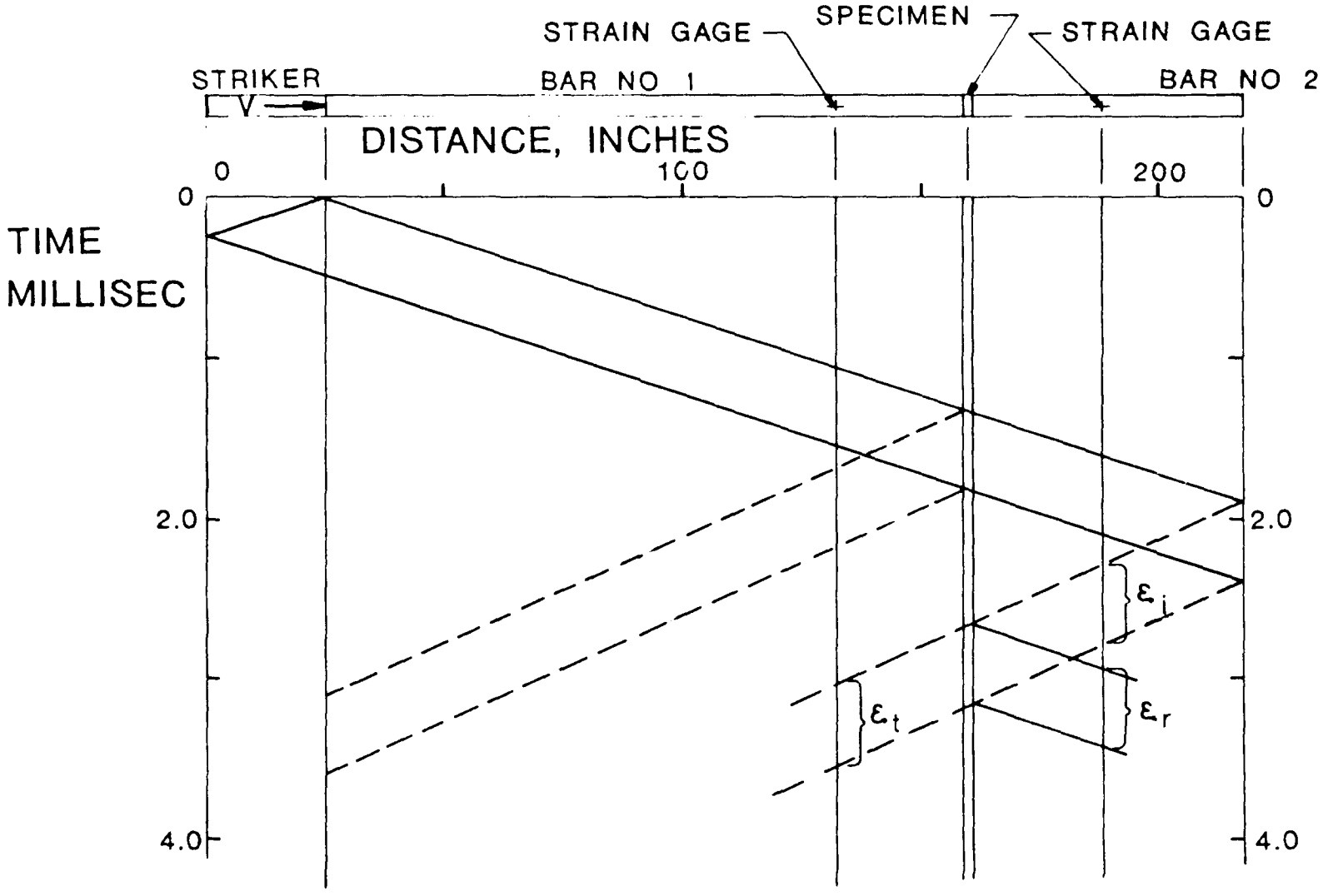

Figure 16. Schematic and Lagrange Diagram for an Indirect Tension SHPB.

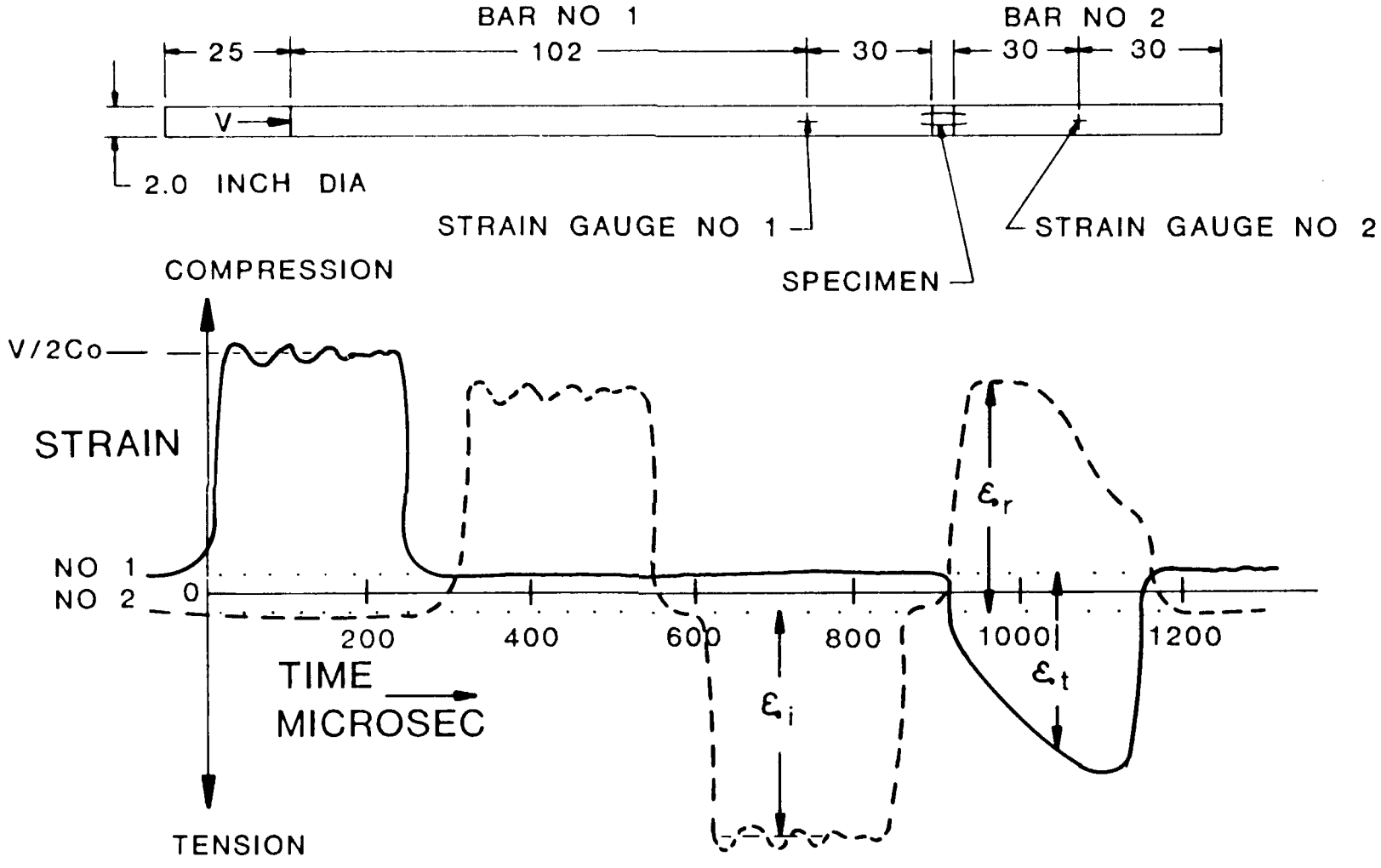

Figure 17. Schematic and Typical Strain Signals for the Indirect Tension ESL-SHPB (All Dimensions in Inches).

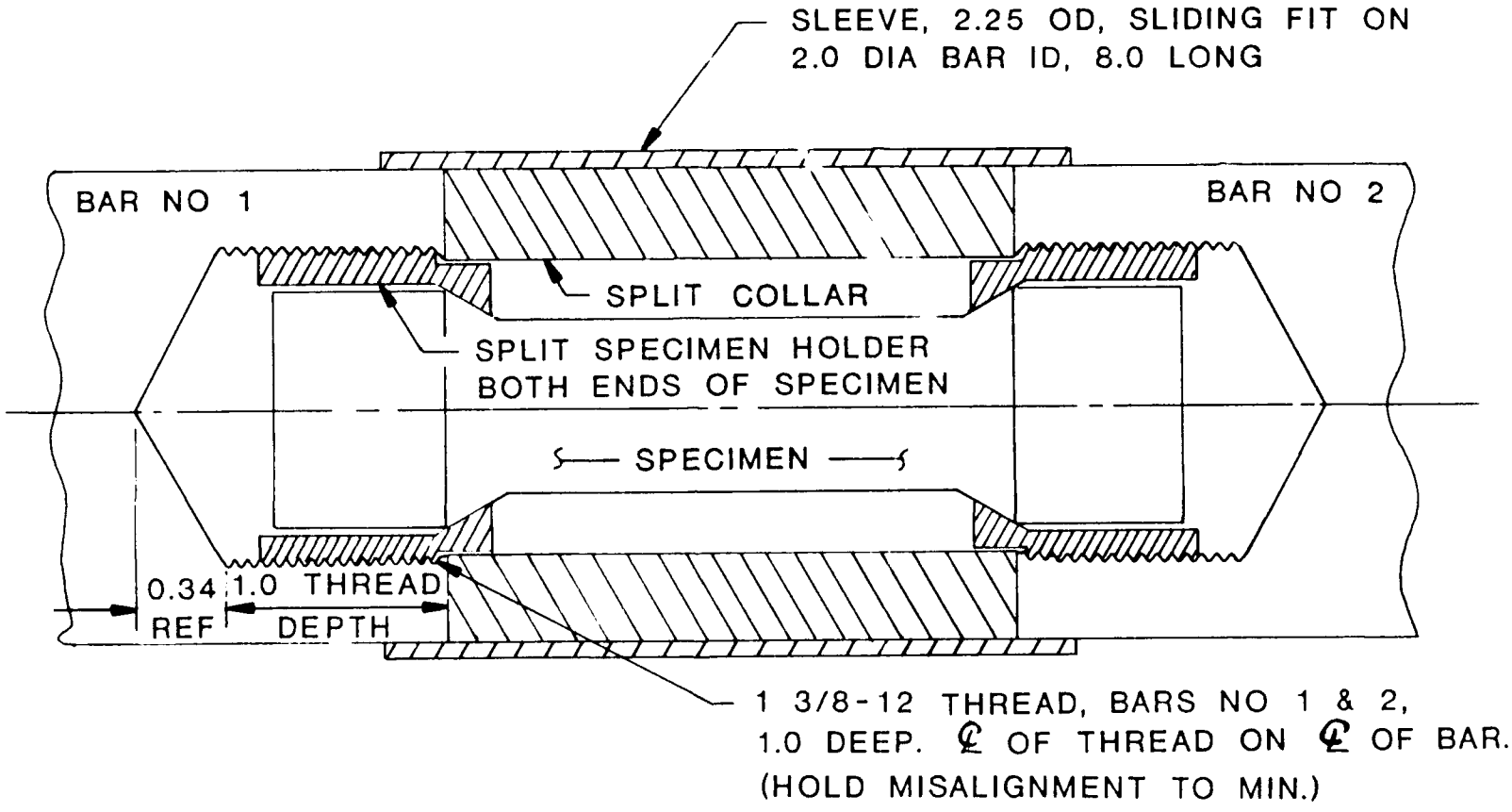

Figure 18. Proposed Dumbbell Tension Specimen for Concrete in the Indirect Tension ESL-SHPB (Dimensions in Inches).

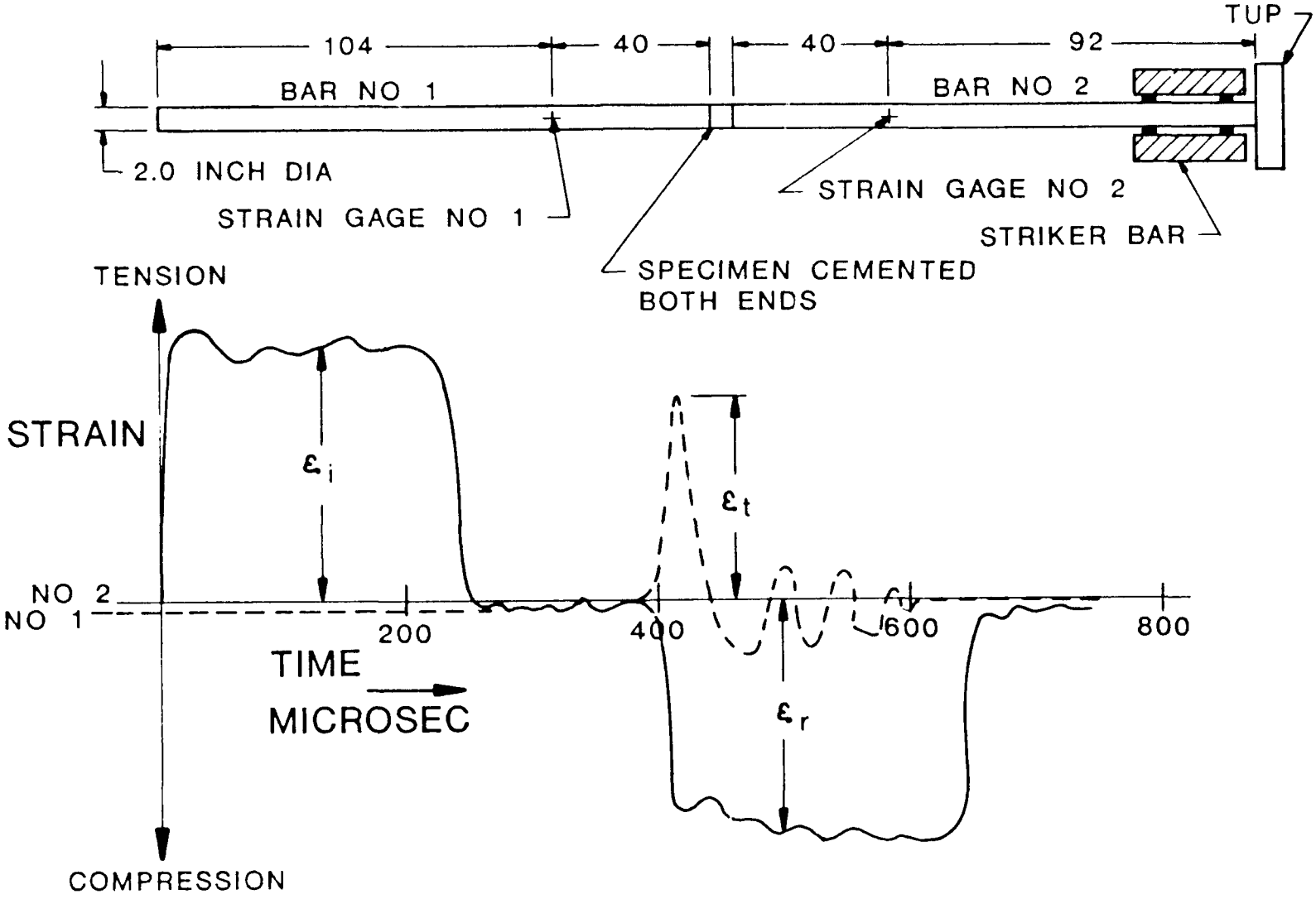

Figure 19. Schematic of Direct Tension ESL-SHPB and Typical Strain Signals.

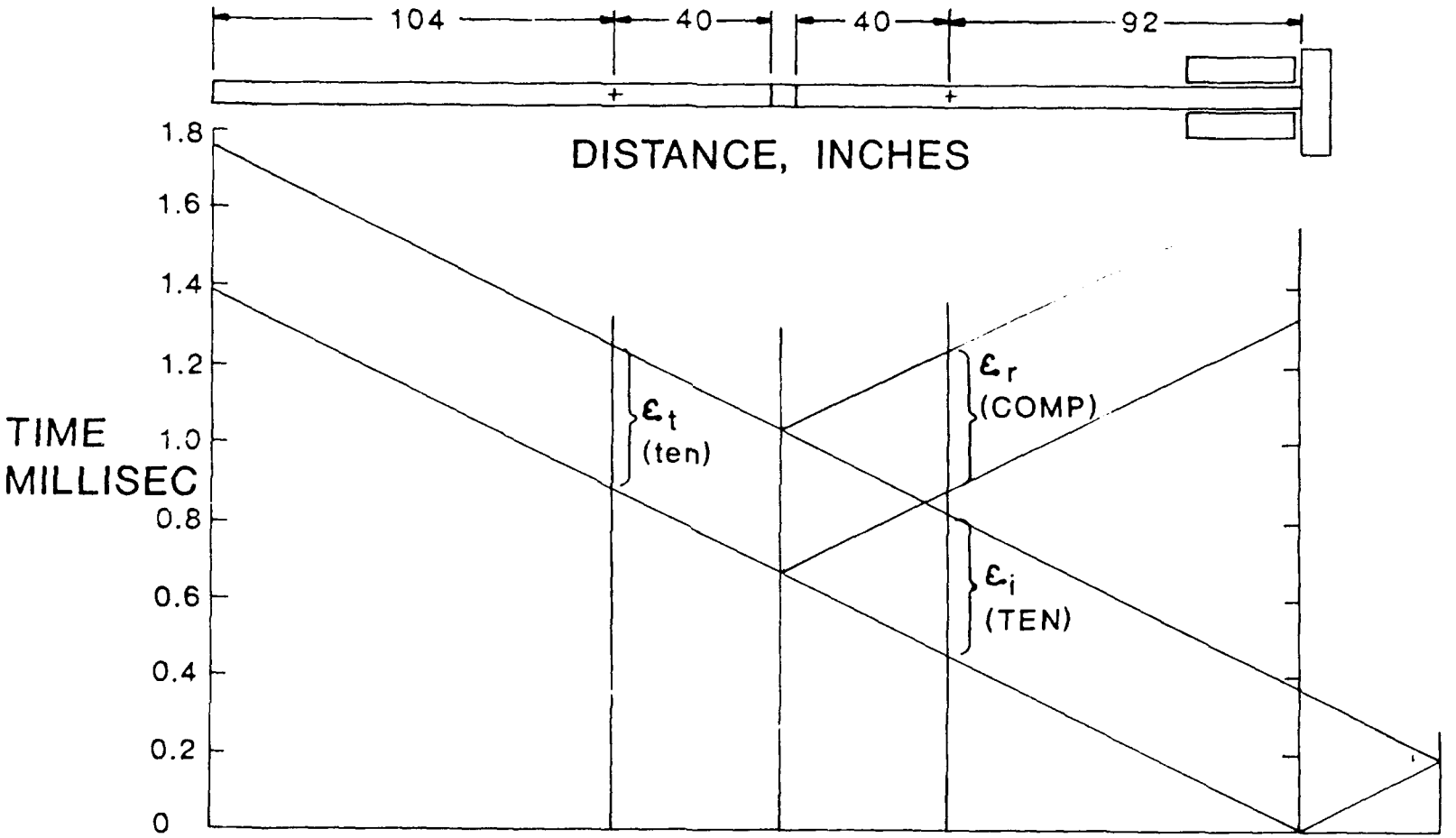

Figure 20. Schematic and Lagrange Diagram for Direct Tension ESL-SHPB.

The specimen gripping for specimens which may be threaded is shown at the bottom of Figure 8. However, for specimens which may not be threaded, a dumbbell arrangement was developed in Reference 16 and a schematic of a similar arrangement to be used for mortar is shown in Figure 18. The method used in Reference 16 showed that some slipping was occurring at the interface between the dumbbell specimen and the specimen holder, which caused some serations in the initial portions of the stress-strain curve and an over prediction of the specimen strain. A modification to a conical interface was made for the specimen and specimen holder shown in Figure 18. If problems still arise it is suggested that an adhesive be used to hold the specimen in place.

The final version of the direct tensile SHPB of ESL is shown schematically in Figures 19 and 20. The principles of operation of the SHPB are described below.

f. The cylindrical striker bar, which slides on Bar 2, is put in motion in a pressure tube and impacts the tup which is screwed into the end of Bar 2.

g. The impact produces an almost rectangular tensile stress pulse in Bar 2. The pulse length in time is $t_S = 2L_S C$. The magnitude of the pulse is not as easily determined analytically as the compressive pulse. The pulse magnitude is calibrated by the strain gauge output and the pressure tube pressure.

h. The tensile pulse propagates away from the impacted end at a speed of C. The tensile incident pulse propagates in Bar 2, and is recorded at Strain Gauge 2, and impinges on a specimen cemented between the two bars. A portion of the pulse is transmitted into Bar 1 and a portion if reflected back into Bar 2. These pulses, incident and reflected in Bar 2 and transmitted in Bar 1 are all recorded. These pulses are then used to form the tensile dynamic stress-strain curve similar to that discussed in 2e and 3e above.

4. Dynamic Stress-Strain Curves

As discussed earlier a dynamic stress-strain curve may be generated by a coincident time display of the integrated incident and reflected pulses versus the transmitted pulse. One method of doing this is by placing the strain gauges equidistant from the specimen and placing an electronic integrator in the reflected strain circuit, and driving the abscissa and ordinate of a x-y plotter, respectively, with the integrated reflected strain and transmitted strain. For the ESL-SHPB all strain signals will be recorded and then corrected for wave dispersion and phase differences using the computer code of Reference 17, prior to a display of the dynamic stress-strain curve.

In addition, stress, strain, or strain rate versus time curves may be generated using the recorded data and Reference 17. For all these curves the calibration constants to be derived later must be applied to the strain signals for final values.

C. ESL SHPB ELECTRONICS AND CALIBRATION

1. Strain Gauge Circuit

Each strain gauge circuit on Bar 1 and 2 are identical and only one arrangement will be shown. Each strain gauge location is located an equal distance of 40-inches (1.016m), on either side of the specimen location, as shown in Figures 15 and 19.

At each strain-gauge location two bielement gauges (Micromeasurements® EA-06-250TB-350) are cemented diametrically opposed on the bar. The arrangement is shown in Figure 21, along with the full bridge schematic. This circuit forms a full four-gauge bridge which is inherently temperature-compensated and gives increased sensitivity from Poisson effect in the transverse gauges.

The gauges are connected to the strain gauge conditioner (Micromeasurements® 2300-2311 system) through the standard plug (Bendix® PT06-14-15 P(SR)) and are connected in the manner described for a "full bridge" in the strain gauge conditioner handbook.

Connections from the strain gauge conditioner to the oscilloscope are direct and straightforward. The oscilloscope is a Nicolet 4094B® four-channel digital instrument with dual-disk recording capability. Normal operation has been that of using a disk for four-channel recording in conjunction with the math pack for titles, delays, etc.

2. Strain Gauge Calibration.

Standard calibration using the calibration switch on the strain gauge conditioner is based on a stressed condition where all gauges see similar or opposing strains. However, for the strain gauge arrangement as shown in Figure 21 the two longitudinal gauges see nearly the same longitudinal strain during a test but the transverse gauges see a strain equal to the negative of the longitudinal strain times Poisson's ratio. Using this fact a calibration constant for the arrangement shown in Figure 21 must be calculated. For the bridge circuit of Figure 21 the output voltages ΔE may be expressed as (Reference 18),

$$\Delta E = \frac{E_e r}{(1+r)^2}\left[\frac{\Delta R_a}{R_a} - \frac{\Delta R_b}{R_b} + \frac{\Delta R_c}{R_c} - \frac{\Delta R_d}{R_d}\right] \tag{38}$$

where ΔR is the change in resistance of the resistor due to strain, R is the original resistance of each resistor, r is the ratio R_d/R_a=1.q, and $E_e$is the circuit excitation voltage.

For the longitudinal gauges, with a known gauge factor GF supplied by the gauge manufacturer, the longitudinal strain ε_L is related to the $\Delta R/R$ of the longitudinal gauge by the relation (Reference 18),

$$(GF)\varepsilon_L = \frac{\Delta R}{R} \tag{39}$$

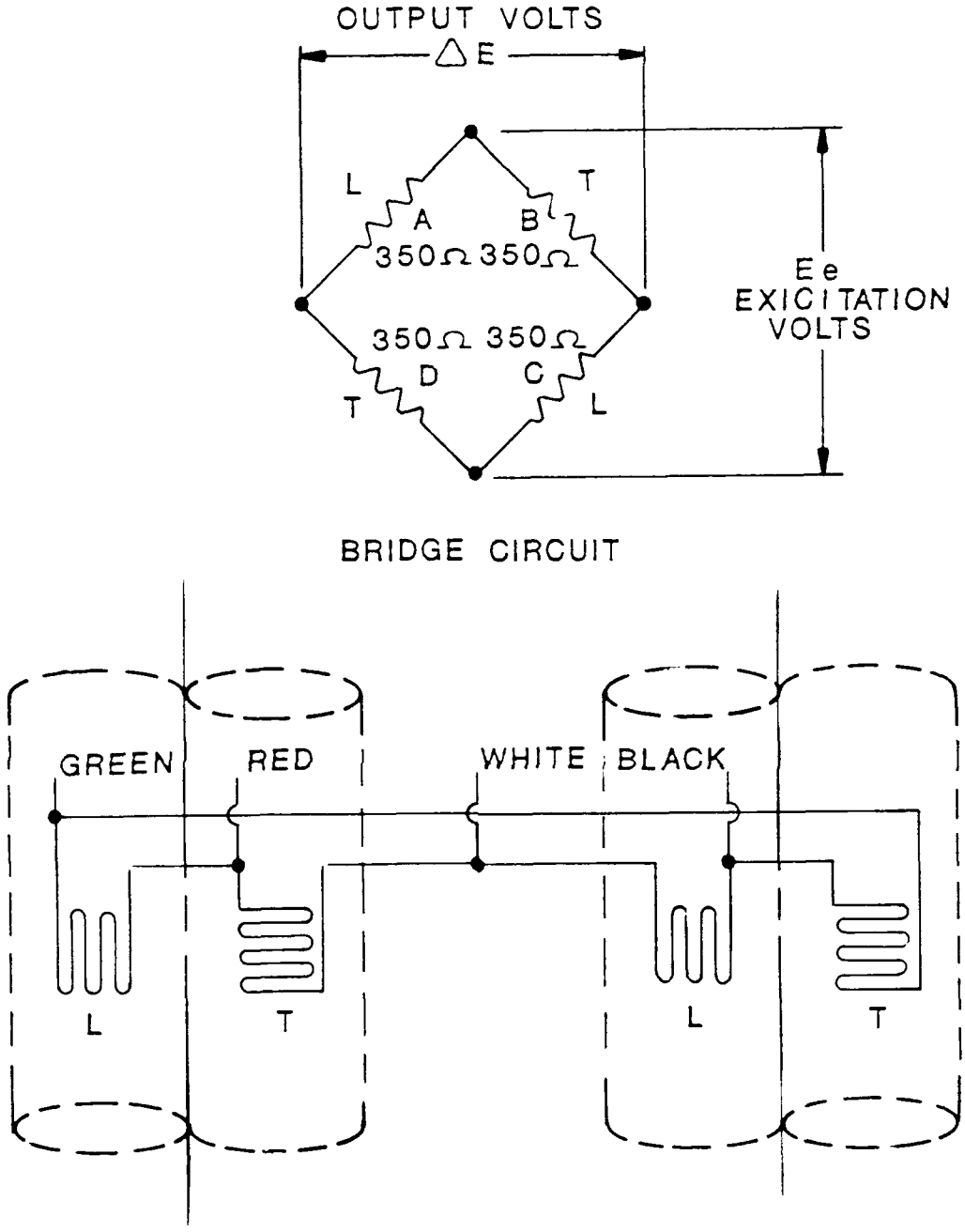

Figure 21. Strain Gauge Arrangement and Wheatstone Bridge Circuit for the ESL-SHPB.

Under the assumption that the strain is uniform over the bar cross-sectional area then

$$\frac{\Delta R_a}{R_a} = \frac{\Delta R_c}{R_c} = (GF)\varepsilon_L \tag{40}$$

Using the same reasoning for the transverse gauges then

$$\frac{\Delta R_b}{R_b} = \frac{\Delta R_d}{R_d} = (GF)\varepsilon_T \tag{41}$$

However, due to the Poisson effect, the transverse strain ε_T is

$$\varepsilon_T = \mu\varepsilon_L \tag{42}$$

where μ is Poisson's ratio and Equation (38) becomes

$$\Delta E = \frac{2E_e r}{(1+r)^2}(1+\mu)\,\varepsilon_L\,(GF) \tag{43}$$

For r=1, E_e=10.0, μ=0.29 and GF=2.04

$$\varepsilon_L \simeq 0.076\Delta E \tag{44}$$

where ε_L is in units of strain and ΔE is in volts.

For calibration a 25.67-inch (0.65m) striker bar was used for impact at a series of chamber pressures. The velocity of the striker bar is determined by using the velocity indicating device at the end of the gas gun barrel. Two infrared light beams and detectors are mounted at 3-inch hole intervals near the end of the barrel. A counter measures the time for this 3-inch transit and the impact velocity V is calculated by dividing the 3-inch distance by the counter time. Using Equation (9) the impact strain may be calculated as

$$\varepsilon_{ic} = -\frac{\sigma}{E} = -\frac{\rho}{E}\,C_o\,\frac{V}{2} \tag{45}$$

where $\rho/E = 1/C_o^2$ and Equation (45) becomes

$$\varepsilon_{ic} = -\frac{V}{2C_o} \tag{46}$$

Equation (46) represents the magnitude of a rectangular stress wave. However, due to dispersion effects and the true three-dimensional nature of the impact the measured stress or strain pulse is not rectangular but has oscillations superimposed on a rectangle, as shown in Figures 15, 17, and 19. For the calibration, the first minimum and major strains, as shown in Figure 15, were calculated using Equation (44) and the recorded strain pulse. The

average of the two values and the strain calculated using Equation (46) were plotted versus the chamber pressure. This process was repeated for an 8-inch (0.2m) striker bar. Based on these tests the calibration equation (Equation (44)) was changed to reflect the average of the curves and was established to be

$$\varepsilon_L = 0.07\Delta E \tag{47}$$

Where ε_L is in strain units of in/in, cm/cm, etc. and ΔE is in volts. Here, care must be exercised and the gain of the strain gauge conditioner must be included in determining the value of ΔE. This same calibration constant is used for both strain gauge circuits. A plot of the calibration is shown in Figure 22.

For the direct tensile mode of operation the velocity transit time is not measured and the strain values of each pulse are determined using Equation (47). During the compression mode the velocity transit time is recorded just as a check on repeatability.

D. OPERATING PROCEDURE

In operation for the compression or direct tension tests the same primary gas bottles, pressure regulators, pressure gauges, and valves are used for both operations. These pieces of equipment must be moved from one end of the SHPB assembly to the other during change from one loading mode to the other. This move requires approximately 2 hours for a complete change.

An operating procedure and checklist for each mode of operation is given in Appendix A.

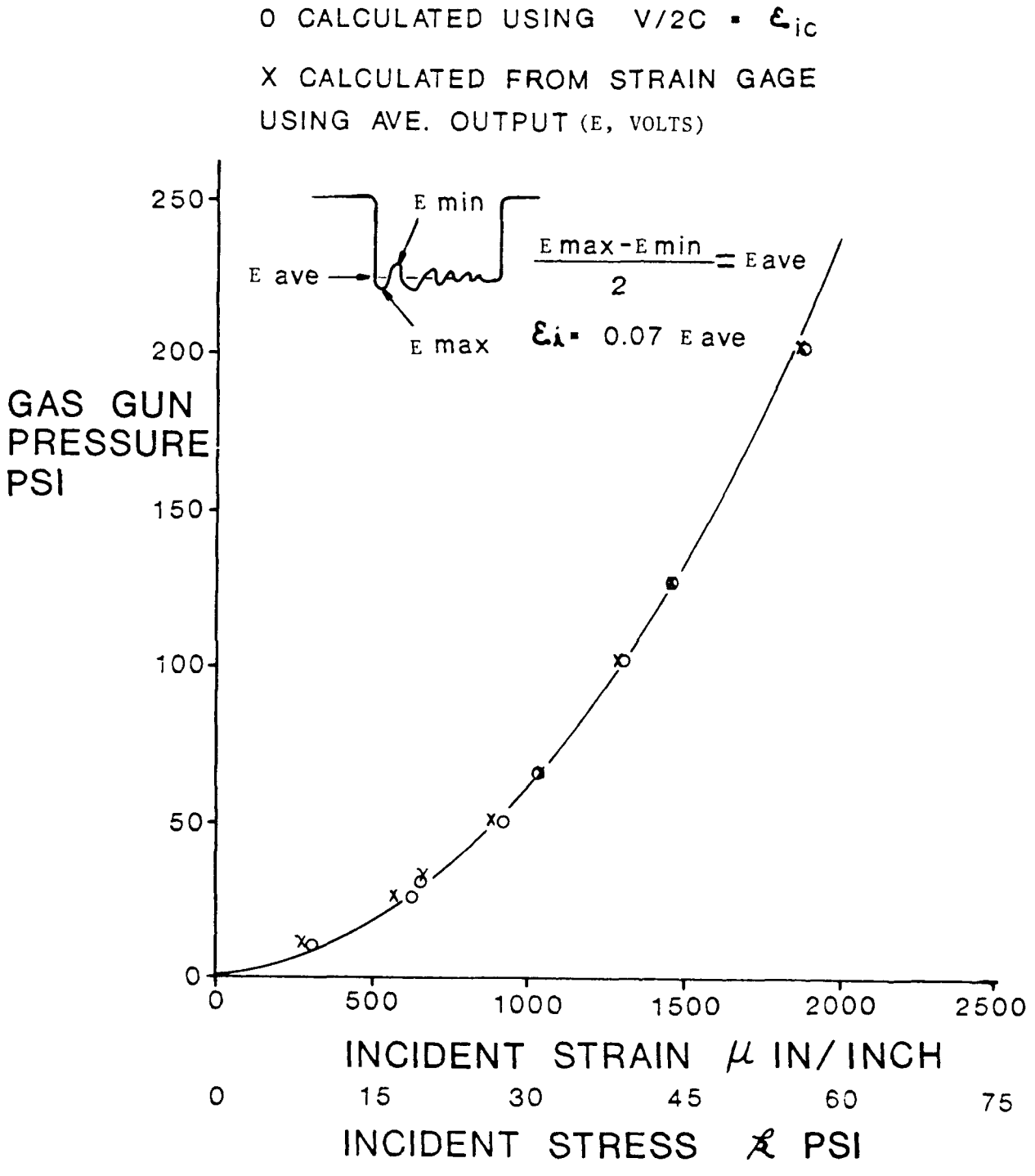

Figure 22. Calibration Curve for Incident Strains.

SECTION IV

RESULTS AND DISCUSSION

A. CONCRETE AND MORTAR TESTS

1. Introduction

As discussed in Section III B.3 the initial attempt at a tensile mode of operation was to be the indirect tension device shown in Figures 17 and 18. For this operation special specimen molds were fabricated and a "dog-bone" type mortar specimens, as shown in Figure 18, were cast. Also as indicated this type mode of operation was not successful and the direct tension device shown schematically in Figure 19 was used for tensile tests.

For the tests reported on here, a distinction is made between mortar and concrete. The mortar specimens were prepared using cement, sand, and water only and concrete specimens were prepared using cement, sand, water, and aggregate. For concrete and mortar four different types of specimens were tested in the SHPB. These four types of specimens were designated as direct compression, direct tension square notch, direct tension saddle notch, and a split cylinder. These four different specimens, 2-inches (5.1cm) nominal length and 2-inches (5.1cm) nominal diameter are shown in place in the SHPB in Figure 23-26.

2. Specimen Preparation

Mortar specimens were initially prepared by casting a large block of mortar using a mixture of Portland cement, local builders sand, and tap water. Coring the mortar resulted in cores nominally 1.80-inches (4.57cm) and were cut to a nominal 1.90 (4.83cm) long. These plain cylinders were tested in direct compression and split cylinder tests. Direct tension specimens were prepared in two different ways. One set was machined by grinding a 0.13-inch (0.32cm) square notch circumferentially around the specimen at the midlength. Another set was machined by grinding a 1-inch (2.54cm) bottom radius natch of 0.13-inch (0.32cm) depth circumferentially at the midlength of the specimen. See Figures 25 and 26 for similar shapes of concrete specimens.

The tolerances of the mortar specimens were loose and, in many instances, the end faces were not parallel. These discrepancies caused a considerable number of problems in trying to test at quasi-static strain rates in the MTS material test machine.

Concrete test specimens were fabricated by the Corps of Engineers Waterways Experiment Station WES for ESL, according to the specifications given in Figure 27. Examples of these specimens are shown in Figures 23-26. These specimens were very precise and very few problems were encountered in testing. The mix recipe for the concrete used by WES is given in Appendix B.

Figure 23. Direct Tension Saddle-Notch Specimen Mounted in the ESL-SHPB.

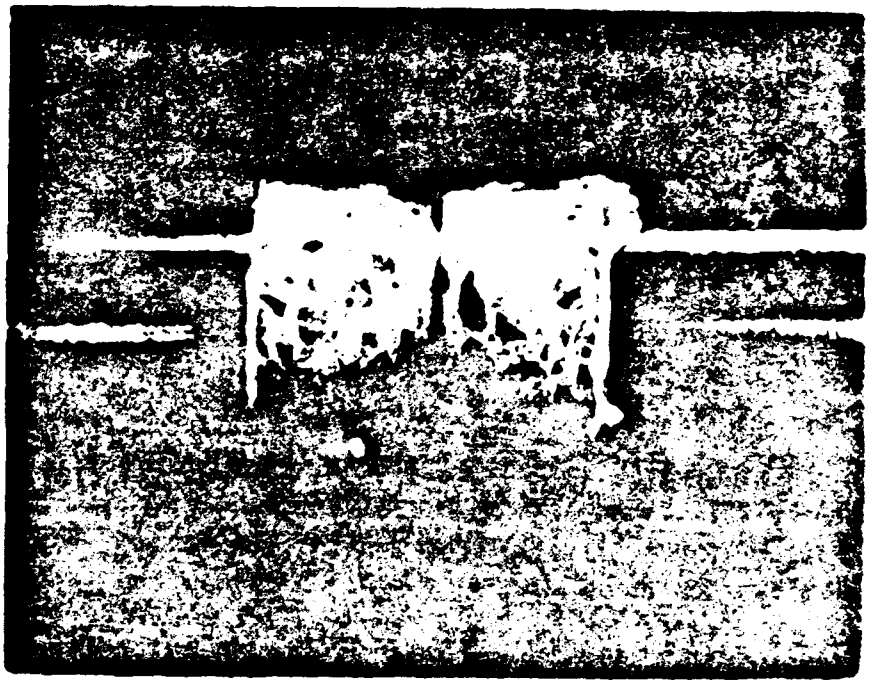

Figure 24. Direct Tension Square-Notch Specimen Mounted in the ESL-SHPB.

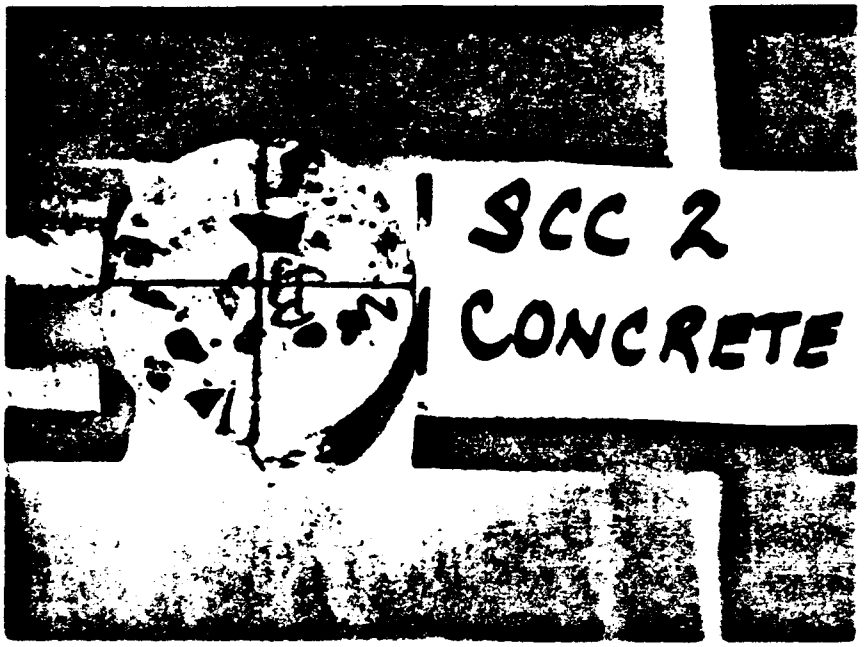

Figure 25. Splitting Cylinder Specimen Mounted in the ESL-SHPB.

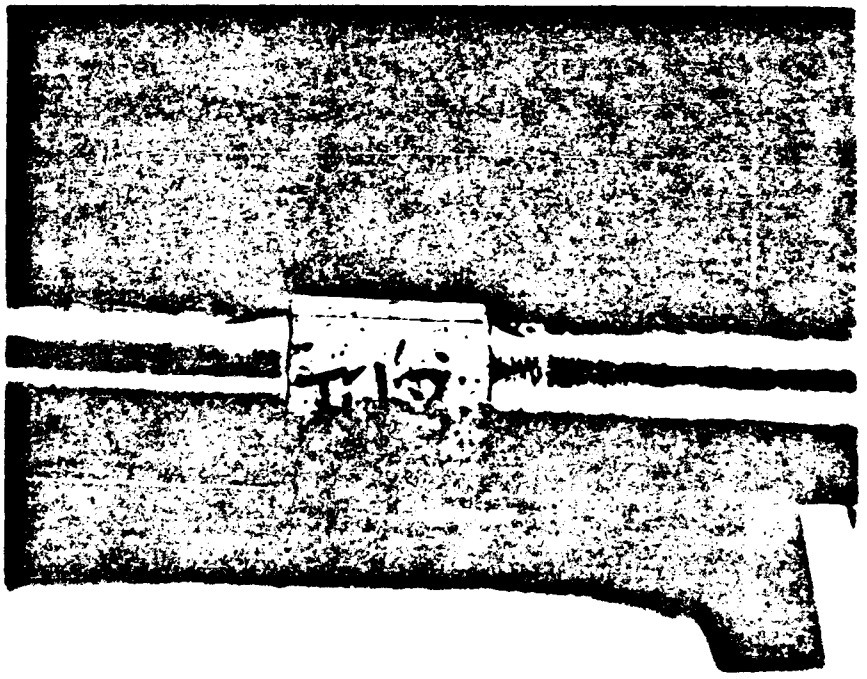

Figure 26. Direct Compression Specimen Mounted in the ESL-SHPB.

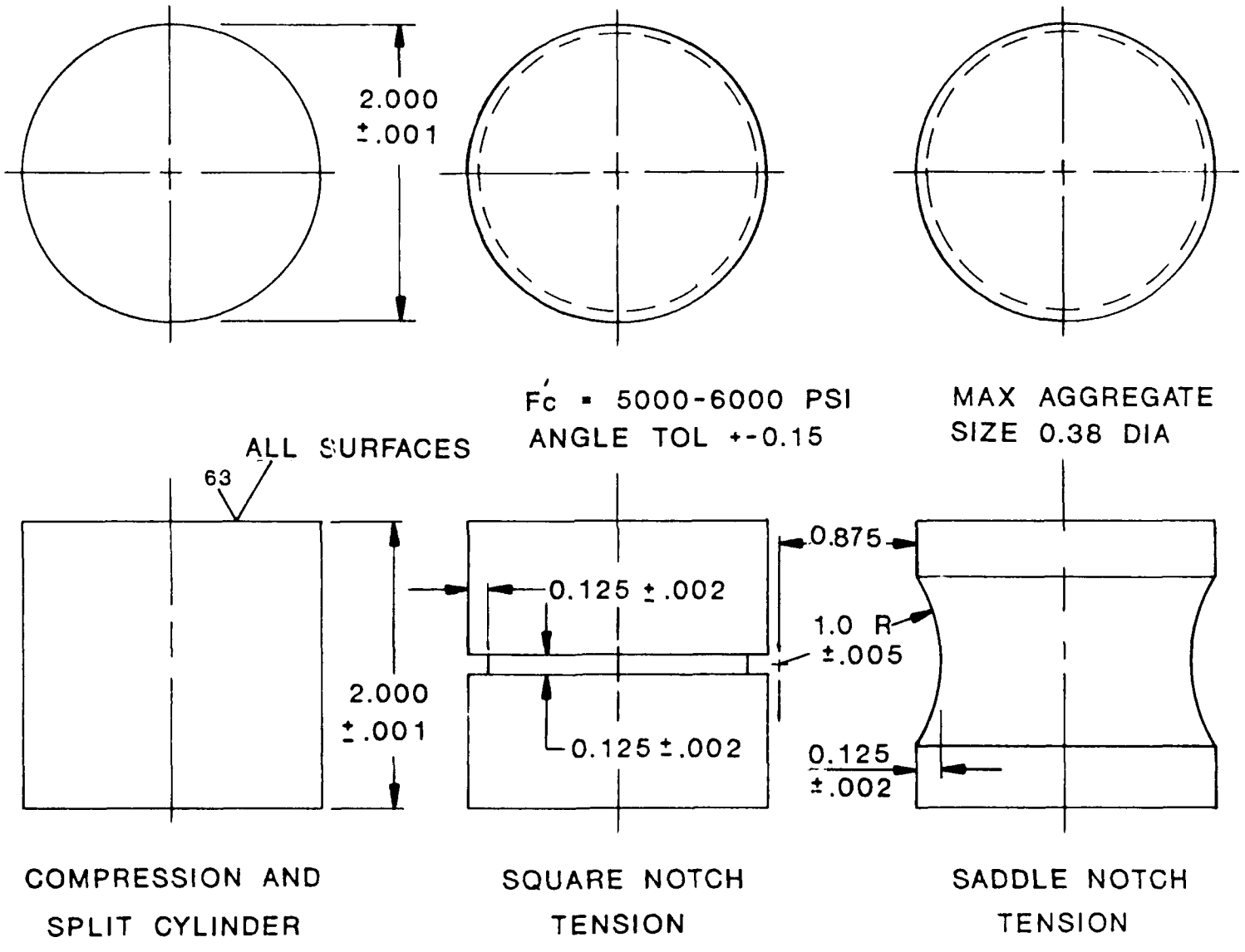

Figure 27. Specifications for Concrete Specimens Fabricated by WES (All Dimensions in Inches).

For direct compression tests the specimens were lightly lubricated (using a molybdenumdisulfide grease) and pressed between the two Bars 1 and 2. They were held in place by friction between the two bars. In the split cylinder test, a plain cylinder was rotated 90° about its longitudinal axis and placed in the bar, as shown in Figure 25. Again the edges in contact with the bars are lightly lubricated and friction holds the specimen in place.

Direct tension specimens were cemented to the bars at each end of the specimen. Before cementing, both the specimen ends and the bar ends were cleaned by the following procedure similar to surface preparation for a strain-gauge placement. Each surface was degreased using a degreaser or trichlorethylene. A Micromeasurements, Inc.©, acidic solution was then applied two times to the surface, followed by Mircromeasurements Inc.© neutralizer solution in two applications. The surfaces were allowed to dry and a thin coating of Tridox© 55 cement paste was applied to each end of the specimen. The two-part cement paste was mixed to about three parts powder to one part liquid. After cement application the specimen was pressed between the bars, aligned, and supported in place for 30 minutes prior to testing.

Low strain rate tests were conducted in the ESL MTS material testing machine. In these low speed tests the direct compression and split cylinder specimens were tested using the large 6-inch diameter platens. A special tension test holder with 2-inch in diameter platens were used for the low-speed tension tests. For these tests the direct tension specimens were cemented to the platens using the same method as described above for SHPB direct tension specimens.

3. Results

For the concrete and mortar tests the major objective was to determine the effects of strain rate on the tensile strength of concrete. As a comparison the compressive strength of concrete was also determined. For determining the tensile strength, two different kinds of specimens were used, i.e., direct tension and splitting cylinder. For the direct tension two different types of tensile specimens were used; a square notched type and a saddle notch type. For the splitting cylinder test a plain cylinder was used and this cylinder specimen was the kind as used in the compression tests. All these specimens are shown mounted in the SHPB in Figures 23-26.

A typical set of strain gauge traces for a square notch specimen is shown in Figure 28 and a set for a saddle notch specimen is shown in Figure 19. These traces are raw data and have not been corrected for dispersion effects. The tensile strength for either the square notch or saddle notch specimens is obtained by taking the peak transmitted stress shown in Figure 28 and 29. These stresses are obtained by applying Equation (47) to get the strain and Equation (35) to determine the stress. The strain rate is normally based on uniform stress along the specimen and is determined by observing the reflected strain at the same time as the transmitted stress. This strain rate is the strain rate observed as the maximum transmitted stress or strain. It is not the maximum strain rate but it is the strain rate associated with the tensile strength.

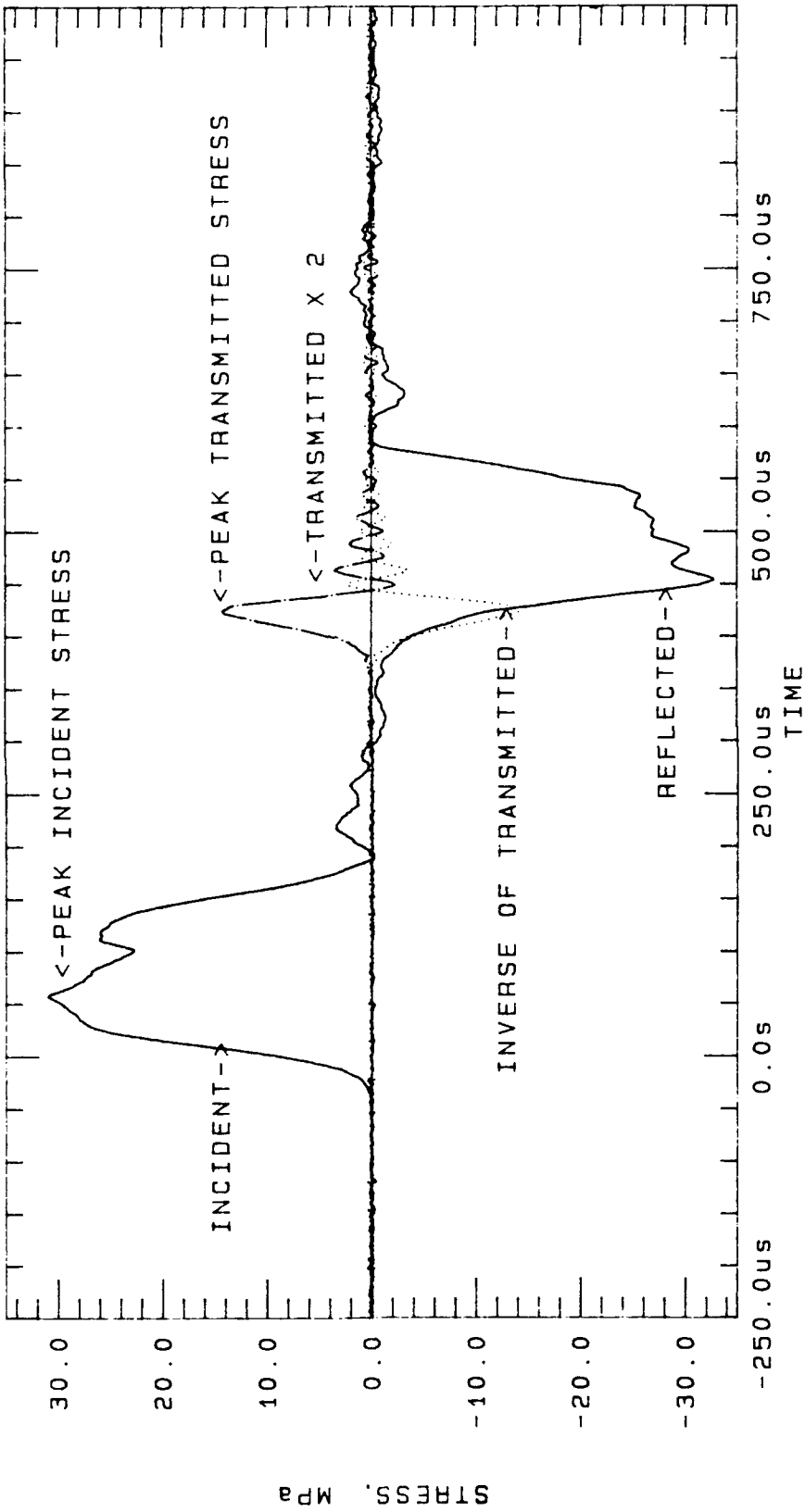

Figure 28. Uncorrected Data Traces for Square-Notched Specimens.

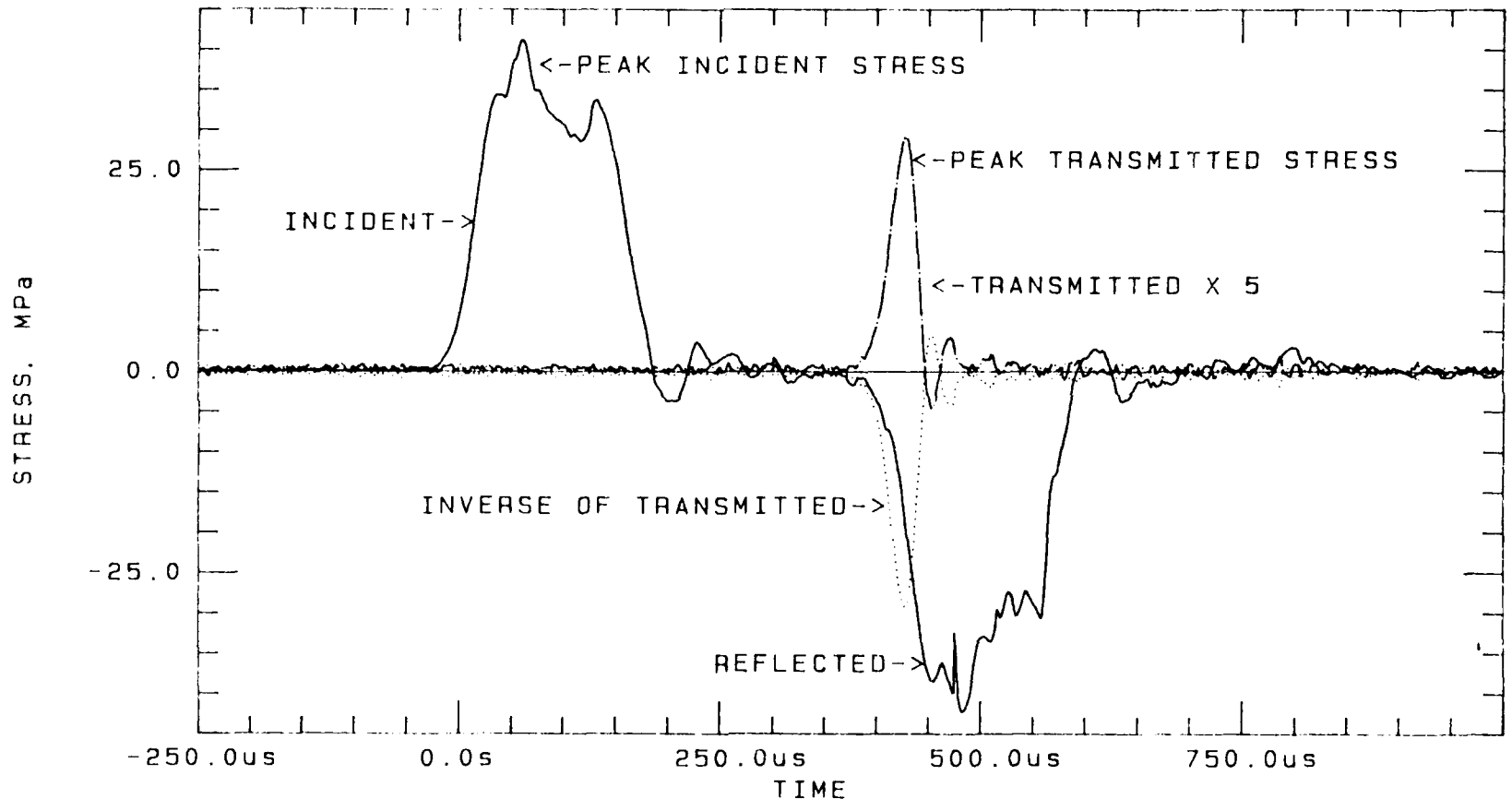

Figure 29. Uncorrected Data Traces for Saddle-Notched Specimens.

In an effort to improve upon the details of these traces, each signal was corrected for dispersion and corrected for phase back to opposite ends of the specimen. The computer code used for these corrections is given in Reference 17. After corrections, the signals are then used to display curves for stress-strain, strain versus time, strain rate versus time, and stresses for each end of the specimen. Displays of stresses at both ends of the specimen are a good indication of how well the basic assumption of uniform stress along the specimen length holds for each specimen. For the same specimen traces displayed in Figures 28 and 29 the stresses on each end of the specimen and the strain rate are given in Figures 30 and 31. In addition, the stress-strain curves for each are shown in Figures 32 and 33.

In an effort to further determine the tensile strength of concrete the splitting cylinder test was attempted in the SHPB. This is believed to be the first time this type specimen has been tested in the SHPB. As shown in Figure 25 this test is a plain cylinder tested with its longitudinal axis perpendicular to the SHPB longitudinal axis. The strain gauge traces for this kind of test are shown in Figure 34. Here the incident and transmitted signals are compressive and the reflected signal is tensile. For analysis purposes the peak of the transmitted compressive signal is converted to a load which is then assumed to be the peak load applied to the specimen, similar to the static loading as shown in Figure 35. The static tensile stress f_t' normal to the load direction as shown in Figure 35 is

$$f_t' = \frac{2P}{\pi DL} \tag{48}$$

where P is the applied load
D is the specimen diameter
L is the specimen length.

The dynamic tensile strength f_{td}' is calculated using Equation 48 where the load P is determined from the maximum transmitted stress $(\sigma_T)_{max}$ times the cross sectional area, A, of the SHPB. $(\sigma_T)_{max}$ is determined using the peak transmitted stress of Figure 34. Equation (48) is then modified for dynamic tensile strength as

$$f_{td}' = \frac{2(\sigma_T)_{max}A}{\pi DL} \tag{49}$$

The static stress distribution is shown in Figure 35 and it has been shown numerically that the dynamic stress distribution is very similar to the static stress distribution. (The numerical calculations are currently being done on a contract from AFESC/RDCM to Civil Engineering Department, Auburn University and have not been published, although several papers are to be published soon.)

The failure of both the static and dynamic splitting cylinders are almost identical. Figure 36 shows a typical failure for a static case and Figure 37 shows a typical failure for a dynamic test. For SHPB splitting cylinder tests, with increasing load rate, the split cylinder halves have increasing velocity and additional fracture occurs during impacts with side

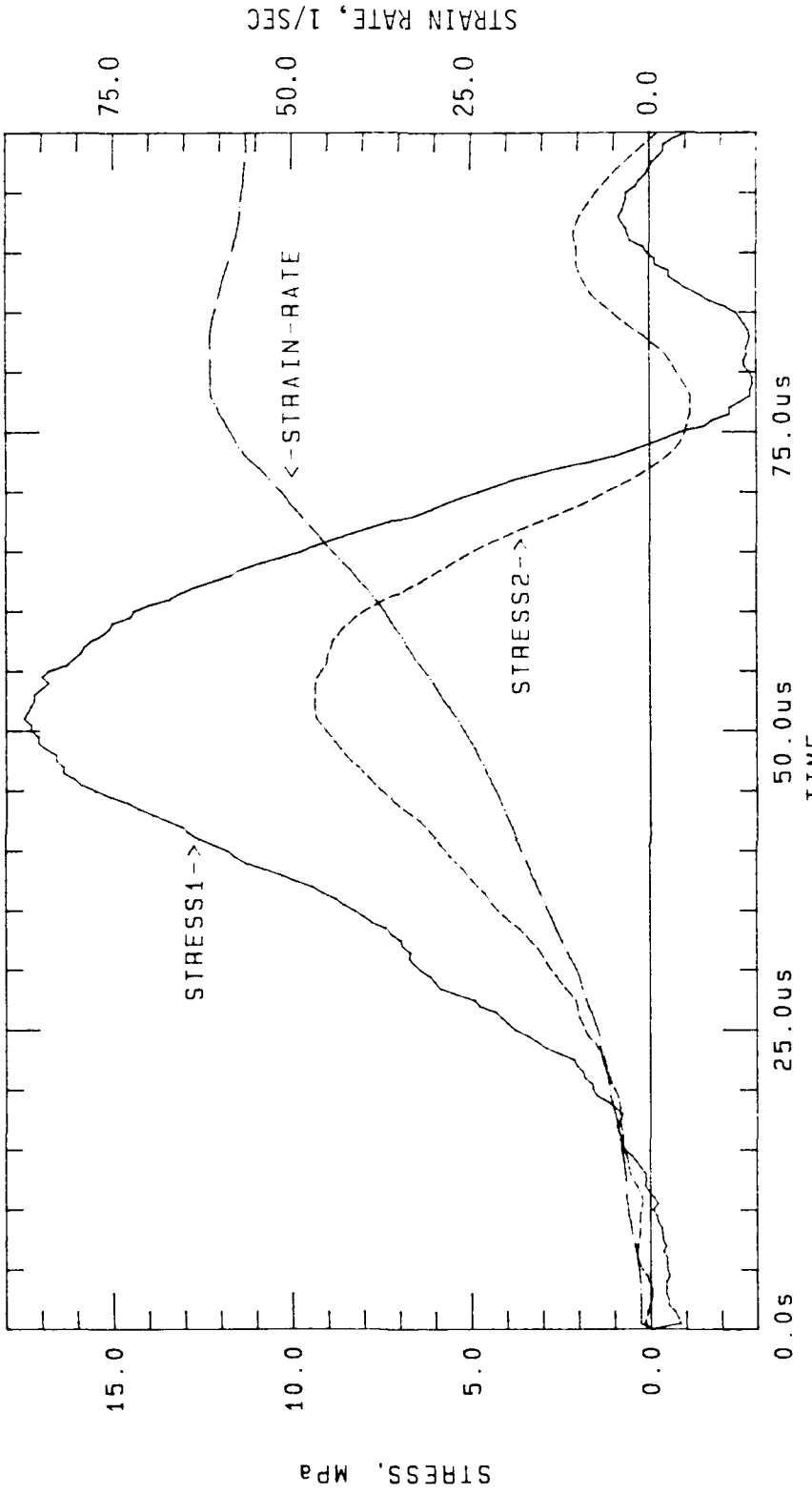

Figure 30. Corrected Front and Rear Specimen Stresses and Strain Rate for the Square-Notched Specimen of Figure 28.

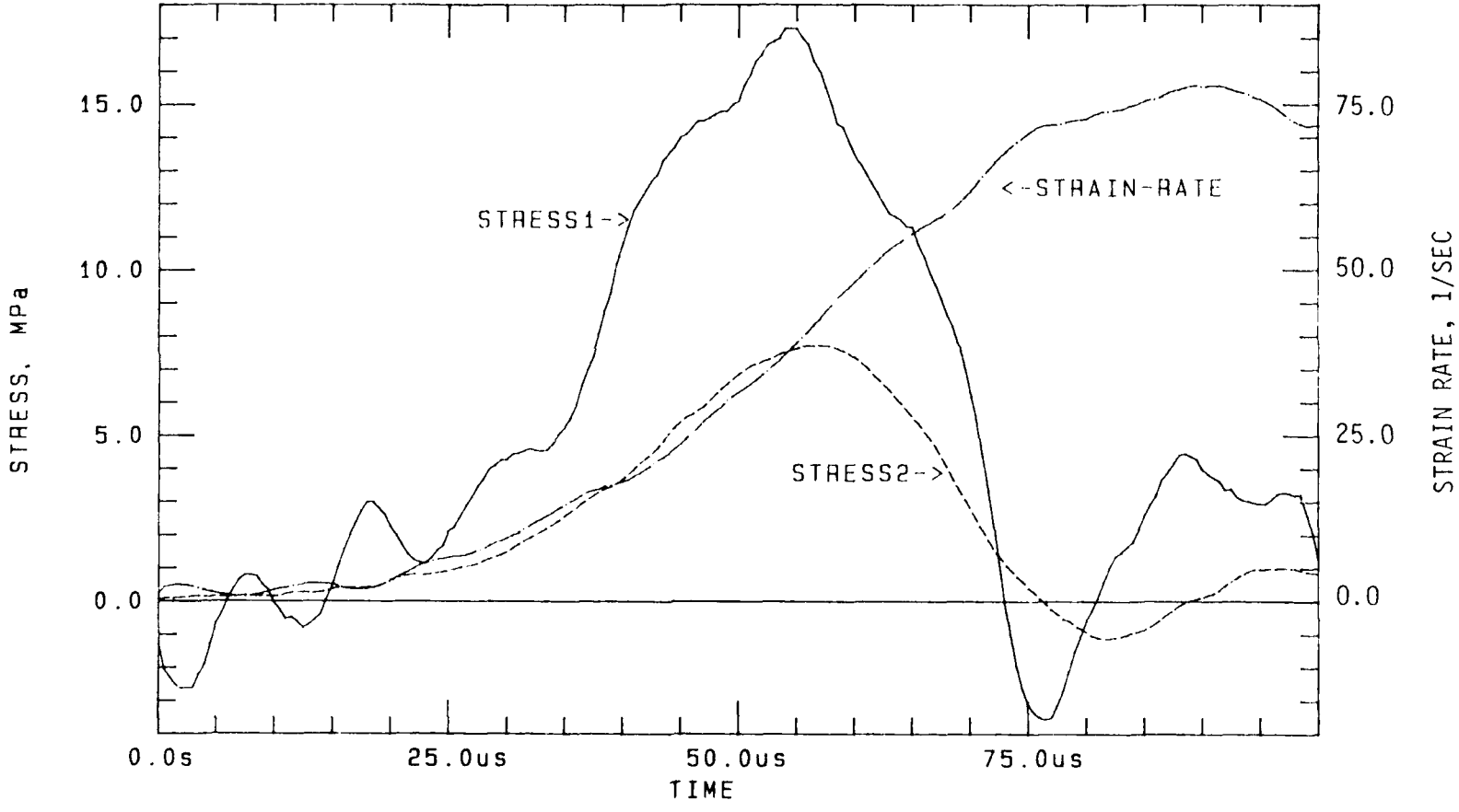

Figure 31. Corrected Front and Rear Specimen Stresses and Strain Rate for the Saddle-Notched Specimen of Figure 29.

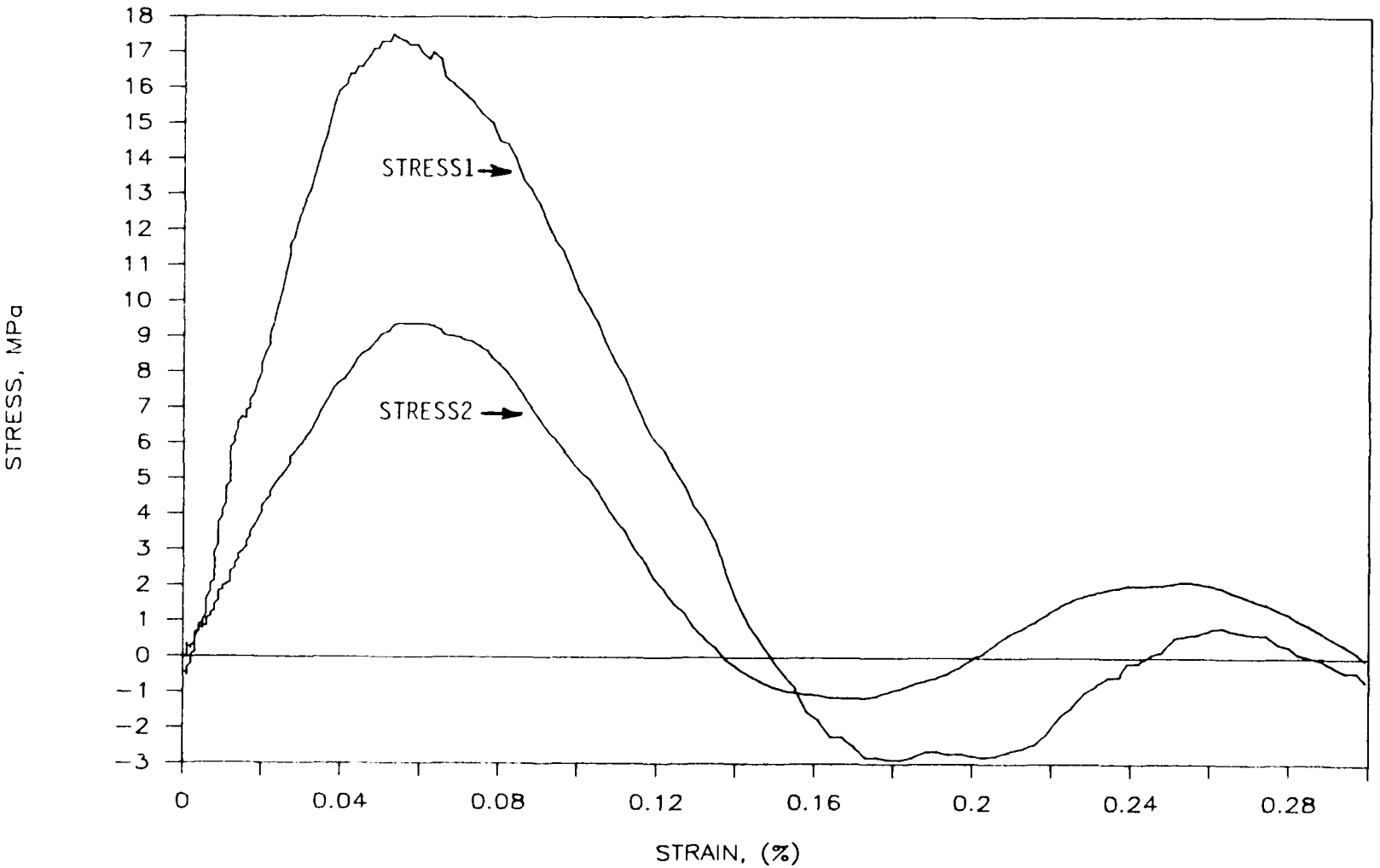

Figure 32. Stress-Strain Curve for Square-Notched Specimen of Figure 28.

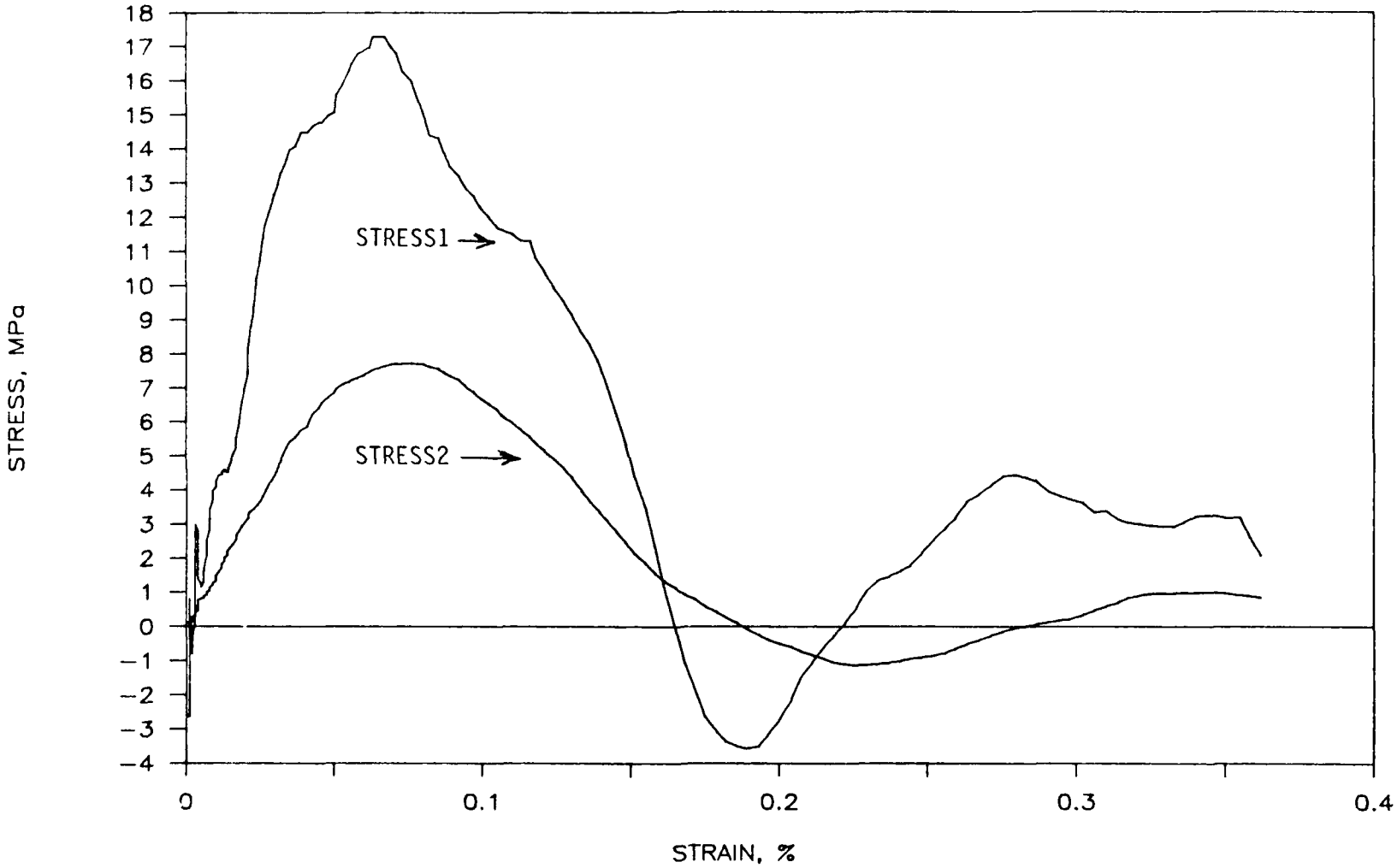

Figure 33. Stress-Strain Curve for Saddle-Notched Specimen of Figure 29.

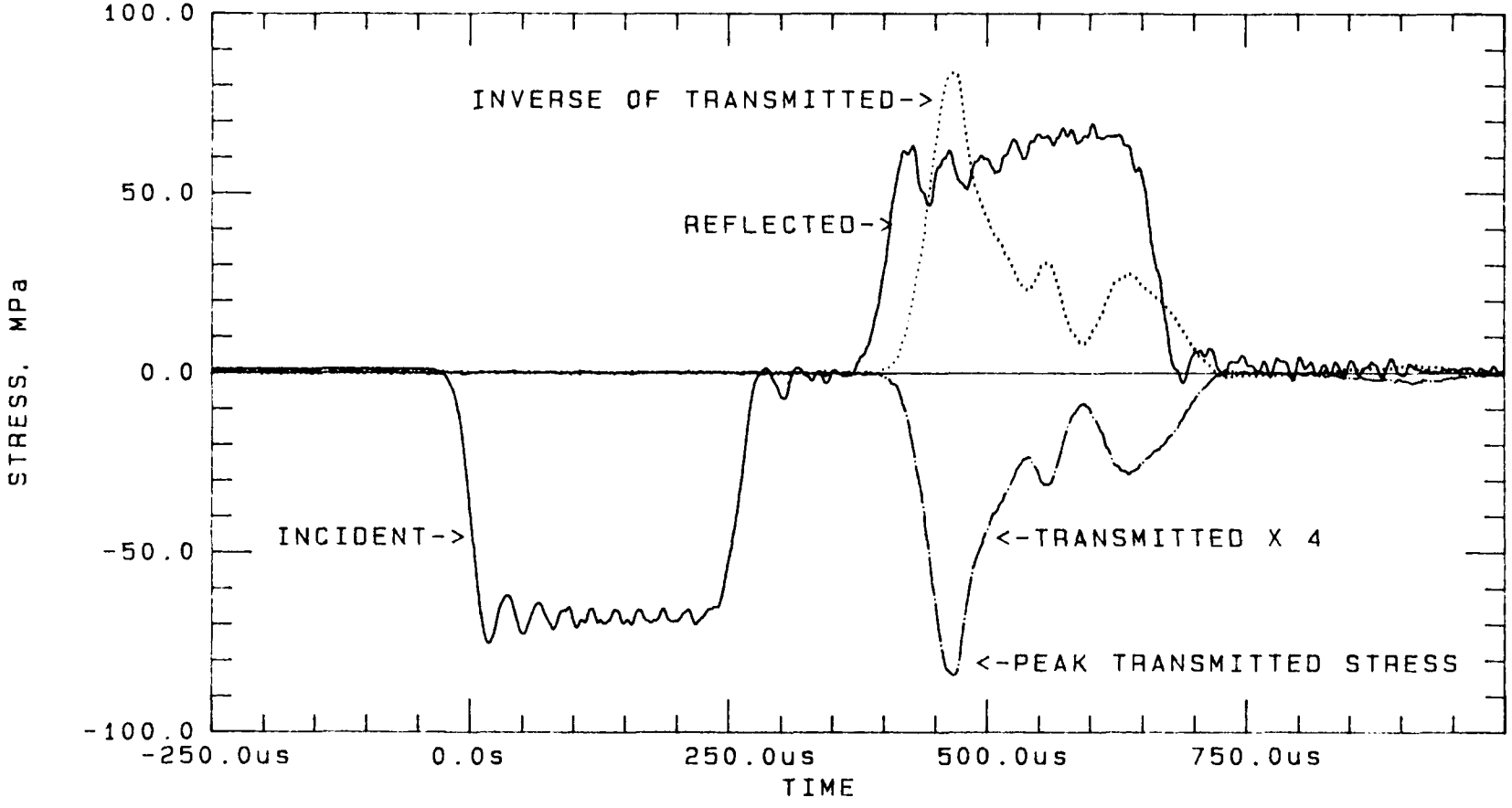

Figure 34. Strain Gauge Traces for a Splitting Cylinder Test.

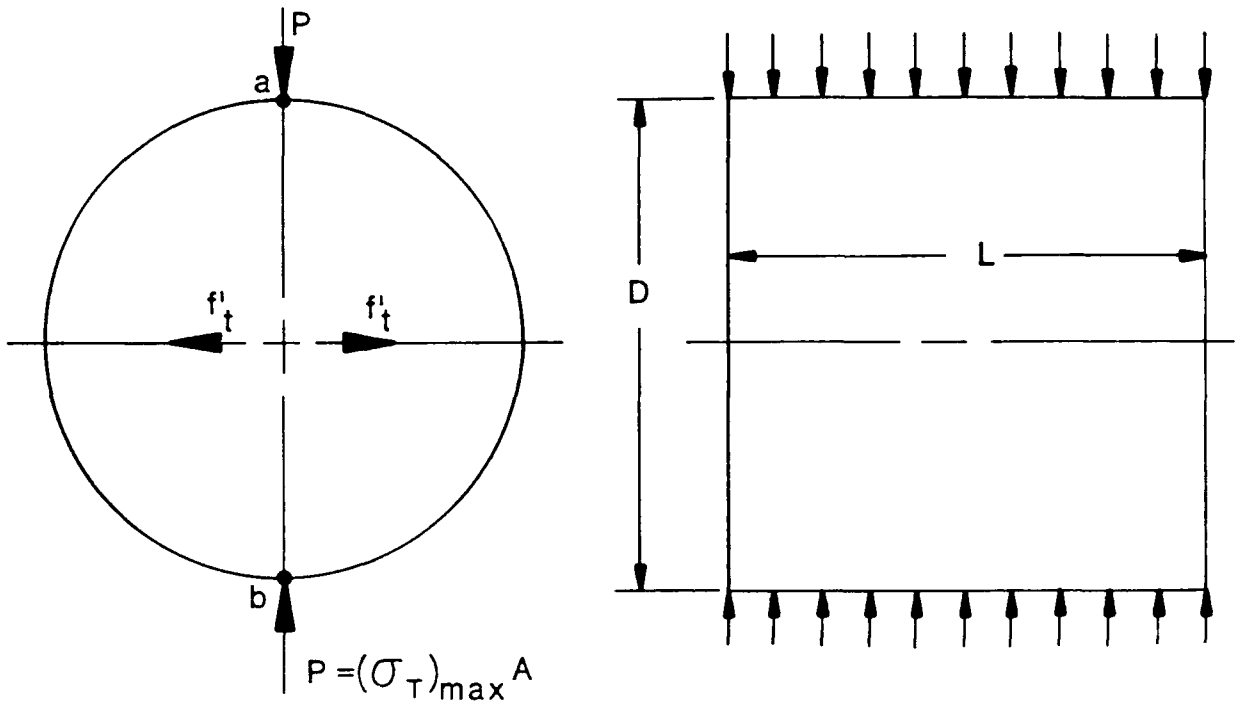

LINE LOAD ALONG THE CYLINDER

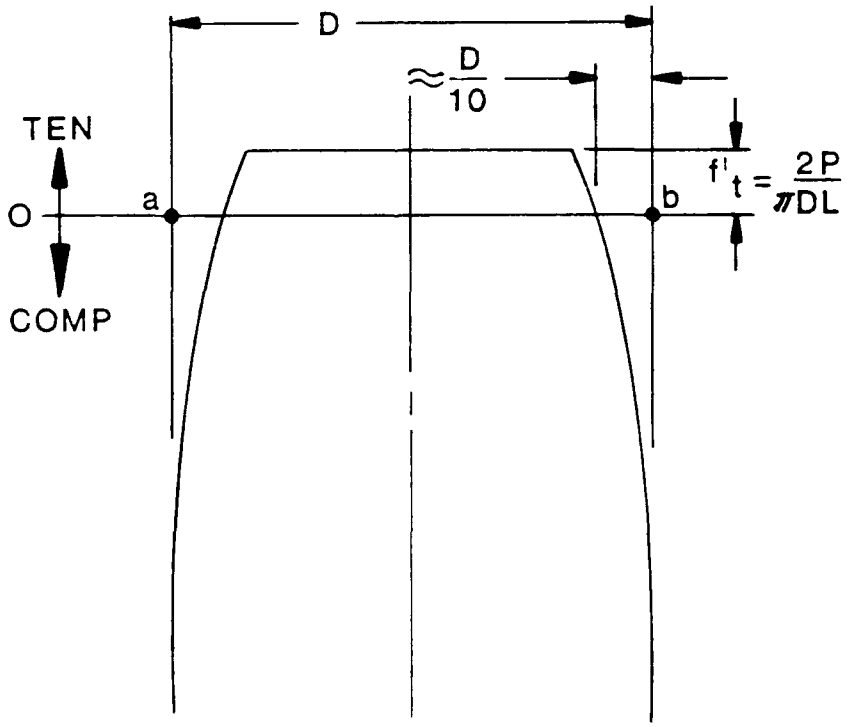

STRESS DISTRIBUTION

Figure 35. Loading Diagram for a Splitting Cylinder Specimen and the Static Stress Distribution.

Figure 36. Static Loading Failure for a Splitting Cylinder Test (Approximate Strain Rate: 3.1×10^{-4}).

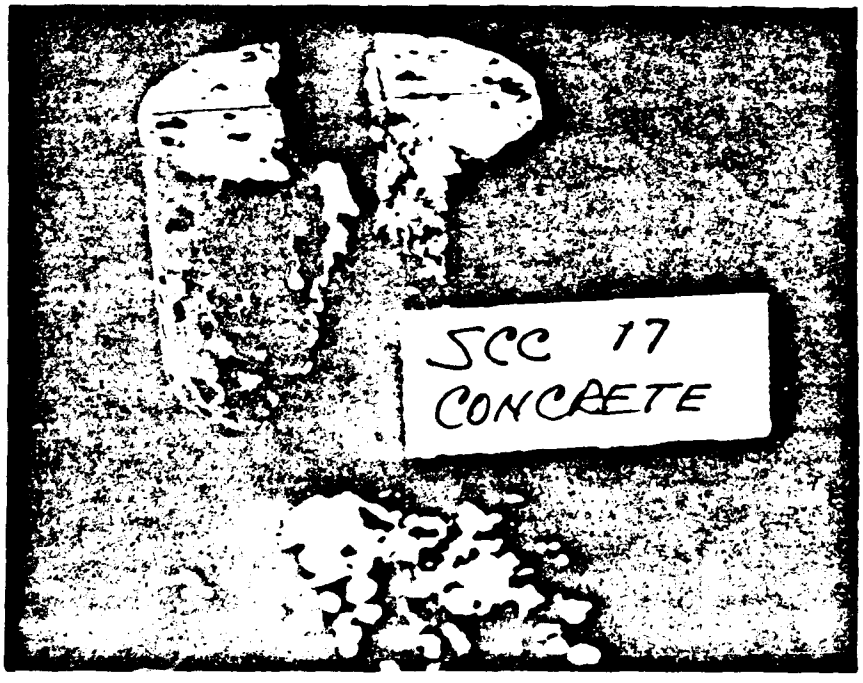

Figure 37. Dynamic Loading Failure for a Splitting Cylinder Test (Approximate Strain Rate: 2.0).

walls of a debris catcher. However high-speed photography shows the halves to be intact after splitting. The high-speed film shows that the fracture begins to occur first near the center and this is in agreement with the numerical calculations which shows that the tensile stress, for a given time, is larger in the center of the specimen than at the edges. Also the compressive stress normal to the failure plane is larger at the edges which reduces the tendency for fracture near the edges.

Direct compression tests were performed in both the SHPB and MTS on plain cylinders of the same concrete mix as in previously discussed tensile test. These tests were used as a basis for comparison with other data, as in almost all discussion, the compressive stress is the major property used in comparison. These tests are very straightforward with the specimen mounted, as shown in Figure 26. The raw data for one of these tests is shown in Figure 38. Stresses of front and rear faces of the specimen along with strain rate are shown in the curves of Figure 39 and stress-strain curves are shown in Figure 40. Also a static stress-strain curve obtained from a 220-day 6-inch diameter, 12-inches long (15.24 x 30.48 cm) cylinder and a 220-day 2-inch diameter, 2-inches long (5.1 x 5.1 cm) cylinder is shown in Figure 40.

4. Discussion

As noted earlier, direct tension tests are difficult and failure appears to occur at most any place along the length of the specimen. This is especially true at the higher strain rates. The two direct tension type specimens show similar response in both the SHPB and the MTS machine. At the higher strain rates of the two machines the specimens fractured at places other than in the reduced section. In the SHPB specimens, multiple fractures occurred in many tests. In all the cases of multiple fractures in the SHPB, a fracture occurred on the incident side of the specimen and at reduced section. A typical double fracture is shown in Figure 41. In some cases, only the incident side fracture occurred. In multiple fractures, it appeared that the fracture at the reduced section occurred first. However when a SHPB single fracture occurred near the incident end, one must assume that this single fracture occurred during the passage of the first pulse through the specimen.

It appears that the direct tension fracture of SHPB specimen occurs in the loading phase of the incident pulse. This is based on observing that the peak of the transmitted pulses of both the direct tension square and saddle notch specimens (Figures 28 and 29) occur during the rise time of the reflected pulse. For clarity, the inverse of these transmitted pulses are also shown in these figures. Also in observing the stresses on the two faces of the direct tension specimens (Figures 30 and 31) there is almost a factor of 2.0 difference between these two stresses. This indicates a nonuniformity of stress along the length of these two kinds of specimens. An alternative method of determining stress uniformity along the specimen length is to compare the wave transit-time across the specimen to the loading time or time-to-failure of the specimen. Uniformity of stress occurs in the specimen

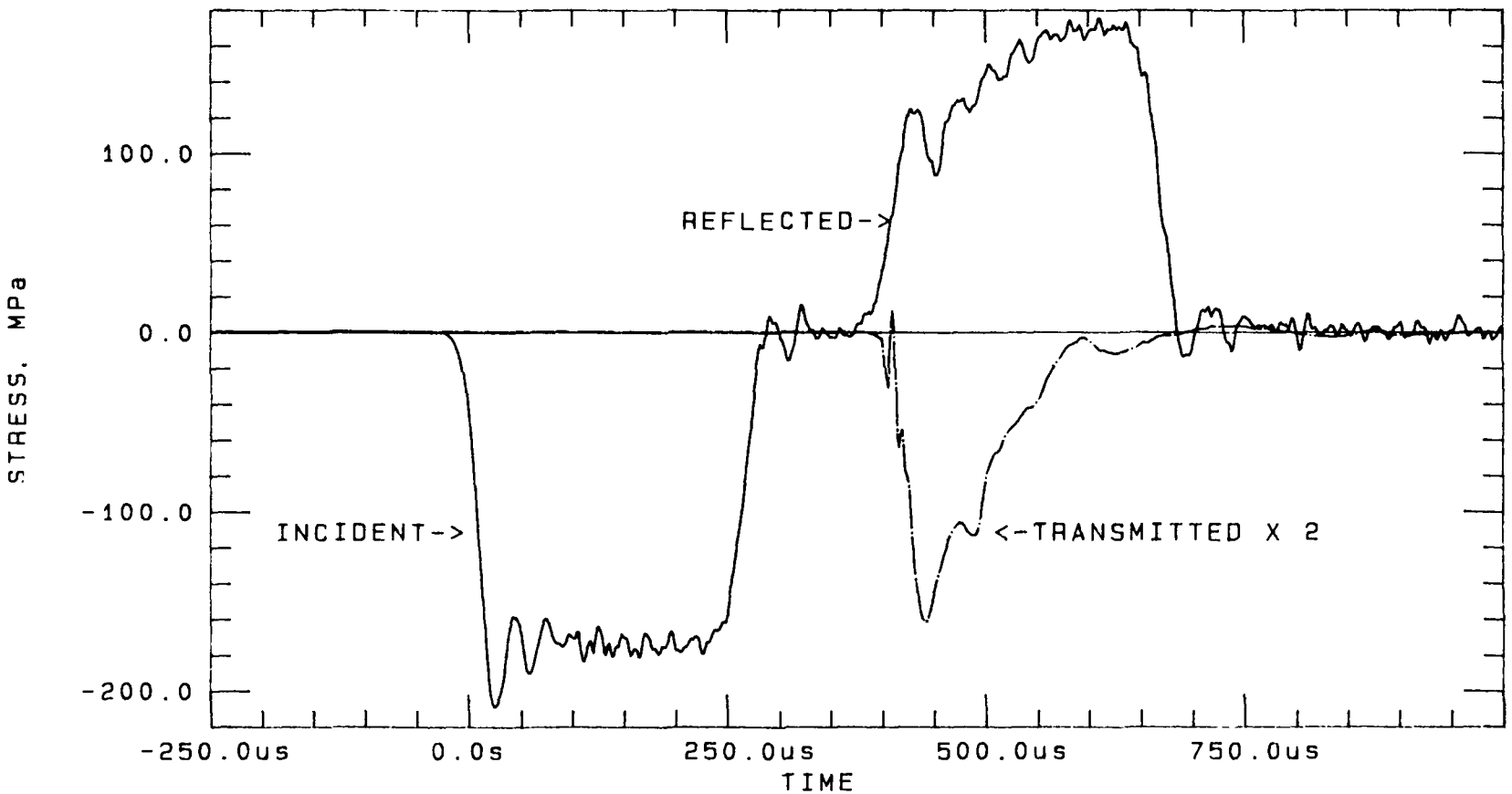

Figure 38. Uncorrected Data Trace for a Direct Compression Specimen.

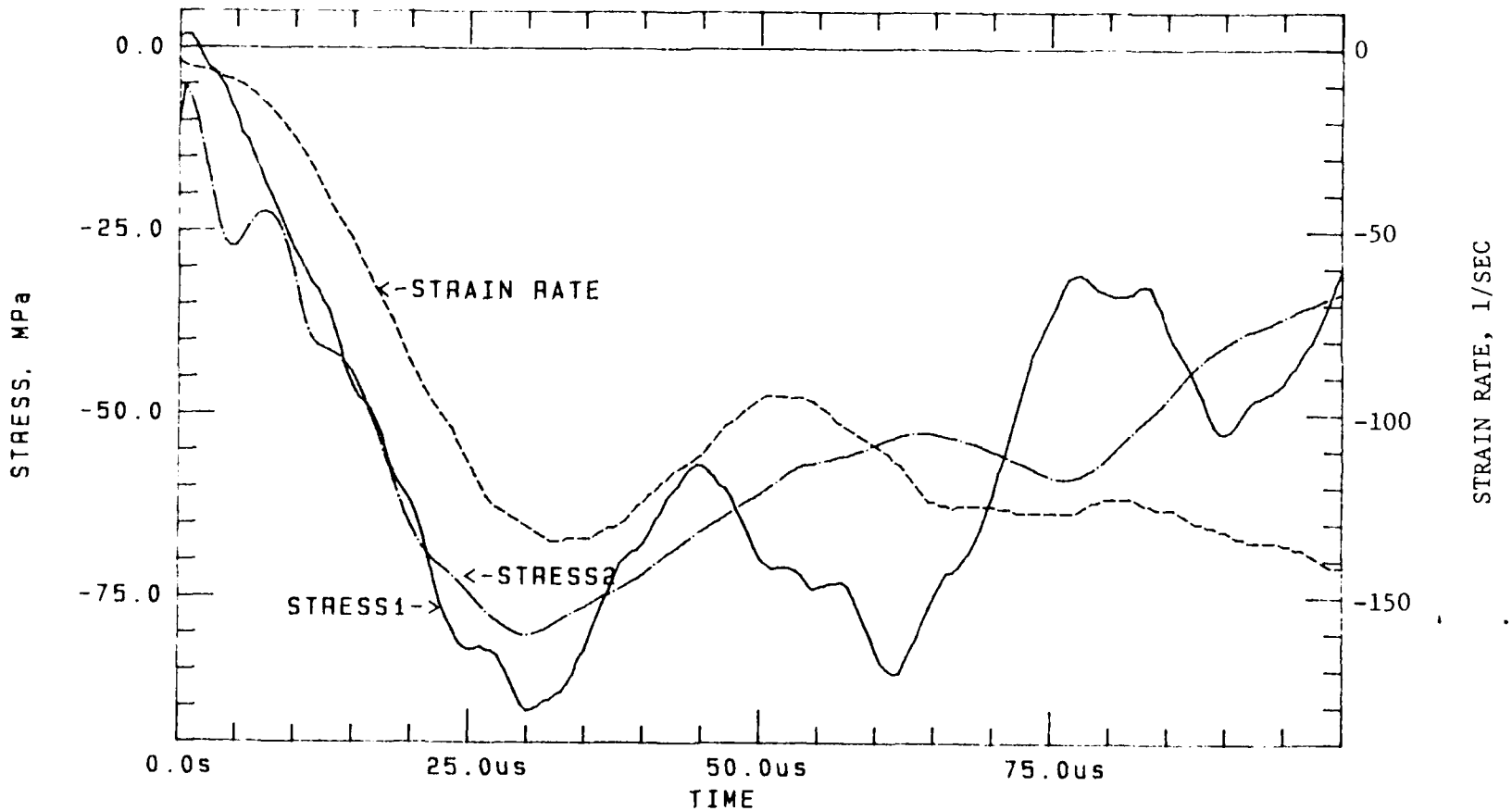

Figure 39. Corrected Front and Rear Specimen Stresses and Strain Rate for the Direct Compression of Figure 38.

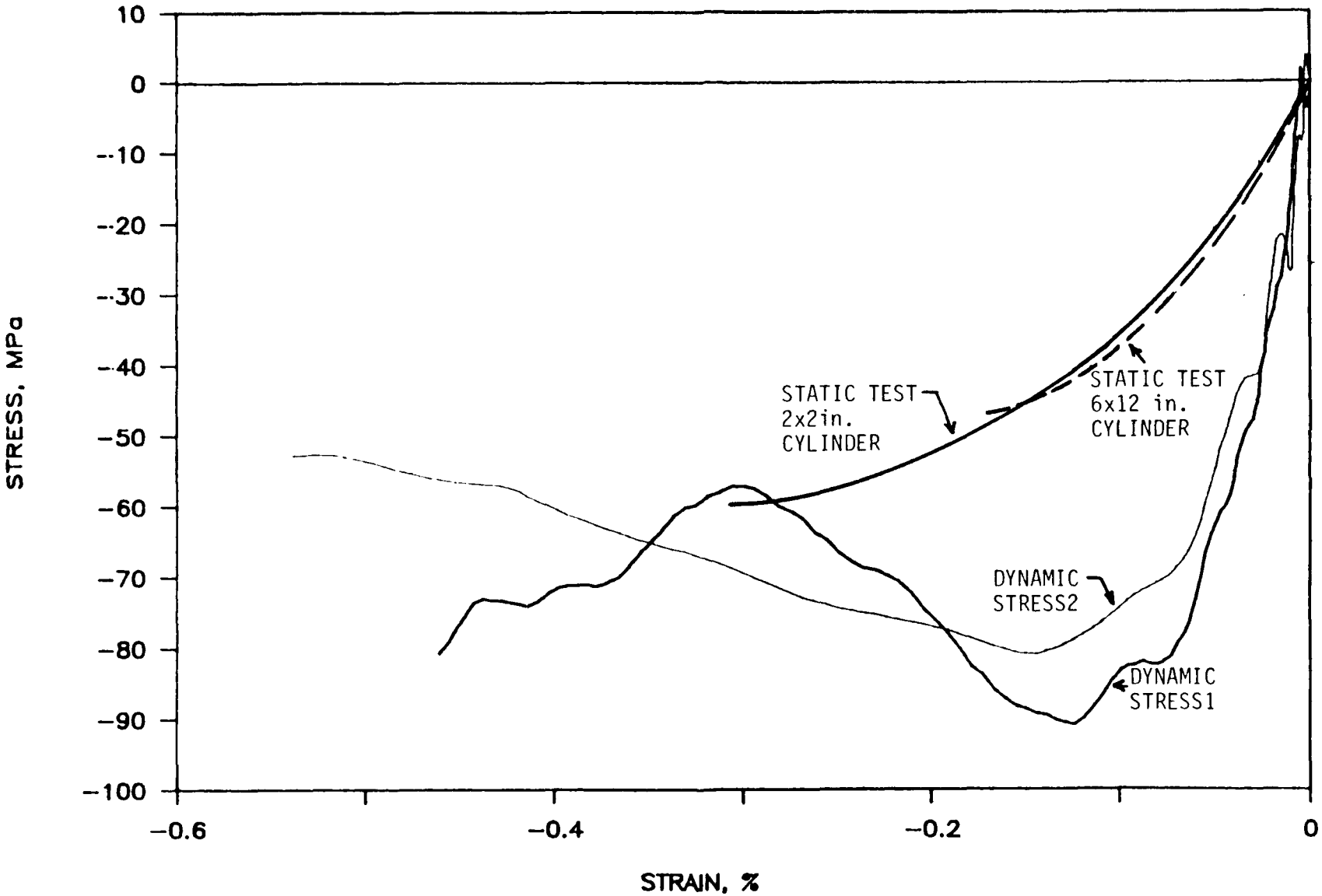

Figure 40. Stress-Strain Curve for the Direct Compression Specimen of Figure 38.

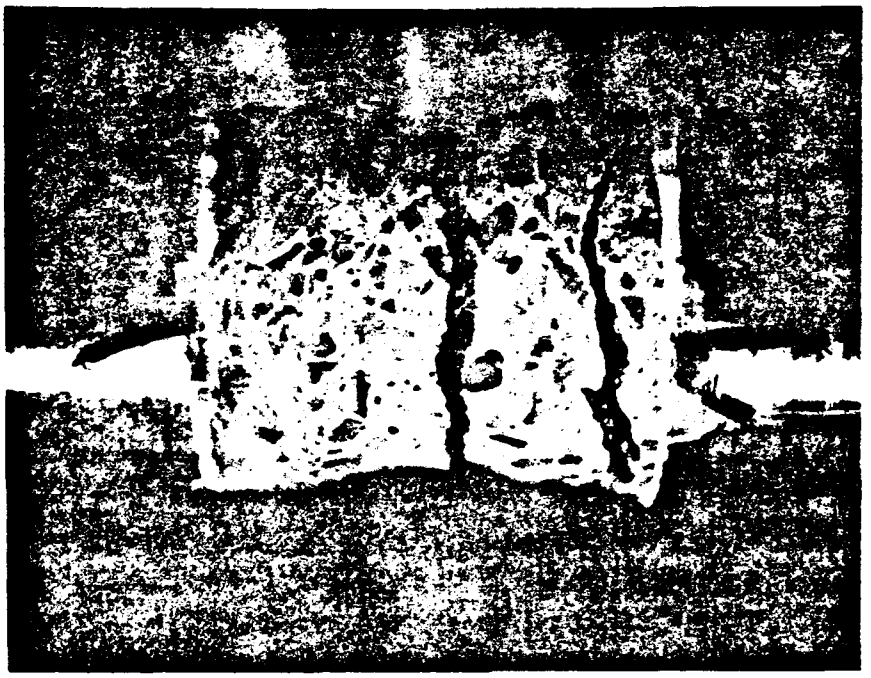

Figure 41. Double Fracture of a Direct Tension Specimen.

after multiple wave reflections within the specimen. A rule of thumb is to assume that approximately 10 transit-times are required for stress uniformity along the specimen length. The wave speed in concrete is approximately 3.7 km/sec (12,000 ft/sec) and the transit-time of a 5.08 cm (2-inch) long specimen in approximately 14 μsec. The time to failure for the direct tensile specimens of Figures 18 and 29 is approximately 50 μsec. The number of specimen transit-times for 50 μsec is only 3.6, which does not meet the 10 required for stress uniformity along the specimen length. This is in agreement with the results obtained above with Figures 30 and 31.

The nonuniformity of stress along the length of the specimen affects only the strain rate of the specimen. The strength calculated from the maximum transmitted stress is correct. However, the strain may not be calculated using Equation (36), but is determined from the load rate, based on the time to fracture, divided by the elastic modulus of the concrete. The rate and resulting strain rate determined by this method must assume a linear elastic material response and experimental observations show this assumption to be justified. This method of calculating strain rate was used for both the splitting cylinder specimens and direct tension specimens and was used in preparing the data for Figure 42.

Some direct tension tests were conducted on mortar specimens of various sizes. Similar results as that of concrete were observed and the only low strain rate data was taken at a strain rate of approximately 10^{-7}/sec. A summary of all the concrete data is shown in Figure 42. In Figure 42 the strength data was displayed by a ratio of the strength data at strain rate to the strength data at a strain rate of approximately 10^{-7}/sec. The strength data at this low strain rate was referred to as the static strength.

The tensile strength ratios reported in Reference 25 are shown in Figure 42 as open squares with a diagonal line and are very high when compared to compressive strength ratios of many researchers. Therefore, based on these two or three data points, the acceptance of the high tensile strength was questionable. However, based on the experimental tensile data collected in this report and some tensile strengths back calculated from spall experiments on concrete walls of Reference 26, these higher tensile strengths appear more acceptable. The spall data of Reference 26 are shown, as open squares with a dot in the middle, in Figure 42.

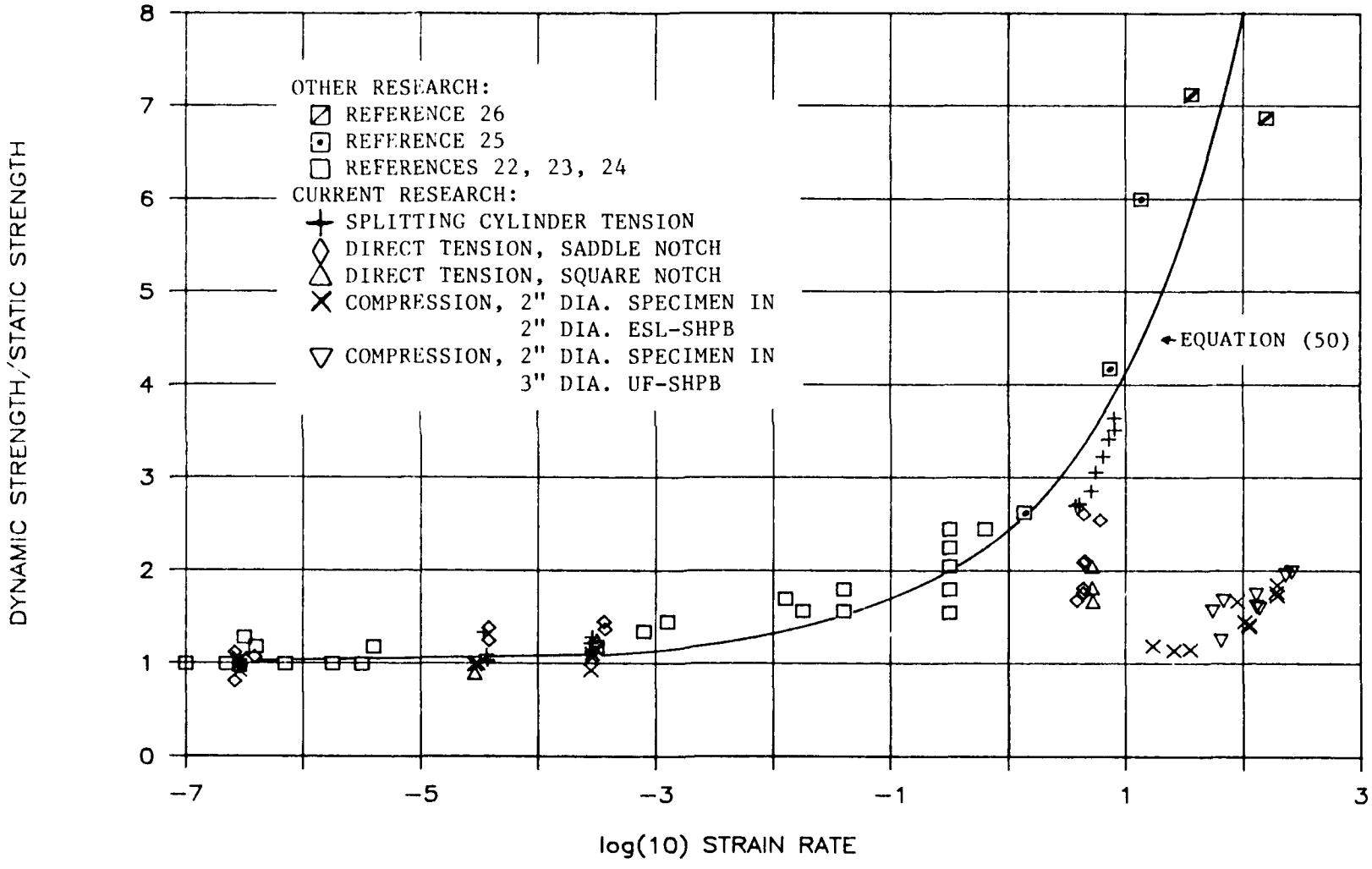

Figure 42. Strength Ratio Versus Log (10) of Strain Rate for Tensile and Compressive Tests of Concrete Specimens Tested in the ESL-SHPB.

Based on all the tensile data shown in Figure 42, an "eyeball" curve is drawn through the data. The curve is based on a similar equation of Reference 23 and given as:

$$\frac{f'_{td}}{f'_{ts}} = \exp(AE^B)$$

$$E = \log_{(10)}[\dot{\varepsilon}_d/\dot{\varepsilon}_s]$$

$$\dot{\varepsilon}_s = 10^{-7}/\text{sec}$$

$$A = 0.00126 \qquad (50)$$

$$B = 3.373$$

ε = Strain Rate

d,s subscripts for dynamic and static

Also displayed in Figure 42 are the data for the splitting cylinder tests. These data are also displayed using the ratio of the strength at a given strain rate to the static strength. As mentioned earlier it appears that the dynamic stress distribution of the splitting cylinder test is very similar to the static stress distribution. However, it has not been determined how accurate the peak tensile stress is when calculated using the peak transmitted compressive stress. The tensile stress calculated using Equation (48) and the SHPB data is in most all cases higher than the SHPB direct tension strength data. This is also true in static data where the splitting cylinder strength data is approximately 10 to 15 percent higher than direct tension strength (Reference 19). For the SHPB data shown in Figure 42 the splitting cylinder strength is 20 to 30 percent higher than the direct tension data.

The effects of strain rate on compressive strength of concrete (same mix as tensile specimens) is shown in Figure 42. Here, as in the case of previous data the tensile strength appears to have a higher strain rate sensitivity than the compressive data. The compressive data of Figures 39 and 40 show very nearly equal stresses on the front and back faces of the specimen. Based on this, one can say that the compressive test meets the SHPB assumption of uniform stress along the specimen length. The static modulus of concrete is shown in Figure 40 along with the dynamic curve obtained from the SHPB tests. It is the authors opinion that the dynamic modulus data obtained from SHPB tests is not valid because any elastic deformation occurs in the rise time of the loading pulse and during that time the specimen is not uniformly loaded along its length. Nonuniformly loaded specimens then have nonuniform strain distribution and may give false modulus data.

B. SOILS TESTS

1. Introduction

Additional soil tests on three different soils were conducted in a manner described in Reference 15. These three soils were designated as mortar sand, 20-30 Ottawa sand, and Eglin sand. The 20-30 Ottawa sand is a very uniform round particle size. The mortar sand is mined locally and has fairly angular grains with approximately 0.5 percent fines. The Eglin sand (collected on Eglin AFB) is similar to the mortar sand except it contains 2.0 to 3.0 percent fines.

2. Specimen Preparation

Specimens for the tests and data presented in Reference 15 and initial tests presented here were prepared by first adding moisture and then compacting to a given volume to give a constant dry density. The specimen diameter of 2-inch (5.1cm) was chosen to match the SHPB diameter. A 4-inch (10.2cm) length specimen was prepared in four 1-inch (2.54cm) lifts. Initially, a dry density was chosen and the proper mass was determined to fill the 2-inch diameter, 4-inch long (5.1 by 10.2cm) volume. The mass was then divided into four equal parts for the four lifts. A schematic of the specimen mounted in the SHPB is shown in Figure 43.

For moist specimens a moisture content was chosen and the proper amount of water was added to the original dry soil. The specimen was then mixed for 5 minutes and let stand for approximately 45 minutes. Before specimen preparation a portion of the mix was weighed and set aside for drying and moisture content determination. Six specimens were prepared and a portion of each was set aside for determining moisture content. The average of all these moisture contents is the moisture content reported for each of the specimens of the particular mix. The density of the moist specimen then becomes the dry density times the sum of one plus the moisture content.

3. Results

For each specimen, wave speed and a transmission ratio were obtained. The wave speed was determined by observing the elapsed time between the beginning of the incident pulse and the beginning of the transmitted pulse. This elapsed time represents the time required for the pulse to travel through the specimen plus the length of the bar between the strain gauges. The length of time required to travel through the bar material may be calculated using this length and wave speed of the bar. When this time of travel in the bar between the strain gauges is subtracted from the total elapsed time, the transit time in the specimen is determined. Using this transit time and specimen length the wave speed in the specimen is obtained.

The transmitted stress ratio was obtained by selecting the peak transmitted stress of Figure 44 and dividing by the peak stress of the incident stress of the same graph.

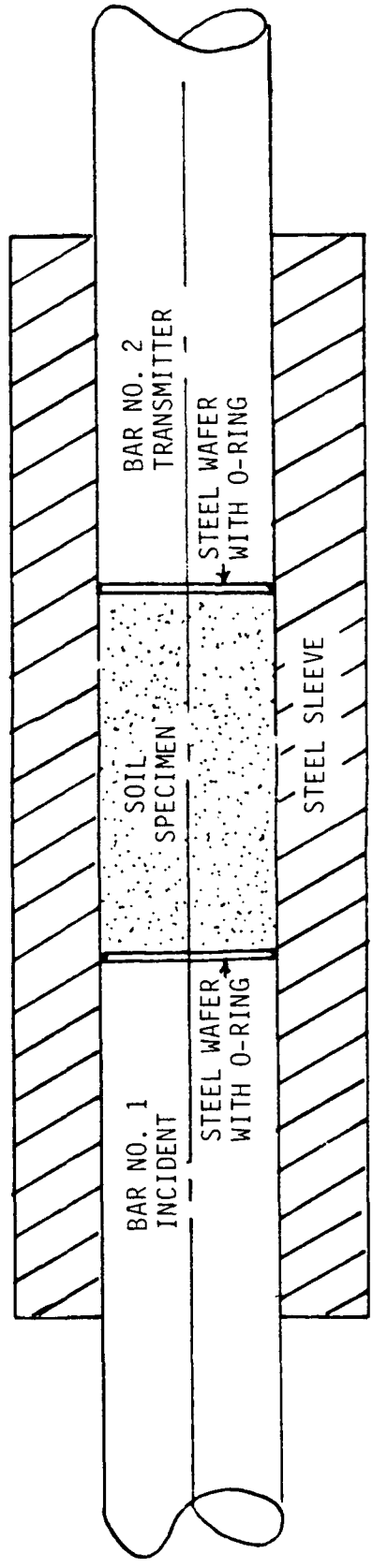

Figure 43. Schematic of Soil Specimen in the SHPB.

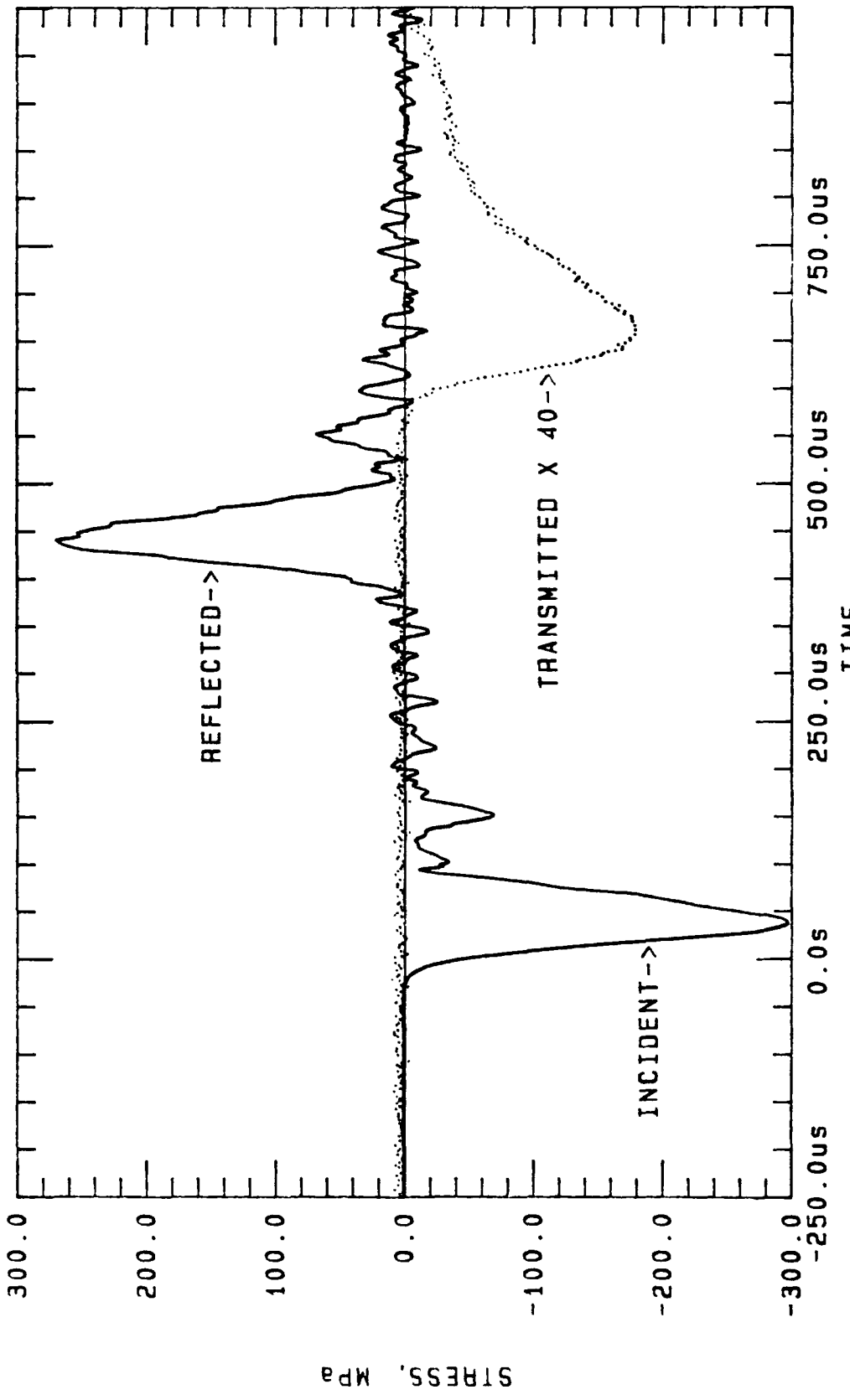

Figure 44. SHPB Soil Specimen Data Trace.

The Eglin sand contained the higher percent of fines, and of the soils tested, showed the highest increase in wave speed and stress transmission ratio. Data obtained using Eglin sand was the only detailed data given here to show the effects of moisture content and compaction. For a given dry density of 1.75g/cc (void ratio of 0.51) and a solid particle density of 2.60g/cc the moisture content at saturation is approximately 0.2. Wave speed data and stress transmission ratios, as a function percent of saturation are shown respectfully in Figures 45 and 46. These data were collected in a metal sleeve without additional confining pressure. Also these specimens were prepared by adding moisture before compaction.

Similar soil tests were conducted at the ESL SHPB facility by Professor Wayne Charlie and graduate student Steve Pierce of Colorado State University, under a USAF-UES Summer Faculty Research Program. (This work is reported under an unpublished final report to AFESC/RDCS). However, most of this work was completed on specimens that were compacted dry with moisture added later through a saturation/desaturation process. These tests were conducted in a triaxial cell, mounted in the ESL SHPB, which had the capability of applying a confining pressure to the specimen. Data for atmospheric pressure are shown in Figures 47 and 48. Similar data on Eglin sand for tests with 45 psi (0.31MPa) confining pressure are shown in Figures 49 and 50.

4. Discussion

Of the five different sandy soils tested in the ESL SHPB by compacting with moisture, all showed similar data as that shown in Figures 45 and 46. Initially, these results were thought to be due to capillarity and its effects on effective stress (Reference 20). Also other researchers (Reference 21) attributed similar effects on shear modulus to that of capillarity. In the work described in Reference 21, the specimens were also compacted with moisture present.

In the case of the data presented in Figures 47 and 48, the specimens were compacted dry, all to same dry density of 1.75g/cc. For the moist specimens, water was introduced by soaking overnight to complete saturation. Subsequently the specimens were desaturated to some soil suction pressure which corresponds to a moisture content on a desaturation pressure/moisture content curve. The results from these tests at atmospheric pressure do not show the increases in wave speed and transmission ratio with increasing moisture content as that of Figures 45 and 46.

These results negate the original thinking that the results of specimen tests when compacted with moisture was due to capillarity, but may be attributable more to compaction energy. Based on this, some further tests were conducted. These tests consisted of an effort to quantify the energy required to compact soil of varying moisture content to the same dry density. This was done by counting the number of blows of a 5.5 pound (2.5 kg) hammer with a 12-inch (30.5 cm) drop, to compact each lift of the 4-inch (10.4 cm) long specimen.

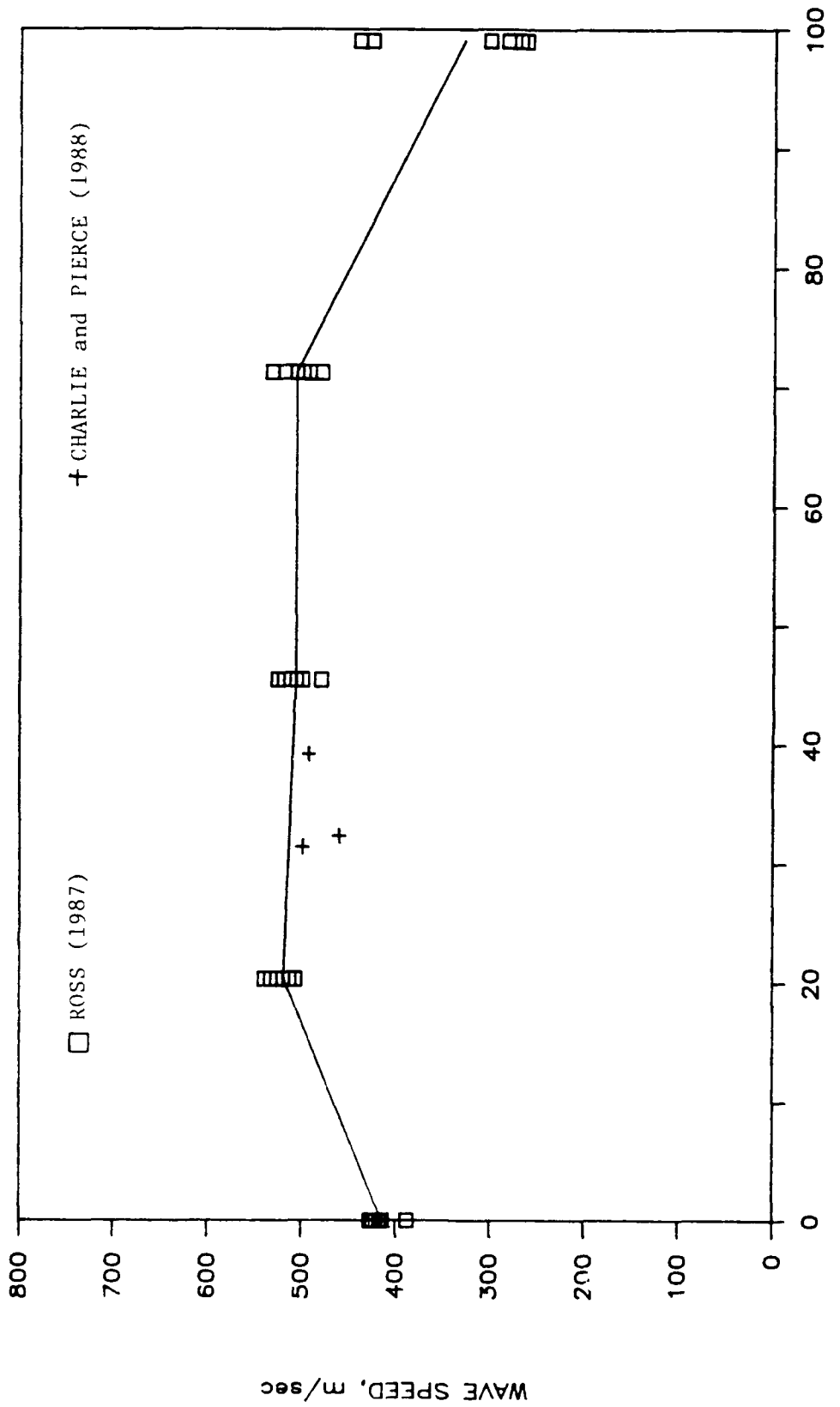

Figure 45. Wave Speed Versus Percent of Saturation for Eglin Sand Compacted With Moisture.

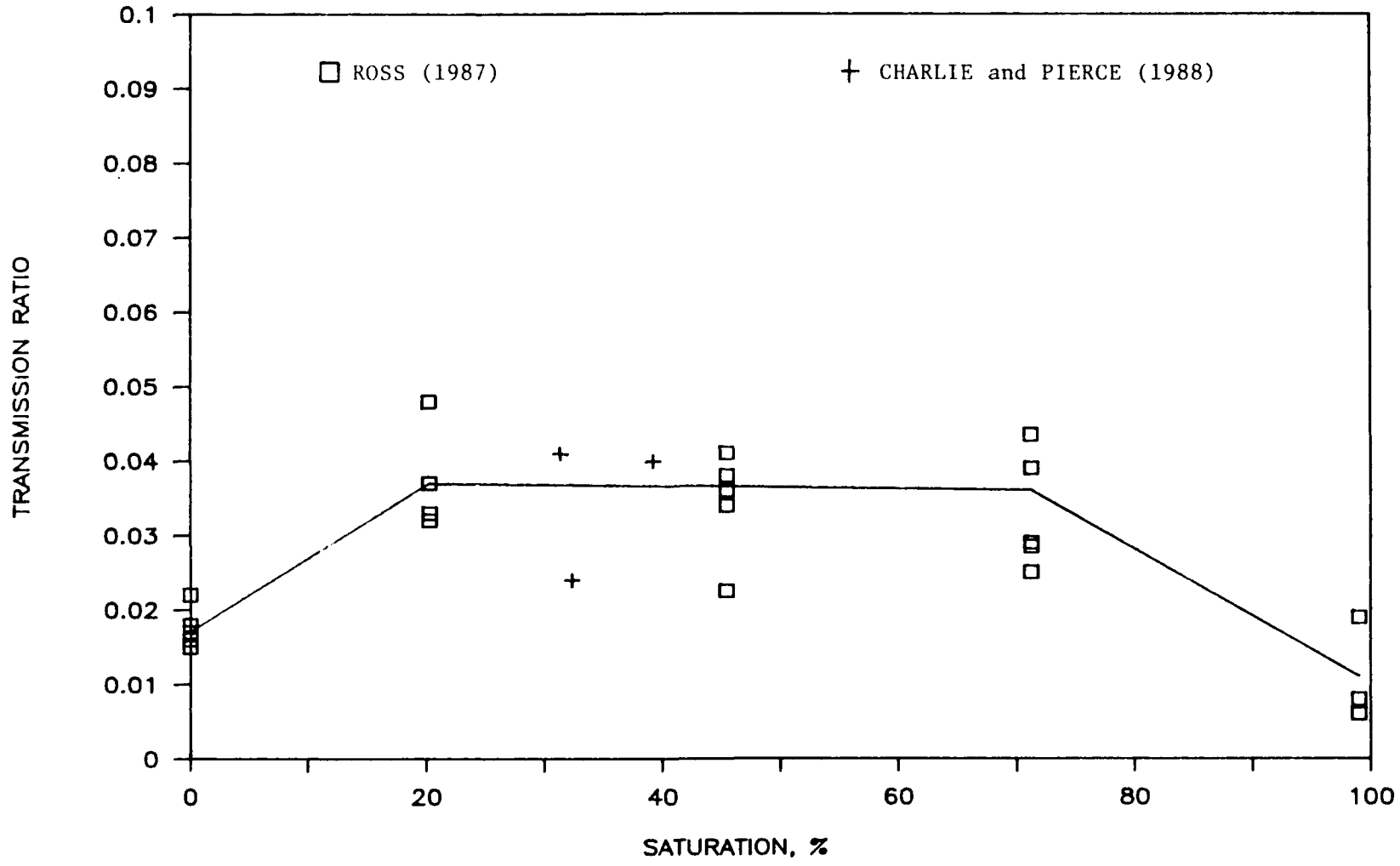

Figure 46. Transmission Ratio Versus Percent of Saturation for Eglin Sand Compacted With Moisture.

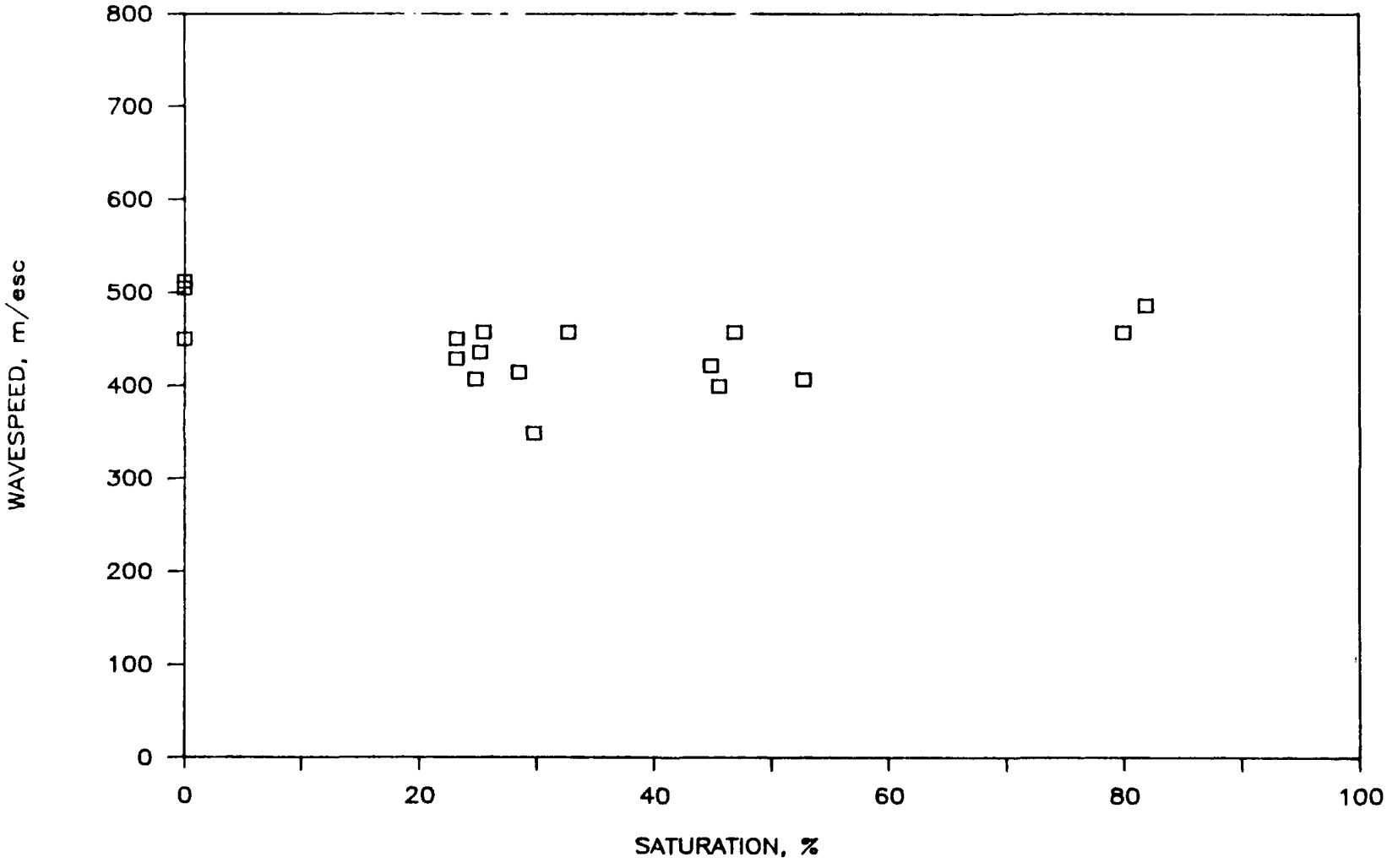

Figure 47. Wave Speed Versus Percent of Saturation for Eglin Sand Compacted Dry and Moisture Added Later. Confining Pressure: Atmospheric.

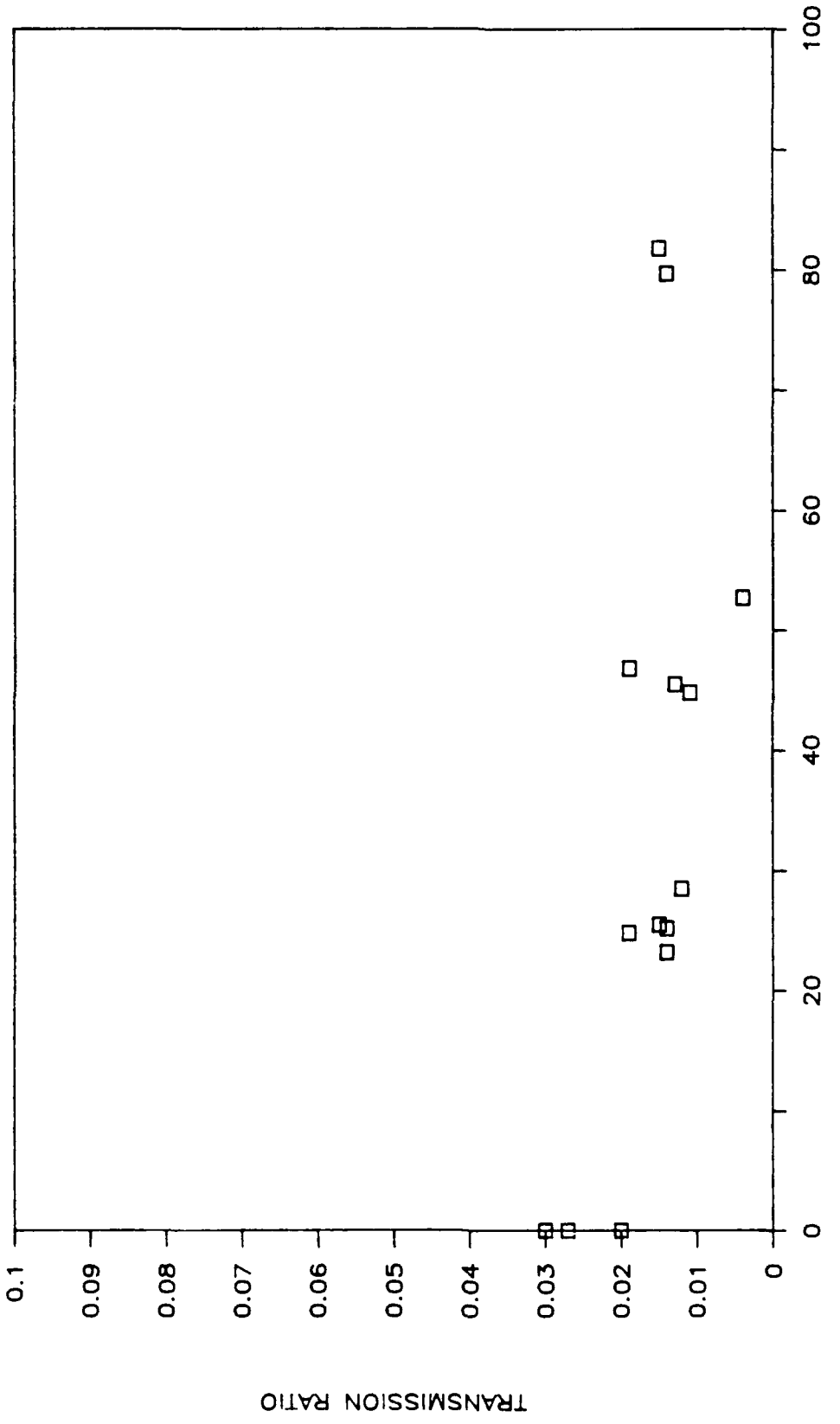

Figure 48. Transmission Ratio Versus Percent of Saturation for Eglin Sand Compacted Dry and Moisture Added Later. Confining Pressure: Atmospheric

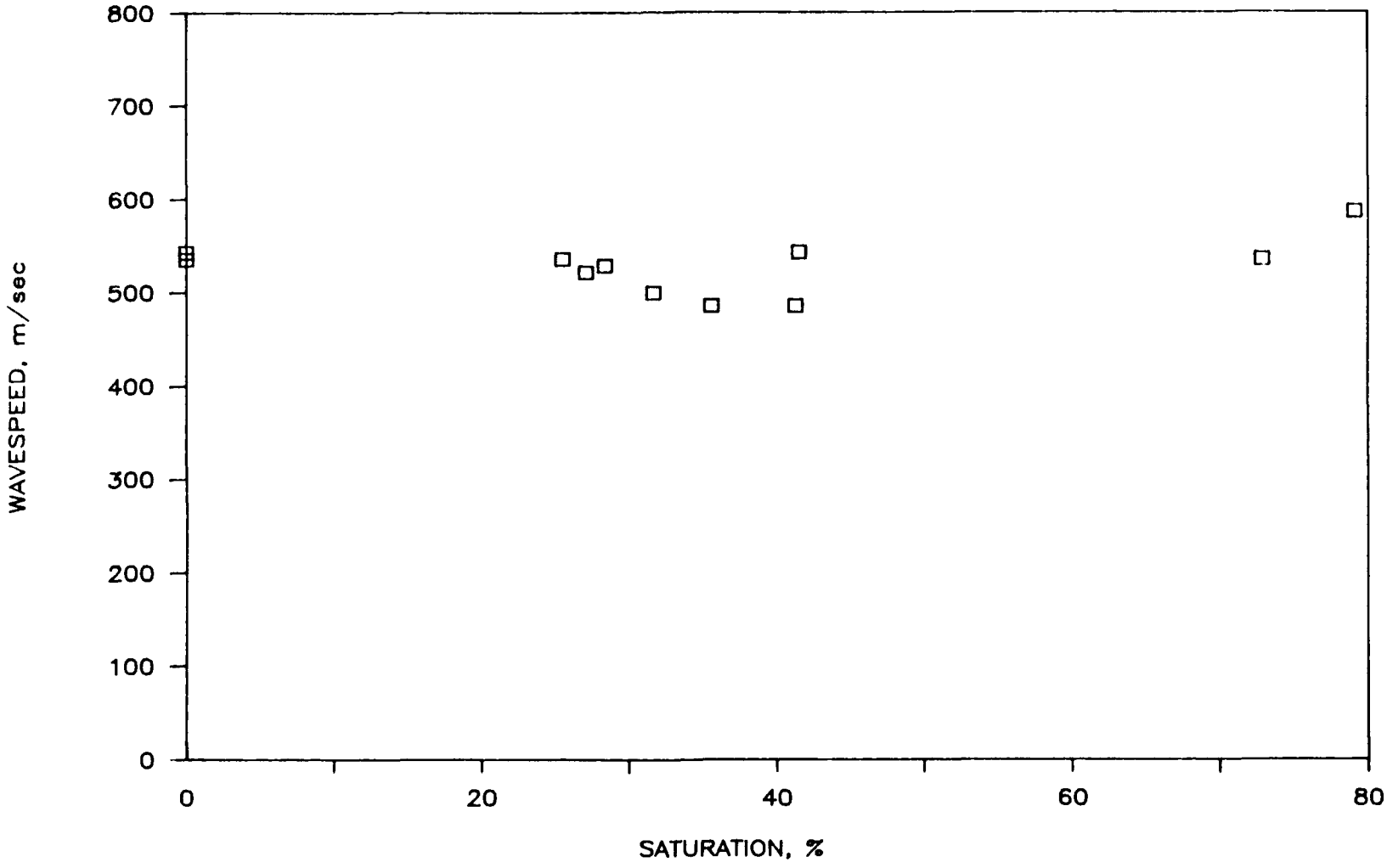

Figure 49. Wave Speed Versus Percent of Saturation for Eglin Sand Compacted Dry and Moisture Added Later. Confining Pressure: 45PSI (0.31MPa).

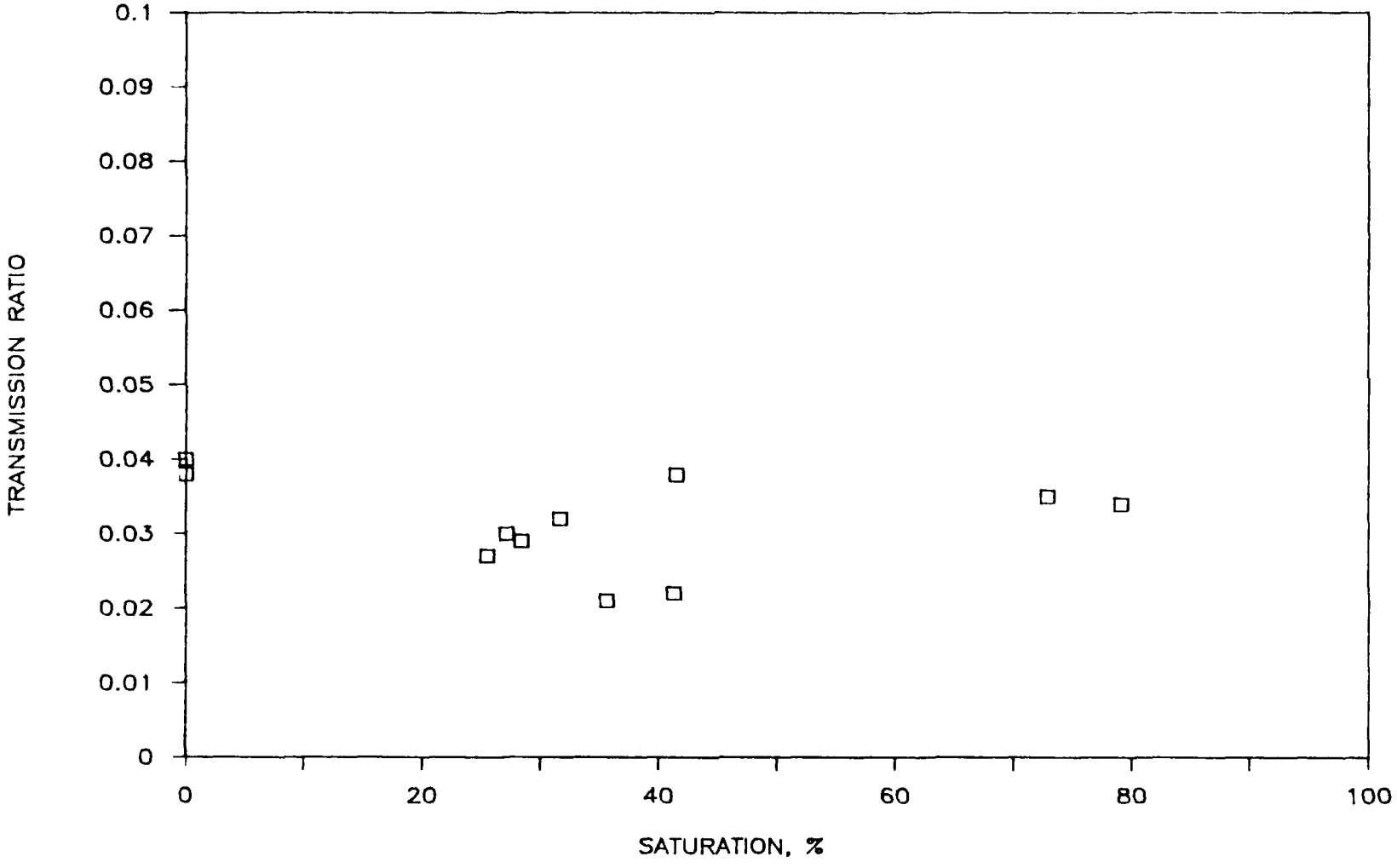

Figure 50. Transmission Ratio Versus Percent of Saturation for Eglin Sand Compacted Dry and Moisture Added Later. Confining Pressure: 45PSI (0.31MPa).

This energy is shown in Figure 51 versus moisture content and shows similar results as that of the SHPB soil specimens that were compacted with moisture present. That is, the energy to compact at all lifts increases with increasing moisture content but then decreases below that of the dry values at 50 to 60 percent saturation. This same general trend is also evident for the data of SHPB soil specimens compacted with moisture and shown in Figures 45 and 46. Results of specimens compacted dry and moisture added later show a rather constant wave speed and transmission ratio versus moisture content. This further tends to show that compaction energy with moisture has a rather strong influence on stiffness, wave speed, and transmissibility of sandy soils. Results of additional tests on specimens with a confining pressure of 45 psi (0.31MPa) compacted dry and then moisture added are shown in Figures 49 and 50. These data are similar as those of Figures 47 and 48 except the effect of confining pressure is to give a uniform increase in wave speed and transmissibility over the range of moisture contents below saturation.

All the soils tests in this study were conducted at a moisture content below saturation. It is recognized that at saturation large increases in stress wave propagation characteristics will occur, however that particular area was intentionally excluded from this work.

Also, it is recognized that the transmitted stress level recorded in the Bar 2 or transmitter bar is not the actual value of stress transmission in the soil. In fact, due to the high impedance mismatch between soil and steel the transmitted stresses are doubled across the rear soil/steel interface. However, the ratio of peak stresses in the incident and transmitter bar served as a convenient comparator between results of different soil tests.

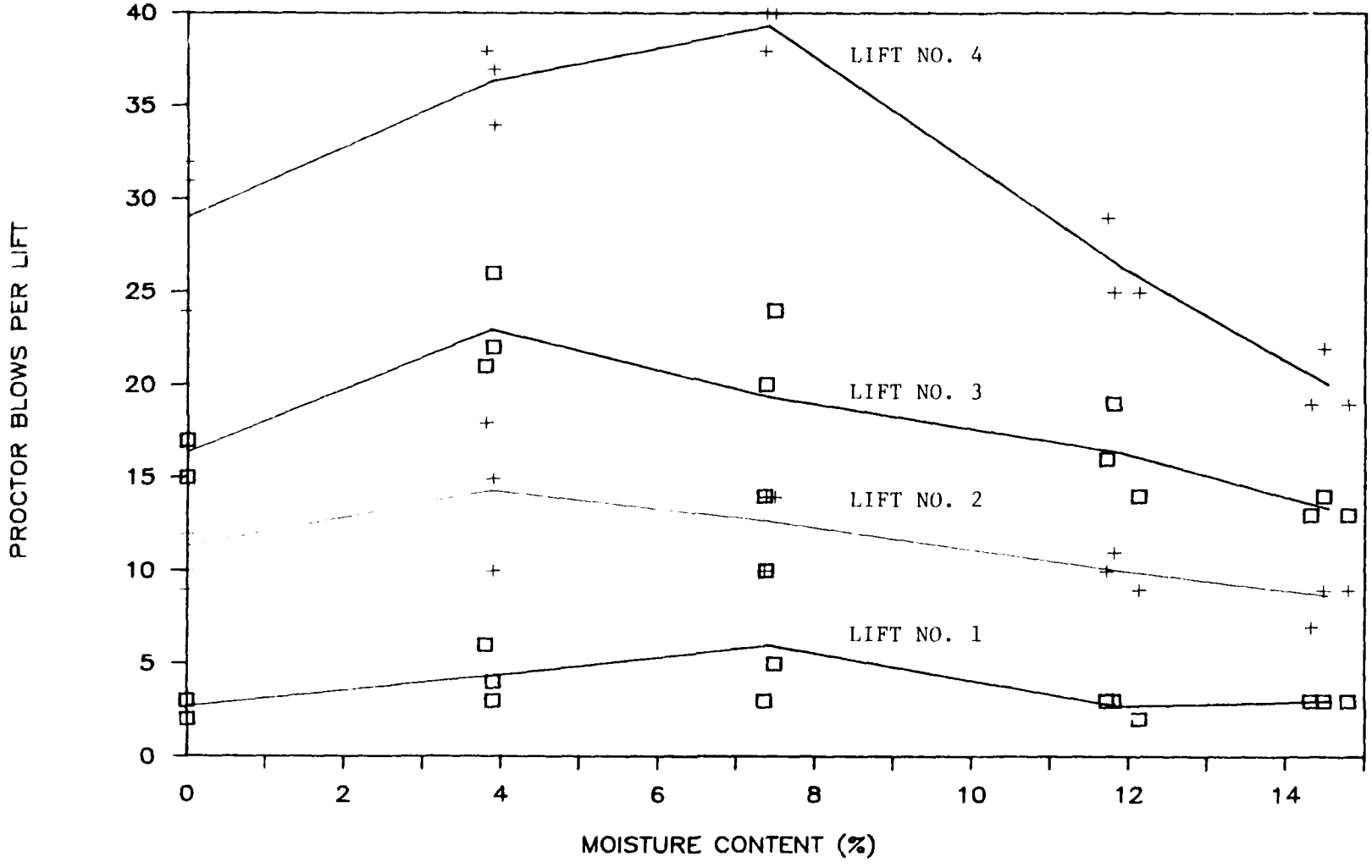

Figure 51. Energy, in Terms of Number of Blows of a 5.5 pound (2.5 kg) Proctor Hammer Dropped 12-inches (30.5 cm), Versus Moisuture Content for Eglin Sand. Number of Blows/Lift Given for Each Lift.

SECTION V

CONCLUSIONS AND RECOMMENDATIONS

A. CONCLUSIONS

1. Large-diameter split-Hopkinson pressure bars (SHPB) can be used to produce high-strain-rate compressive and tensile strength data of concrete.

2. High-strain-rate direct tension data appears not to satisfy the SHPB assumption of uniform stress along the specimen length.

3. Based on SHPB tests, the splitting cylinder specimen shows real promise as a tensile strength test specimen for high-strain-rate tests. However no stress-strain data are obtained by this method.

4. The stress distribution of the low- and high-load rate-splitting cylinder tests are similar.

5. Both compressive and tensile concrete strength show monotonically increasing values with increasing strain rate.

6. The tensile concrete strength shows a larger increasing strain rate sensitivity than that of compressive strength at the same strain rates.

7. Sandy soils tested at large compressive dynamic strains, with prior compaction and moisture, show increases in wave speed, stiffness, and pressure transmissibility up to approximately 50 percent saturation but show decreases beyond that.

8. The effects of compaction, more so than capillarity, appear to dominate the stress wave propagation characteristics in sandy soils.

B. RECOMMENDATIONS

1. Continue development of SHPB direct tension specimens and specimen grips for high strain rate tests. This method shows the greatest promise for tensile stress-strain data at high strain rates.

2. Continue clarification of SHPB splitting cylinder tests to determine accuracy of tensile strength obtained by this method.

3. Continue tests at high strain rates on cementitious materials to develop predictive equations of strength as a function of strain rate and model some details of constitutive relations.

4. Explore the effects of compaction and moisture content on stress wave propagation in sandy soils to better identify the important parameters and predict relations between these parameters.

REFERENCES

1. Lindholm, U. S., Techniques in Metals Research, Edited by R. F. Bunshah, Vol. 5, Part 1, Interscience N. Y. 1971

2. Nicholas, T., "Material Behavior at High Strain Rates," Chapter 8 of Impact Dynamics, Zukas, J. R., Editor, John Wiley & Sons NY, pp 280, 1982

3. Hopkinson, B., "A Method of Measuring the Pressure Produced in the Detonation of High Explosives or by the Impact of Bullets," Phil. Trans., Royal Soc of London, Series A, 1914, pp 437-456

4. Davies, R. M., Phil Trans Royal Soc of London, A., 140, p375, 1948

5. Kolsky, H., "An Investigation of the Mechanical Properties of Material at Very High Rates of Loading," Proc. Phys. Soc. (London) Ser B, Vol 62, pp 676-704, 1949

6. Lindholm, U. S., "Some Experiments With the Split-Hopkinson Pressure Bar," J. Mech. Phys. Solids, Vol 12, pp 317-335, 1964

7. Nicholas, T., "Tensile Testing of Materials at High Rates of Strain," Experimental Mechanics, 21(5), 177-185, May, 1981

8. Malvern, L. E., and Ross, C. A., Dynamic Response of Concrete and Concrete Structures, Final Technical Report, AFOSR Contract No. F49620-83-K007, May 1986

9. Harding, J. "Tensile Impact Testing of Fiber Reinforced Composites," 20th Annual Meeting, Soc. of Eng. Sci. Univ of Delaware Newark, DE, Aug. 1983

10. Sierakowski, R. L., Nevill, G. E., Jr., Ross, C, A., and Jones E. R., Studies on the Dynamic Fracture Characteristics of Composites, AFATL-TR-72-44, USAF Armament Laboratory, Eglin AFB, FL., Mar. 1972

11. Ross, C. A., and Sierakowski, R. L., "Dynamic Compressive Properties of a Metal Matrix Composite Material," Proceedings of the 16 Annual SAMPE Conf, Vol 16, P. 109, April 1971

12. Young, C., and Powell, C. N., "Lateral Inertia Effects on Rock Failure in Split Hopkinson-Bar Experiments," 20th US Symposium on Rock Mechanics, 1979

13. Kormeling, H. A., Zielinski, A. J., and Reinhardt, H. W., Experiments on Concrete Under Single and Repeated Impact Loading, Report No. 5-80-3, Delft University of Technology, Stevin Laboratory, May 1980

14. Felice, C. W., Brown, J. A., Gaffney, E. S. and Olsen, J. M. "An Investigation into the High Strain Rate Behavior of Compacted Sand Using the Split-Hopkinson Pressure Bar Technique," Proceedings of 2nd Symposium on the Interaction of Non-Nuclear Munitions With Structures, Panama City Beach, FL, April 1985, pp 391-396

15. Ross, C. A., Nash, P. T., and Friesenhahn, G. J., Pressure Waves in Soils Using a Split-Hopkinson Pressure Bar, ESL-TR-86-29 Air Force Engineering and Services Laboratory, Tyndall AFB FL, July 1986

16. Ross, C. A., Cook, W. H., and Wilson, L. L.,"Dynamic Tensile Tests of Composite Materials Using a Split-Hopkinson Pressure Bar," Experimental Techniques," pp 30-33, Nov, 1984.

17. Malvern, L. E., Jenkins, D. A., Jerome, E., and Gong, J. C., Dispersion Correction for Split-Hopkinson Bar Data, ESL-TR-88-04 Air Force Engineering and Services Laboratory, Tyndall AFB, FL. July 1988.

18. Dally, J. W. and Riley, W. F., Experimental Stress Analysis, McGraw-Hill Book Co., 1965, pp. 446-479.

19. Neville, A. M., Properties of Concrete, J. Wiley & Sons N.Y., N.Y., 1973, p. 490.

20. Ross, C. A., Thompson, P. Y., Charlie, W. A., and Doehring, D. O., "Transmission of Pressure Waves in Partially Saturated Soils," Accepted for Publication in Experimental Mechanics, Mar 1988

21. Wu, S., Gray, D. H., and Rickart, F. E., "Capillary Effects on Dynamic Modulus of Sands and Silts," J. of Geotechnical Eng., ASCE Vol. 110, No. 9, 1948, pp 1188-1203

22. Kormeling, H. A.., et al, Experiments on Concrete and Single and Repeated Uniaxial Impact Tensile Loads, Report 50-80-3, Stevin Lab., Delft Univ. of Tech. Netherlands, 1980.

23. John, R., and Shah, S. P., "Effects of High Strength and Rate of Loading on Fracture Parameters of Concrete," SEM-RILEM International Conf on Fracture of Concrete and Rock, Houston, TX, June 1987, pp 35-52.

24. Oh, B. H., "Behavior of Concrete Under Dynamic Tensile Loads," ACI Materials Journal, Jan-Feb 1987, pp 8-13.

25. Mellinger, F. M. and Birkimer, D. L., Measurement of Stress and Strain on Cylindrical Test Specimens of Rock and Concrete Under Impact Loading, Tech. Rept. No 4-46 Ohio River Div. Lab., Corps of Eng., Cincinnati Ohio 45227, Apr. 1966.

26. McVay, M. K., Spall Damage of Concrete Structures, Tech. Rept. SL-88-22, Waterways Experiment Station Corps of Eng. Vicksburg MS, June 1988.

APPENDIX A

A. OPERATING PROCEDURE

1. Introduction

For the operating procedure in general, the two areas which are common to most all tests are the gas gun system which launches the striker bar and the instrumentation used to record the strain signatures of the two strain-gauge positions. The gas gun operation is slightly different for the compression and tensile mode of operation and each will be covered separately.

2. Compressive Mode

A schematic of the pneumatic system for the compression mode operation is shown in Figure A-1. The general operating procedure is as follows:

1. Turn on main power for oscilloscope and strain gauge conditioner and allow to warm up.

2. Turn on main cylinder gas valves and set regulators. Approximately 200 psi (1.38MPa) for main line and 50 psi (0.35MPa) for quick opening valve.

3. Set trigger time on oscilloscope. Approximately 250 sec is a good setting.

4. Display test title on oscilloscope if desired.

5. Set excitation voltage and gain on all channels being used on strain gauge conditioner.

6. Set desired volts full-scale on all channels being used on the oscilloscope.

7. Open bleed valve C and push striker bar down the barrel. Close bleed valve C.

8. Move the Bar 1 to within approximate 1/8-inch (3 mm) of the end of the barrel.

9. Sandwich the specimen in between the Bars 1 and 2 using a thin film of lubricant on each end. Molybdenumdisulfide is an excellent lubricant.

10. Adjust the end stop on Bar 2.

11. Balance the strain gauge circuits of the strain gauge conditioner.

12. Adjust traces of channels to be used on oscilloscope to centerline of viewing screen (use GRID position on function knob).

13. Set trigger voltage level. Trigger should always be made on incident pulse, Strain Gauge 1 in compressive mode, and Strain Gauge 2 in tensile mode.

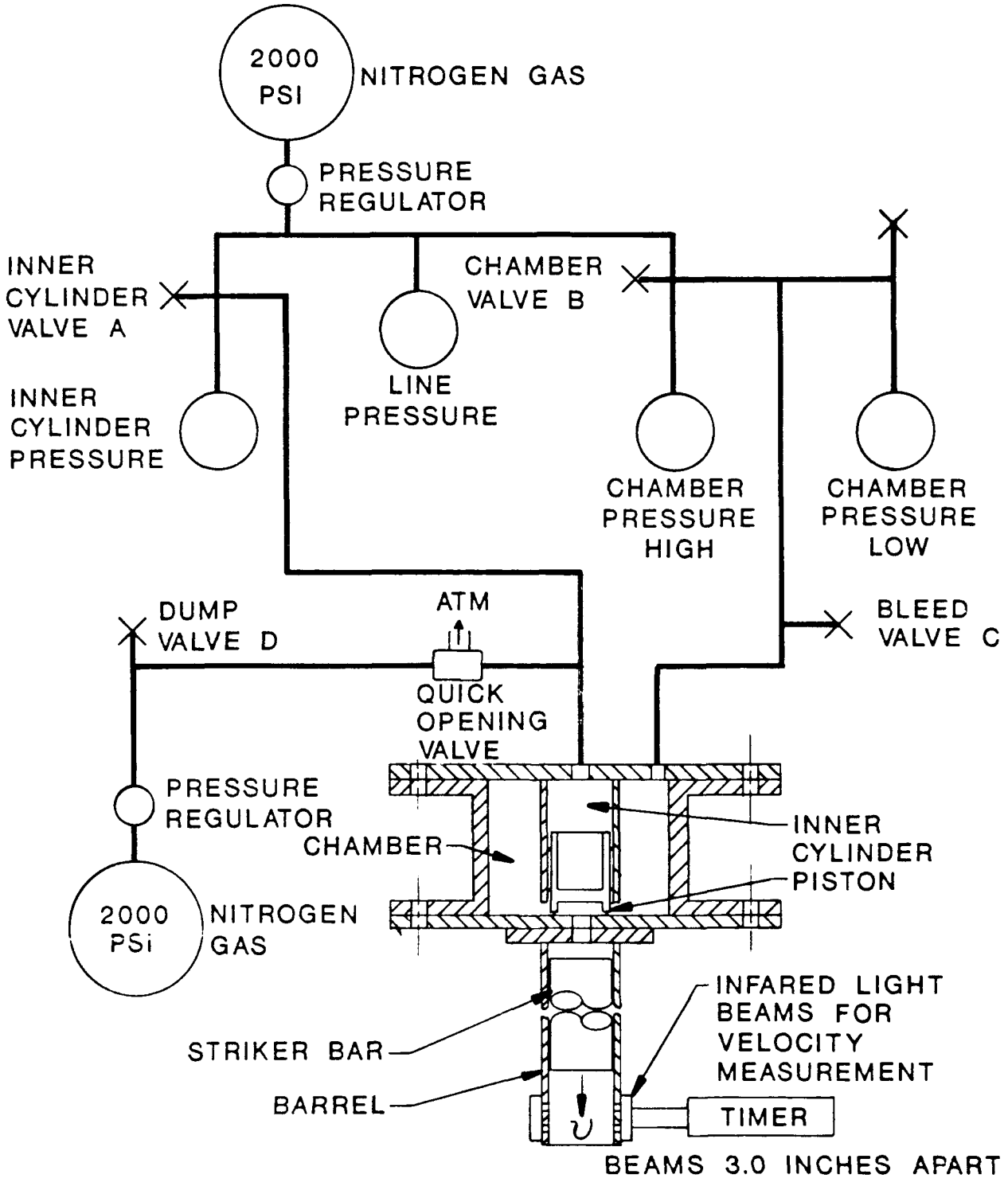

Figure A-1. Schematic of Pneumatic System for the Compressive Mode of Operation.

14. Set oscilloscope vertical and horizontal gains to "OFF".

15. Set oscilloscope function on selection to "invert." Title will not be recorded on disk if in "Prgm" position.

16. Set oscilloscope memory selection to "All."

17. Set oscilloscope to switch to "Norm" and arm oscilloscope to "live" and "hold next" mode.

18. Arm timer of velocity indicator.

19. Open inner cylinder Valve A and pressurize inner cylinder to approximately one-third the desired chamber pressure. Close Valve A.

20. Open chamber pressure Valve B and pressurize chamber to desired pressure. Close Valve B.

21. Double check to see if time and oscilloscope are still armed.

22. Open dump Valve D to "fire" position. After striker impacts Bar 1 return the Valve D to the "safe" position.

23. In case of emergency the chamber pressure may be released, without firing the system, by opening the Bleed Valve C.

3. Tensile Mode

A schematic of the pneumatic system for the tensile mode operation is shown in Figure A-2. The general operating procedures is as follows:

1.-6. Same as for compressive mode

7. Tighten tup on threaded end of Bar 2 and place the tup end of Bar 2 to approximately 0.5-inch (13 mm) inside the pressure tube.

8. Move the striker bar down the pressure tube. Use flexible rod in slot of pressure tube.

9. Cement the specimen in between Bar 1 and Bar 2. Take care that Bar 2 is not moved or rotated during this operation.

10.-17. Same as for compressive mode.

18. Open chamber pressure valve B and pressurize chamber to desired pressure. Close Valve B. (Inner cylinder and Valve A is not used in tensile mode operation).

19. Double check to see if oscilloscope is still armed.

20.-21. Same as 22.-23. of compressive mode.

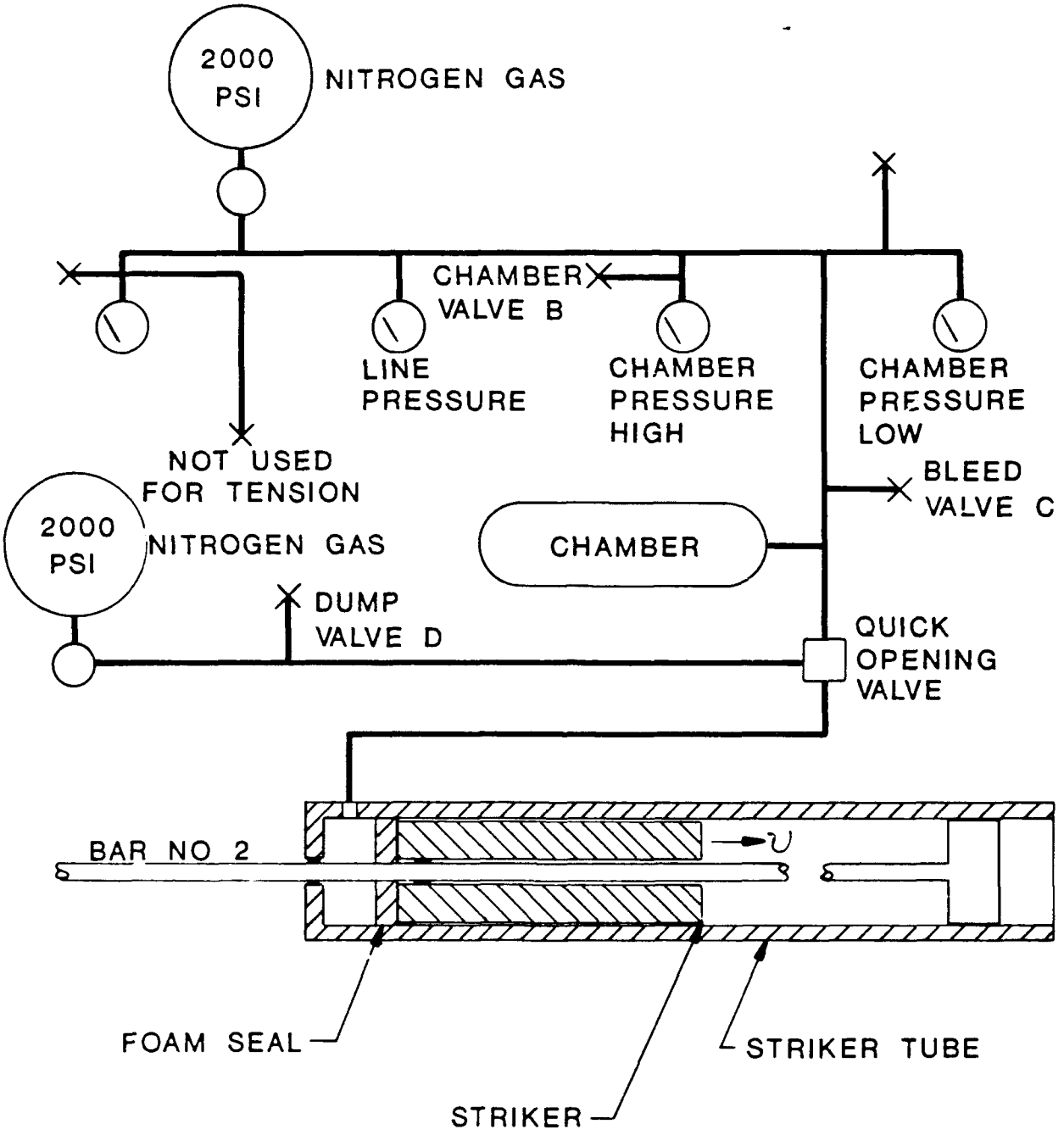

Figure A-2. Schematic of Pneumatic System for the Tensile Mode of Operation.

APPENDIX B

MIX RECIPE USED FOR WES CONCRETE

DEPARTMENT OF THE ARMY
WATERWAYS EXPERIMENT STATION, CORPS OF ENGINEERS
P O BOX 631
VICKSBURG, MISSISSIPPI 39180 0631

REPLY TO
ATTENTION OF

November 16, 1988

Structures Laboratory

Dr. C. A. Ross
Headquarters, Air Force Engineering
and Services Center
Tyndall Air Force Base, Florida 32403-6001

Dear Allen:

The mixture proportions for a 1-cu-yd batch of the concrete used to make your specimens are as follows:

Portland cement (Type I)	544 lb
Fly ash (Class F)	60 lb
Fine aggregate	1,397 lb
Coarse aggregate	1,785 lb
Anti-air-entraining admixture	1.2 lb
Water-reducing admixture	36.2 oz
Water	290 lb

The fine aggregate is a natural (siliceous) sand meeting ASTM C 33 specifications. The coarse aggregate is a 3/8-in. nominal maximum size limestone. All aggregate weights are saturated surface dry weights. The anti-air-entraining admixture is Halliburton D-Air, and the water-reducing admixture is Hunt Process HPSR.

If you need any further information, please let me know.

Sincerely,

Mike

Michael I. Hammons, PE
Research Civil Engineer
Concrete Technology Division